CAIT-UTC-NC13

Dynamic Effects and Friction Values of Bridge Moves for ABC Bridges

FINAL REPORT
2017

Submitted by:

Kris Johnson
Graduate Research Assistant

Marc Maguire
Assistant Professor

Marvin Halling
Professor

Paul Barr
Professor

Sattar Dorafshan
Graduate Research Assistant

Utah State University
4110 Old Main Hill
Logan, UT 84322-4110

External Project Manager

Michael P. Culmo
CME Associates, Inc.
333 East River Drive Suite 400
East Hartford, CT 06108

In cooperation with

Rutgers, The State University of New Jersey
and
The National Cooperative Highway Research Program (NCHRP)
and
U.S. Department of Transportation
Federal Highway Administration

Disclaimer Statement

The contents of this report reflect the views of the authors, who are responsible for the facts and the accuracy of the information presented herein. This document is disseminated under the sponsorship of the Department of Transportation, University Transportation Centers Program, in the interest of information exchange. The U.S. Government assumes no liability for the contents or use thereof.

The Center for Advanced Infrastructure and Transportation (CAIT) is a National UTC Consortium led by Rutgers, The State University. Members of the consortium are the University of Delaware, Utah State University, Columbia University, New Jersey Institute of Technology, Princeton University, University of Texas at El Paso, Virginia Polytechnic Institute and University of South Florida. The Center is funded by the U.S. Department of Transportation.

TECHNICAL REPORT STANDARD TITLE PAGE

1. Report No.	2. Government Accession No.	3. Recipient's Catalog No.
CAIT-UTC-NC13		

4. Title and Subtitle	5. Report Date
Dynamic Effects and Friction Values of Bridge Moves for ABC Bridges	November 2017
	6. Performing Organization Code Utah State University/CAIT
7. Author(s) Kris Johnson; Marvin Halling, Ph.D., P.E.; Sattar Dorafshan; Marc Maguire, Ph.D., P.E.; Paul Barr, Ph.D., P.E.; Michael Culmo	8. Performing Organization Report No. CAIT-UTC-NC13
9. Performing Organization Name and Address Utah State University 4110 Old Main Hill Logan, UT 84322-4110	10. Work Unit No. 11. Contract or Grant No. DTRT13-G-UTC28
12. Sponsoring Agency Name and Address Center for Advanced Infrastructure and Transportation Rutgers, The State University of New Jersey 100 Brett Road. Piscatawav. NJ 08854	13. Type of Report and Period Covered Final Report 12/01/14 to 11/30/16 14. Sponsoring Agency Code

15. Supplementary Notes
U.S. Department of Transportation/OST-R
1200 New Jersey Avenue, SE, Washington, DC 20590-0001

16. Abstract

The effects of the Self-Propelled Modular Transports (SPMT) vehicles on pre-cast bridge decks during transportation were investigated as the part one of this report. The dynamic response SPMTs were investigated during several possible load cases and three load cases, by conducting following experiments. Nine accelerometers were attached to a SMPT in different location facing three major directions, i.e., longitudinal, transverse, and vertical. The SMPT was operated in each motion case while carrying different weight including: Heavy Load Case (100 Tons), Medium Load Case (50 Tons), and Light Load Case (15 Tons). The accelerations were recorded after each experiment by the attached sensors and then post-processed to obtain the critical motion case. It was found that traversing a long stretch of uneven ground was critical for the vertical direction (The Long Run Motion Case) and rapid decelerations were critical for the horizontal direction (The Start and Stop Motion Case). Transverse accelerations were found to not be critical for the horizontal direction. Increasing the payload of the SPMT was found to decrease measured accelerations significantly. Acceleration data was recorded from the platform in various locations during these maneuvers. The data collected was used to develop design response spectra, treating the problem similarly to an earthquake design scenario. Peak platform acceleration (PPA), for vertical and horizontal directions, can be obtained using the empirical formulas which take the percentage of SPMT capacity into account. Then, the period of the system (SPMT and the falsework) needs to be calculated. Based on period, the spectral acceleration and associated dynamic effects can be computed using the synthesized design spectrums.

Additionally, multiple tests were carried out to determine the effects of surface roughness, lubricant's type, siding speed, and contact pressure on the coefficient of friction during bridge slides in Slide-In Bridge Construction (SIBC). Tests were performed using three different levels of surface roughness. Type 304 stainless steel was tested for two of the mating surfaces each with different surface finishes. Tests were also conducted using carbon steel in order to determine how well the bridge would slide if steel bridge girders were placed directly on the PTFE pads. If the performance of the steel was satisfactory, it could eliminate the need for contractors to purchase and install stainless steel sheets for the sliding surface. Each surface was tested with the following types of lubricants: silicone grease, automotive motor oil, graphite, dish soap and a dry surface for baseline comparison. Additionally, four different applied pressures and two different speeds were investigated. This testing matrix resulted in around 60 unique combinations in which performance data was collected and used for comparison. It was concluded that stainless steel with a #2B finish (just lightly polished) performed similar to the #8 mirror finish (highly polished). This option is preferred due to its lower cost and availability. Using carbon steel resulted in much higher COF as expected and is not recommended due to the increase of horizontal force required to push the bridge into place. The same was true for the stainless steel with a #1 surface finish. All of the lubricants studied, resulted in significantly lower COF values than the baseline testing without lubricant with exception to the graphite. Using motor oil, grease, or liquid soap for a bridge slide will give satisfactory friction values. It is recommended that lubrication such as these always be used.

17. Key Words	18. Distribution Statement
ABC Bridge Construction, SPMT, Slide in Bridge Construction, Bearing Friction, Bearing Lubricants	

19. Security Classification (of this report)	20. Security Classification (of this page)	21. No. of Pages	22. Price
Unclassified	Unclassified	129	

Form DOT F 1700.7 (8-69)

Table of Contents

Part One: Bridge Dynamics

Chapter 1: Introduction

Self-Propelled Modular Transport (SPMT) vehicles were introduced to the bridge industry in 2008 and have been used routinely since. SPMTs are mainly used to transport super-heavy bridges from a prefabrication site to their final position. Each SPMT module can be attached to the other modules for moving very large structures, forming a combination of multi-axle platforms operated by computer interface. A module can pivot 360 degrees, lift, carry and set large loads at walking speed. Moving bridges with SMPTs significantly reduces traffic disruption and provides more safety for the workers and the public.

The bridge transportation process falls in the temporary works category which usually is done by contractors. SPMTs move at walking speed, but the dynamic forces applied to the weight as the SPMT moves can be an issue. Sudden stops, turns, rotations can occur during transport and there is currently limited guidance for this in design. These dynamic forces are typically the responsibility of the contractor and the design engineer.

To investigate the dynamic effects of SPMT movement to the bridge and falsework, the research team conducted a series of experiments. This report represents the tests procedures followed by the findings of this experiment. Chapter 2 includes an outline of the tests with sensor placement and properties. In Chapter 3 different load cases are explained along with schematic drawings of each load case. Chapter 4 is dedicated to the investigating accelerometer time history to determine critical motion cases. Design spectrum, using the recorded time histories for critical motion cases, and the selected methodology is presented in Chapter 5. In Chapter 6 the proposed AASHTO LRFD Design Spectra are defined to design the falsework for both vertical and horizontal directions.

Chapter 2: Outline of Experiment

The purpose of this experiment was to find the worst case applied accelerations to a transported structure. Sensors were placed directly on the SPMT as well as on the payload (crane weights). The SPMT was taken through several severe motion cases and under three load cases. The following section outlines the details of the experiment.

Placement of the Sensors

Nine accelerometers were installed in three different locations on the SPMT platform and the payload. Each accelerometer was mounted magnetically in one of three principle directions: Longitudinal, Transverse and Vertical. Positive longitudinal is defined as the forward direction of the SPMT. Positive transverse is defined as perpendicular to the longitudinal direction on the platform plane, using the right hand rule with positive vertical defined as opposite of gravity (i.e. up). The direction of each sensor is shown in Table 2.1. Specifications for the accelerometers are presented in Appendix A.

A cluster of three sensors, measuring the three principle directions, were attached to the front left side, the back left side and on top of the metal weights on the platform. The sensor placements are shown in Figure 2.1. Three Bridge Diagnostics Inc. (BDI) nodes were used to connect the sensors to the base station and laptop.

To simulate the condition of the SPMTs carrying a bridge, a payload consisting of metal crane weights was secured to the platform. Three load cases defined as Heavy, Medium and Light, with 100 Tons, 50 Tons and 15 Tons of payload, respectively.

Table 2.1 Sensor's Placement on the SPMT

Positon	Sensor's name	Direction
Front-left on platform	A2130	Longitudinal
	A2131	Transverse
	A2132	Vertical
Back-right on platform	A2133	Longitudinal
	A2089	Transverse
	A2090	Vertical
On the weights	A1036	Longitudinal
	A1035	Transverse
	A2087	Vertical

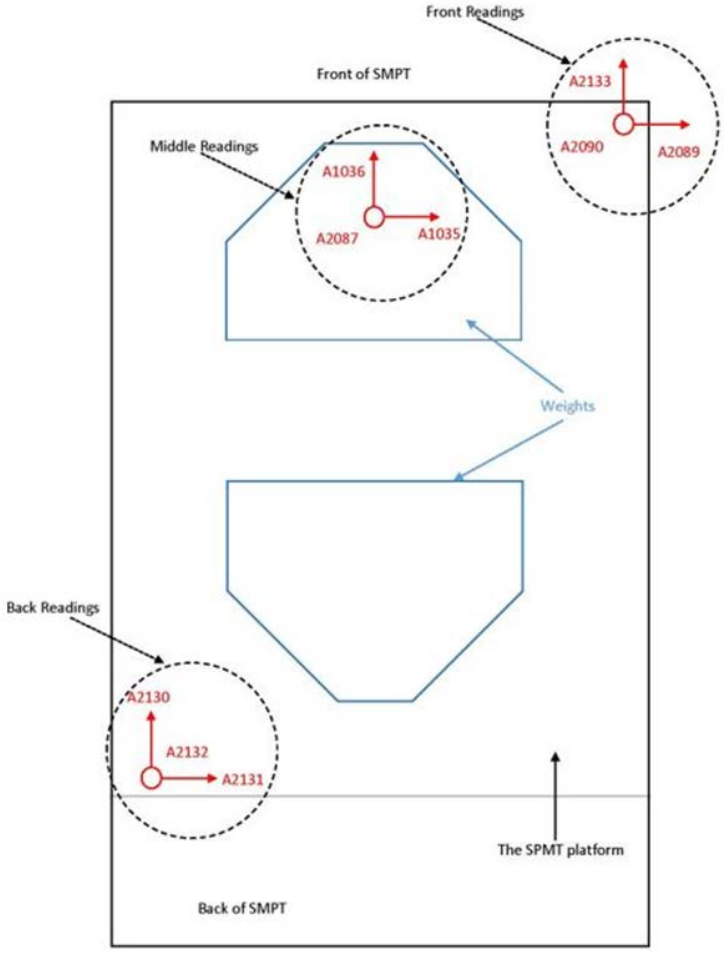

Figure 2.1 Schematic plan view of the sensor's placement

Motion Cases

The following scenarios, referred to as Motion Cases in this report, were defined and investigated to cover all possible extreme events during the cargo transport:

- "Start and Stop": A sudden brake or a rapid take off can cause considerable longitudinal accelerations. This scenario is considered the most common event and can occur several times during one carriage, although typically not to the extreme.
- "Up and Down": Bouncing of the vehicle can cause significant acceleration in vertical direction. This may occur during raising or lowering of the cargo into place.
- "90 Degree Turn": Turning while moving a bridge deck on the road can create both longitudinal and transverse accelerations.
- "Long Run": During a transport, it is possible to encounter uneven ground or the weight of the loaded SPMT can create uneven ground in poorly prepared roadbed. This motion case is characterized by a long run of road unevenness with locations of well and poorly compacted soil, causing significant vertical accelerations.
- "Rotation": SPMTs can rotate 360 degrees causing accelerations in horizontal directions.

For each load case, defined in the following section, all of the five motion cases were performed. During the test, the operator of the SPMT was asked to simulate extreme events.

Chapter 3: Load Cases

Three load cases were selected based on the operational payload weight of SPMTs. Since the maneuvering of the hydraulically powered SPMT is known to be affected the weight, it was loaded with three different payloads in addition to its own weight: 15 Tons, 50 Tons and 100 Tons.

Heavy Load Case (100 Tons)

The vehicle was loaded with two stacks of crane counter weights: nine steel plates on one side and eight on the other side. Each individual plate weighed 5 Tons (Figure 3.1). Additionally, a steel platform on which the weights were placed weighed 15 Tons, thus the total load on the SPMT was 100 Tons. As mentioned in Chapter 2, on the top of the front stack, a cluster of three accelerometers was installed at the elevation of 108 in. from the SPMT's platform bottom. This test was consisted of following cases:

- **SPMT1: Test, checking the sensors.** Note the results of this will not be reported for brevity.
- **SPMT2: Up and down.** Two up-down cycles for this motion case were carried out.
- **SPMT3: Misfire.** The vehicle was started before the running of data acquisition system. Note the results of this will not be reported for brevity.
- **SPMT4: Start and stop.** This test was conducted in backward direction. During the test the SPMT was started and stopped three times (a, b and c).
- **SPMT5: Start and stop.** This test was conducted in backward direction. During the test the SPMT started and stopped three times (a, b and c).
- **SPMT6: Start and stop.** This test was conducted in forward direction. During the test the SPMT started and stopped three times (a, b and c).

- **SPMT7: Start and stop.** This test was conducted in forward direction. During the test the SPMT started and stopped three times (a, b and c).
- **SPMT8: 90 degree turn.** The SPMT was turned for 90 degrees to the South without stopping.
- **SPMT9: Long run.** The SPMT was moved forward at a constant fast walking pace while on uneven ground.
- **SPMT10: Long run.** The SPMT was moved backward at a constant fast walking pace while on uneven ground.
- **SPMT 11: Rotation.** The SPMT was rotated 360 degrees clockwise.

The map for the heavy load case is shown in Figure 3.2.

Figure 3.1. The steel weights on SPMT for heavy loading

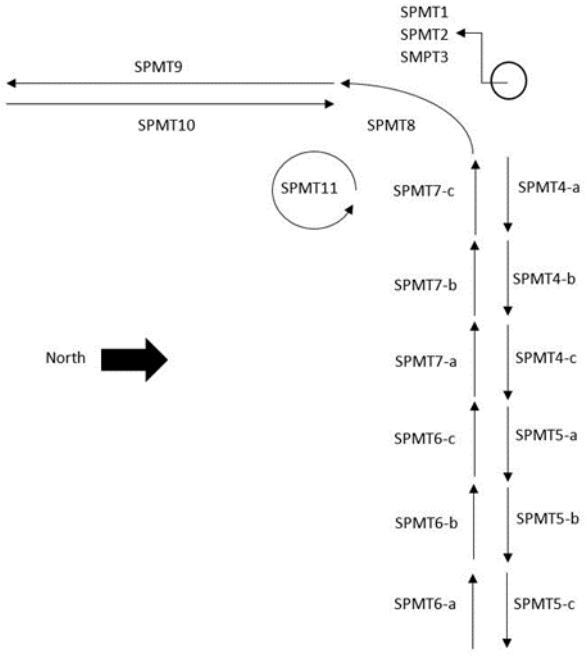

Figure 3.2. The schematic view for heavy load case

Medium Load Case (50 Tons)

The vehicle was loaded with two stacks of crane counter weights: four steel plates on one side and four on the other side. Additionally, a steel platform on which the weights were placed weighed 15 Tons, thus the total load on the SPMT was 50 Tons. As mentioned in Chapter 2, on the top of the front stack, a cluster of three accelerometers was installed at the elevation of 51 in. from the SPMT's platform bottom. This load case consisted of following motion cases:

- **SPMT12: Test, checking the sensors.**: Note the results of this will not be reported for brevity.
- **SPMT13: Moving back into original position.** Note the results of this will not be reported for brevity.
- **SMPT14: Start and stop.** This test was conducted in backward direction. During the test the SPMT was started and stopped three times (a, b and c).

- **SMPT15: Start and stop.** This test was conducted in backward direction. During the test the SPMT started and stopped three times (a, b and c).
- **SMPT16: Start and stop.** This test was conducted in forward direction. During the test the SPMT started and stopped three times (a, b and c).
- **SMPT17: Start and stop.** This test was conducted in forward direction. During the test the SPMT started and stopped three times (a, b and c).
- **SPMT18: 90 degree turn.** The SPMT was turned for 90 degrees to the South without stopping.
- **SPMT19: Long run.** The SPMT was moved forward at a constant fast walking pace while on uneven ground.
- **SPMT20: Long run.** The SPMT was moved backward at a constant fast walking pace while on uneven ground.
- **SPMT21: Rotation.** The SPMT was rotated 360 degrees counter clockwise.
- **SPMT22: Up and down.** Two up-down cycles for this motion case were carried out.

Figure 3.3 presents a schematic map of the route for the motion cases for the 50 Tons load case.

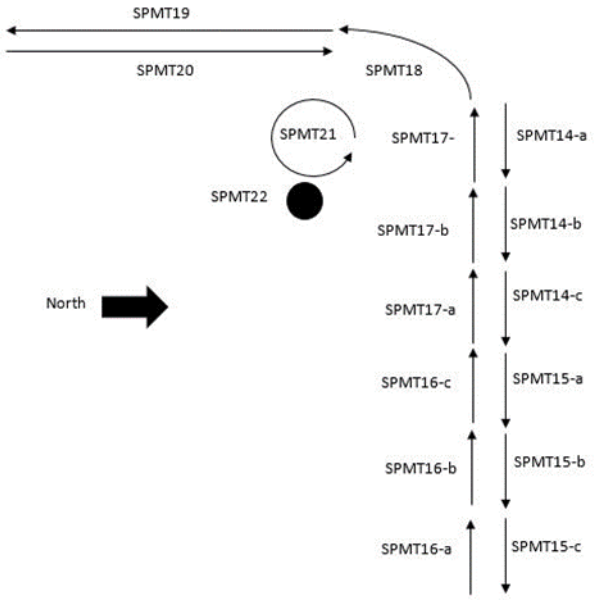

Figure 3.3. A schematic plan view of the medium load case test

Light Load Case (15 Tons)

All the steel weights were unloaded and only the platform of SPMT remained. The total carrying weight by the SPMT was 15 Tons in this case. The light load case was consisted of the following motion cases:

- **SPMT23: Test, checking the sensors.** Note the results of this will not be reported for brevity.
- **SPMT24: Up and down.** Two up-down cycles for this motion case were carried out.
- **SPMT25: Moving back into original position.** Note the results of this will not be reported for brevity.
- **SMPT26: Start and stop.** This test was conducted in backward direction. During the test the SPMT was started and stopped three times (a, b and c).
- **SMPT27: Start and stop.** This test was conducted in backward direction. During the test the SPMT was started and stopped three times (a, b and c).

- **SMPT28: Start and stop.** This test was conducted in forward direction. During the test the SPMT was started and stopped three times (a, b and c).
- **SMPT29: Start and stop.** This test was conducted in forward direction. During the test the SPMT was started and stopped three times (a, b and c).
- **SPMT30: 90 degree turn.** The SPMT was turned for 90 degrees to the South without stopping.
- **SPMT31: Long run.** The SPMT was moved forward at a constant fast walking pace while on uneven ground.
- **SPMT32: Long run.** The SPMT was moved backward at a constant fast walking pace while on uneven ground
- **SPMT32: Rotation.** The SPMT was rotated 360 degrees counter clockwise.

Figure 3.4 presents a schematic map of the route for the motion cases for the 15 Tons load case.

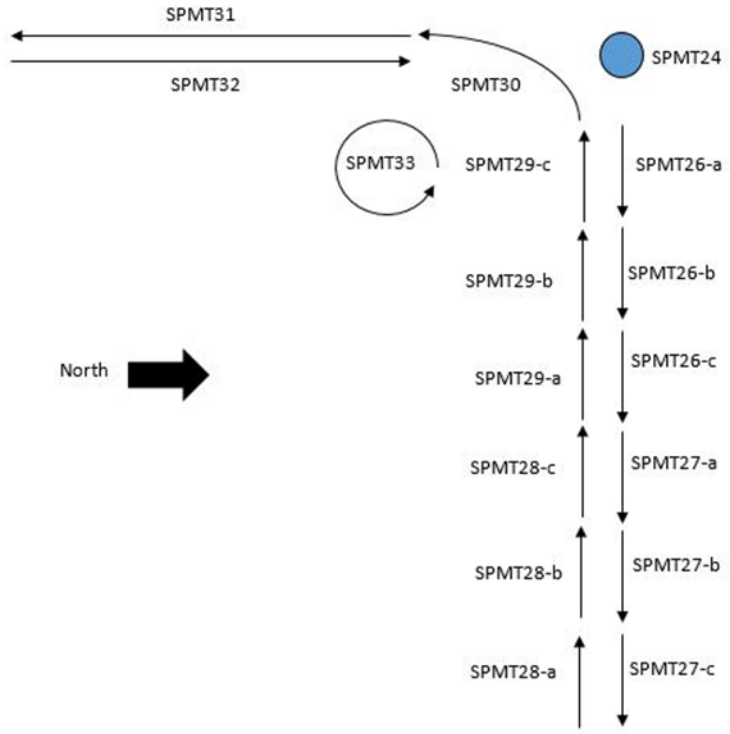

Figure 3.4. A schematic plan view of the light load case test

Chapter 4: Experimental Results

The sensors were divided into three clusters based on their locations. Each cluster consists of three sensors, one for each principle direction. The clusters are grouped together as follows (see Figure 1):

- Cluster 1 (Front Readings): including three sensors in three defined directions located in front of the SPMT (A2133-L, A2089-T, and A2090-V).
- Cluster 2 (Middle Readings): including three sensors in three defined directions located in the middle of the SPMT i.e. on top of the weights (A1036-L, A1035-T, and A2087-V).
- Cluster 3 (Back Readings): including three sensors in three defined directions located in back of the SPMT (A2130-L, A2131-T, and A2132-V).

All accelerometers were sampled at a rate of 100 Hz during the experiment. The recorded accelerations, i.e., time history data, were then post-processed to determine the absolute maximum value of accelerations and the corresponding motion case for each load case. The load case in which the maximums were observed can be considered as the critical cases for design purposes.

Peak Platform Accelerations

The peak platform accelerations (PPA) for each cluster, load case and motion case are presented in Table 4.1 through Table 4.3 for Cluster 1 through Cluster 3, respectively. All time history plots for the absolute maximum acceleration data recorded for each motion and load case are presented in Appendix B.

Table 4.1. Maximum accelerations for Cluster 1 (top of SPMT platform)

Motion Case	Principle Direction	15 Tons	50 Tons	100 Tons

Start and Stop	Longitudinal	0.34g	0.23g	0.25g
	Vertical	0.57g	0.22g	0.13g
	Transverse	0.10g	0.08g	0.07g
Long Run	Longitudinal	0.11g	0.15g	0.06g
	Vertical	0.57g	0.12g	0.08g
	Transverse	0.14g	0.10g	0.08g
Up and Down	Longitudinal	0.06g	0.04g	0.04g
	Vertical	0.05g	0.06g	0.07g
	Transverse	0.06g	0.03g	0.05g
90 Degree Turn	Longitudinal	0.05g	0.03g	0.04g
	Vertical	0.05g	0.04g	0.07g
	Transverse	0.07g	0.06g	0.04g
Rotation	Longitudinal	0.04g	0.02g	0.03g
	Vertical	0.08g	0.04g	0.04g
	Transverse	0.12g	0.11g	0.07g

Table 4.2. Maximum accelerations from Cluster 2 (top of payload)

Motion Case	**Principle Direction**	**15 Tons**	**50 Tons**	**100 Tons**
Start and Stop	Longitudinal	0.34g	0.29g	0.28g
	Vertical	0.59g	0.14g	0.10g
	Transverse	0.09g	0.08g	0.07g
Long Run	Longitudinal	0.11g	0.16g	0.06g
	Vertical	0.34g	0.12g	0.07g
	Transverse	0.13g	0.12g	0.09g
Up and Down	Longitudinal	0.06g	0.05g	0.05g
	Vertical	0.04g	0.05g	0.05g
	Transverse	0.05g	0.02g	0.05g
90 Degree Turn	Longitudinal	0.05g	0.08g	0.04g
	Vertical	0.03g	0.05g	0.03g
	Transverse	0.06g	0.06g	0.05g
Rotation	Longitudinal	0.03g	0.03g	0.03g
	Vertical	0.04g	0.03g	0.03g
	Transverse	0.10g	0.09g	0.06g

Table 4.3. Peak platform accelerations from Cluster 3 (top of SPMT platform)

Motion Case	**Principle Direction**	**15 Tons**	**50 Tons**	**100 Tons**
Start and Stop	Longitudinal	0.33g	0.23g	0.25g
	Vertical	0.18g	0.12g	0.18g
	Transverse	0.09g	0.07g	0.07g
	Longitudinal	0.11g	0.16g	0.06g

Long Run	Vertical	0.25g	0.13g	0.13g
	Transverse	0.12g	0.08g	0.07g
Up and Down	Longitudinal	0.06g	0.04g	0.04g
	Vertical	0.08g	0.06g	0.04g
	Transverse	0.05g	0.02g	0.04g
90 Degree Turn	Longitudinal	0.05g	0.03g	0.03g
	Vertical	0.05g	0.05g	0.05g
	Transverse	0.05g	0.05g	0.04g
Rotation	Longitudinal	0.06g	0.03g	0.03g
	Vertical	0.06g	0.03g	0.04g
	Transverse	0.11g	0.06g	0.03g

Comparing the values between Cluster 1 through Cluster 3, the maximum accelerations are very similar between motion and load cases. The largest differences have come between the transverse directions for the rotation load case which was likely affected by the evenness of the driving surface, as discussed in more detail below. This unevenness can also be seen in the time history plots for this load case, 4.1.A notable exception is the vertical acceleration during the Long Run for the 15 Tons load case, in which Cluster 1 reported 0.57g compared to 0.25g. This is also exhibited when comparing the Start and Stop motion case for the 15 Tons load case (compare 0.57g to 0.18g in Table 4.1 and Table 4.3). This difference was likely related to the center of rotation of the SPMT system, which includes the 30 feet long power pack which houses the hydraulic system. Realistically, due to measurement and testing error, most readings between Cluster 1, 2 and Cluster 3 provide identical results.

According to Table 4.1 through Table 4.3, for the 100 Tons load case, the maximum longitudinal acceleration occurred during the Start and Stop motion case (SPMT 7) with the maximum value of 0.28g. The maximum vertical acceleration occurred during the Start and Stop motion case (SPMT 7) with 0.18g acceleration. The maximum transverse acceleration for this load case happened during the Long Run motion case (SPMT 9) with 0.08g acceleration. For the 100 Tons load case, the Start and Stop motion case had the controlling acceleration in longitudinal and

vertical directions. The maximum transverse acceleration for the 100 Tons load case occurred during the Long Run motion case (SPMT 10) with 0.07g acceleration.

For the 50 Tons load case, the maximum longitudinal acceleration occurred during the Start and Stop motion case (SPMT 17) with a maximum value of 0.23g. The maximum vertical acceleration occurred during the Start and Stop motion case (SPMT 17) with 0.21g acceleration. However, the maximum transverse acceleration for this load case was happened during the Rotation motion case (SPMT 21) with 0.11g acceleration. Similar to the heavy load case, the controlling motion case for longitudinal and vertical accelerations was Start and Stop, but the Rotation motion case controlled the transverse acceleration.

For the 15 Tons load case, the maximum longitudinal acceleration occurred during the Start and Stop motion case (SPMT 29) with the maximum value of 0.34g while the maximum vertical acceleration also occurred during the Start and Stop motion case (SPMT 28) with a value of 0.57g. The maximum transverse acceleration for 15 Tons load case was recorded during the Long Run motion case (SPMT 31) with 0.14g acceleration. The controlling motion cases for longitudinal, vertical and transverse accelerations recorded during Start and Stop, Start and Stop, and Long Run motion cases, respectively.

The transverse accelerations were significantly affected by the gravity reference of the sensors. If the SPMT platform tilted to the side slowly due to uneven ground or natural changes in elevation the sensor would register a change in acceleration, even though this change is pseudo-static. For instance: the maximum transverse acceleration occurred during the Long Run motion case and, as shown in Figure 4.1, due to unevenness of the road, the accelerometer readings were slowly skewed, with maximum dynamic vibration as indicated by the arrow. Therefore, the actual value of transverse acceleration that the falsework or carried structure would experience

dynamically is less than 0.08g (approximately 0.04g) and occurred over a very short time period, which is likely to have little effect on the falsework or bridge structure. This phenomenon is consistent across all transverse accelerations in all motion and load cases.

Figure 4.2 through Figure 4.5 represent the maximum Longitudinal, Transverse and Vertical acceleration time histories. Figure 4.2 presents the maximum longitudinal acceleration time history from SPMT29. This time history was characterized by the three main stop and start maneuvers where each stop and start had a significant positive and negative pulse. The negative pulse was always larger than the positive pulse in which the vehicle was stopping. This indicated that an emergency stop for SPMT was more critical for design than an abrupt start. Figure 4.3 presents the acceleration time history for SPMT31 which was the maximum transverse time history and occurred during a Long Run Motion Case. The transverse accelerations were pulses of very short duration as opposed to the large impulses noticed during the longitudinal accelerations of the Start and Stop Motion Case. Figure 4.4 presents the acceleration time history for SPMT28 which was the maximum vertical time history that occurred during a Start and Stop Motion Case. Figure 4.5 presents the acceleration time history for SPMT32 which was the maximum vertical time history that occurred during a Long Run Motion Case. The time histories for maximum vertical accelerations were significantly different, with the Long Run Motion Case exhibiting a longer and more sustained vertical shaking than the relatively short duration Start and Stop accelerations.

Maximum vertical accelerations were considerably higher in the Start and Stop Motion case than any other (e.g., 0.59g in Table 4.2). However, this is somewhat misleading because of the rotation of the platform during the starting and stopping maneuver. During a stop, vertical accelerations were generated by the rotation of the platform about some point between the center of the platform and the back axle, due to the heavy power pack attachment. During a large bridge

move it was assumed that more than one SPMT will be linked, whether directly attached or through the attachment of the falsework and bridge assembly. By linking the SPMTs this rotation was assumed to be restrained significantly so only the horizontal readings from the Start and Stop Motion Case should be considered for design values (elaborated in the following chapter).

Maximum vertical accelerations during the Long Run Motion Case were caused by the velocity of the SPMT navigating uneven ground. For this reason, vertical accelerations from the Long Run Motion Case were considered critical to design. Maximum longitudinal accelerations were significant in the Long Run Motion Case, but rarely controlling simply based on the maximum measured accelerations. The maximum vertical accelerations during the Long Run Motion Case were 0.57g, 0.13g and 0.13g, for 15 Tons, 50 Tons and 100 Tons respectively.

The motion cases of Up and Down, 90 Degree Turn and Rotation did not exhibit the most severe Longitudinal, Transverse or Vertical accelerations when compared to the Start and Stop and Long Run Motion Cases. For this reason, the results from the Start and Stop and Long Run Motion Cases were recommended for development of the design specifications.

In general, maximum accelerations occurred during the 15 Tons load case. This was likely due to the higher velocities achievable with lower loads, the ability of the SPMT to stop and change in center of rotation of the SPMT and power pack. The operator also expressed some concern at breaking the SPMT hydraulics at higher loads which may have affected the maximum accelerations at the 100 Tons load.

From the data presented above and in the time history plots of the data the following conclusions can be made:

- Maximum horizontal accelerations (Longitudinal and Transverse) are always controlled by the longitudinal acceleration. Transverse accelerations had significantly

lower values in all motion and load cases. For this reason, the longitudinal accelerations are used the following sections for design in both horizontal directions.

- The Start and Stop and Long Run Motion Cases are most critical for design.
- The maximum horizontal (longitudinal) acceleration (0.34g) was recorded during the Start and Stop motion case in all load cases and is recommended for the development of the design procedure.
- The maximum vertical acceleration was recorded during Start and Stop motion case, but the Long Run Motion Case is considered controlling for vertical accelerations because of the way a system of SPMTs would behave during a bridge move.
- The maximum vertical acceleration during the Long Run Motion Case was 0.57g and is recommended for development of the design procedure outlined in the following chapter.

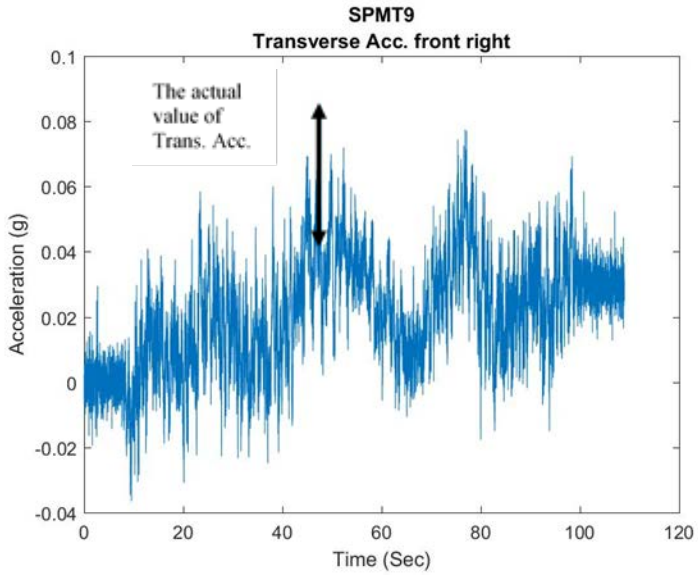

Figure 4.1. Time history for maximum transverse acceleration for Cluster 1 with 100 Tons load case

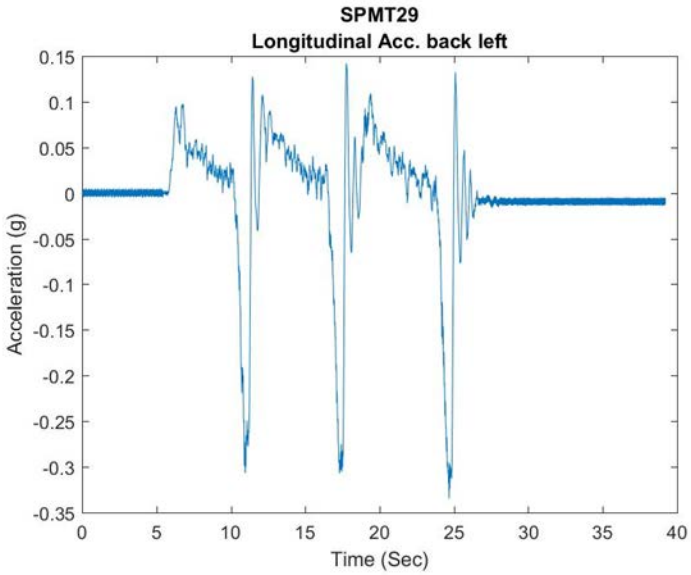

Figure 4.2. SPMT29 acceleration time history, Cluster 1, longitudinal acceleration absolute maximum

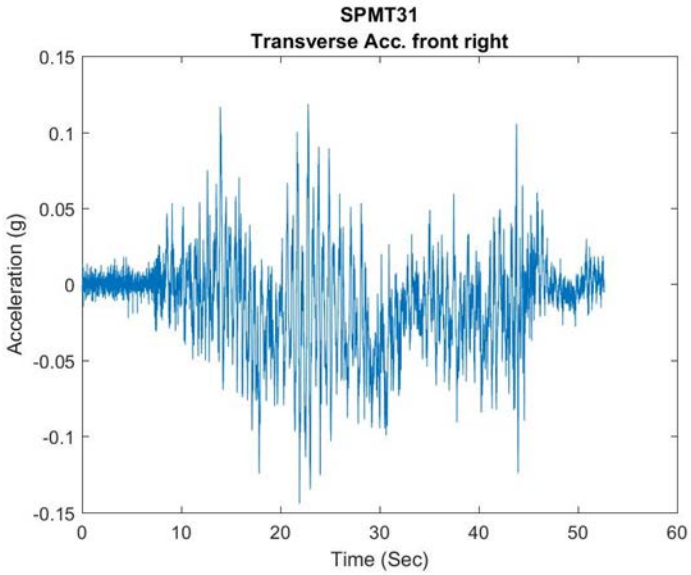

Figure 4.3. SPMT31 acceleration time history, Cluster 1, transverse acceleration absolute maximum

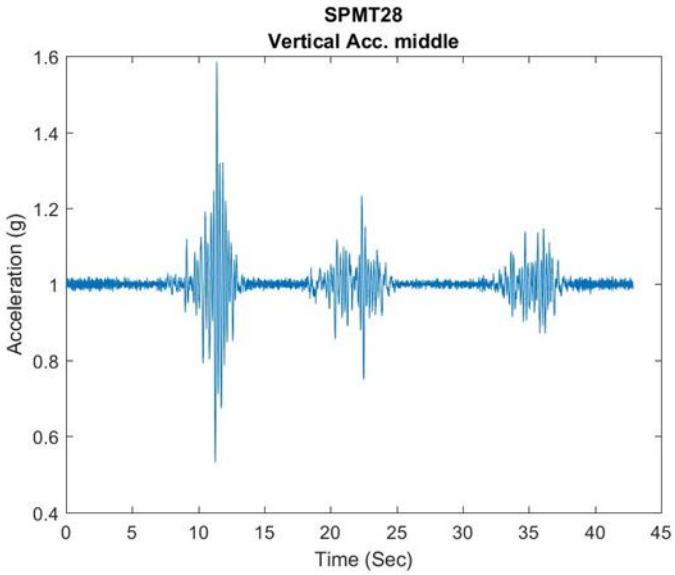

Figure 4.4. SPMT28 acceleration time history, Cluster 2, maximum vertical acceleration from start and stop motion case

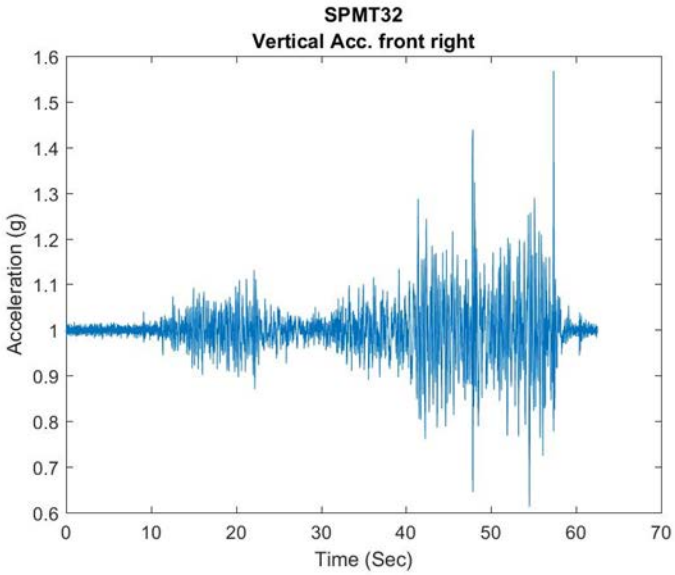

Figure 4.5. SPMT32 acceleration time history, Cluster 1, maximum vertical acceleration from long run motion case

Chapter 5: Response Spectra

For design purposes, the time history accelerations presented in the previous section and Appendix B, are difficult to use. For this reason, response spectra were generated in this chapter using single degree of freedom assumptions similar to those already used for AASHTO LRFD earthquake design. The assumed single degree of freedom (SDOF) system uses the platform accelerations as a dynamic problem with base excitation (Figure 5.1). Therefore, the following differential equation needs to be solved to get the dynamic response of the system (falsework and bridge).

$$\ddot{u} + 2\zeta\omega\dot{u} + \omega^2 u = -\ddot{u}_p \quad (1)$$

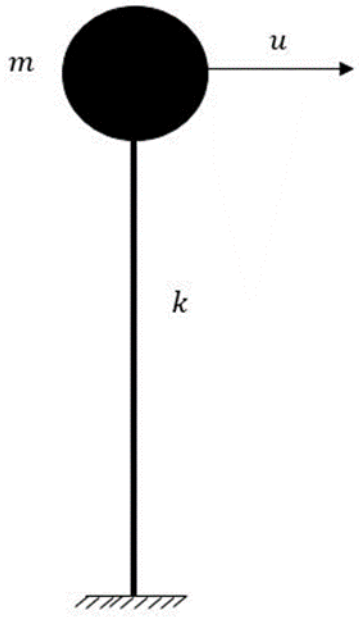

Figure 5.1. SDOF system

Where $u, \dot{u}, \ddot{u},$ and $\ddot{u}_p$ are the displacement of the system, velocity of the system, acceleration of the system, and the platform acceleration, respectively, at any time interval of the

experiment. The value $\zeta \; and \; \omega$ are the damping ratio of the system and the natural frequency of the system, respectively.

Platform accelerations ($\ddot{u}_p$) are the measured time history graphs for each motion case in each load case. To solve equation (1), the Newmark-beta method (Chopra,1995) was used. This method assumes a constant acceleration at each time history interval of the time history (0.01 s). Damping ratio, ζ, and the natural frequency ω are assumed deterministic. For SPMT and the falsework, the damping ratio $\zeta = 0.02$ was selected. The period of the system ($2\pi/\omega$) was analyzed between 0.02 second and 4 second increasing with 0.01 second time-steps. The pseudo acceleration response history of each time history for each period is then calculated and the maximum value of pseudo acceleration in each period was determined and plotted versus period to obtain the response spectra graphs presented below.

Spectrum for Vertical Direction

The Long Run Motion Cases were selected to obtain the spectrum graphs in vertical direction as they were deemed most critical for vertical vibrations. The Long Run motion cases were carried out twice for each load case with three vertically oriented accelerometers, therefore six spectrum graphs were obtained.

The response spectra accelerations were significantly affected by the operator during each incident, for instance, the breaking and turning speeds, as well as the terrain. Thus, a composite mean acceleration spectra and mean acceleration plus one standard deviation of the spectra have also been calculated. In the following response spectra, the mean graph (labeled as μ) provides a proper estimation of the imposed accelerations to the SPMT during the transportation. For

spectrum graphs to cover most of the Long Run Motion Cases, the mean plus one standard deviation graph (labeled as $\mu + \sigma$) is plotted.

Figure 5.2 presents all vertical spectrum graphs for the 15 Tons load case with grey dashed lines. The μ graph and the $\mu + \sigma$ composites are also presented with solid black and gray lines, respectively. The maximum pseudo acceleration at the minimum period (0.01second) is consistent with the peak platform acceleration (PPA) at each load case. The estimated PPA for 15 Ton Load Case in the $\mu + \sigma$ composite is approximately 0.85g. As shown in Figure 5.2, the period at the maximum pseudo acceleration is at a period of 0.26 second with the maximum vertical acceleration of 2.3g. Also after the period of 1.5 second, the graph levels out considerably. The maximum acceleration and the period of the maximum acceleration are thought to be highly dependent on the roughness of the terrain and behavior of the operator, and therefore, highly variable.

Figure 5.3 presents all vertical spectrum graphs for the 50 Tons Load Case with grey dashed lines. The μ graph and the $\mu + \sigma$ composites are also presented with solid black and gray lines, respectively. The estimated PPA for 50 Tons Load Case in the $\mu + \sigma$ composite is approximately 0.19g. The maximum pseudo acceleration occurs at a period of 0.28 second with a pseudo acceleration of 1.07g. After this point, the graph begins to level off and is near zero after 2.5 second.

Figure 5.4 presents all vertical spectrum graphs for the 100 Tons Load Case. The μ graph and the $\mu + \sigma$ composites are also presented with solid black and gray lines, respectively. The estimated PPA for the 100 Tons Load Case in the $\mu + \sigma$ composite is approximately 0.21g. The maximum pseudo acceleration occurs at a period of 0.36 second with a pseudo acceleration of 0.62g. After this point, similar to Figure 5.3 and Figure 5.4, the pseudo acceleration drops to near zero after the period of 2.5 second.

Clearly, the maximum pseudo accelerations decrease significantly as the SPMT load increases. Furthermore, it seems as the payload increases, the period of the maximum pseudo acceleration response increases. This implies pseudo accelerations have a dependence on SPMT velocity and it was noticed that maximum attainable velocity during the Long Run Motion Case decreased with increased SPMT load because the terrain was essentially unchanged from iteration to iteration. Exact velocities were not measured, but maximum velocities were estimated at approximately 4 mph (fast walk) during the Long Run Motion Case, but slightly decreased between the 15 Tons to 50 Tons to 100 Tons Load Cases.

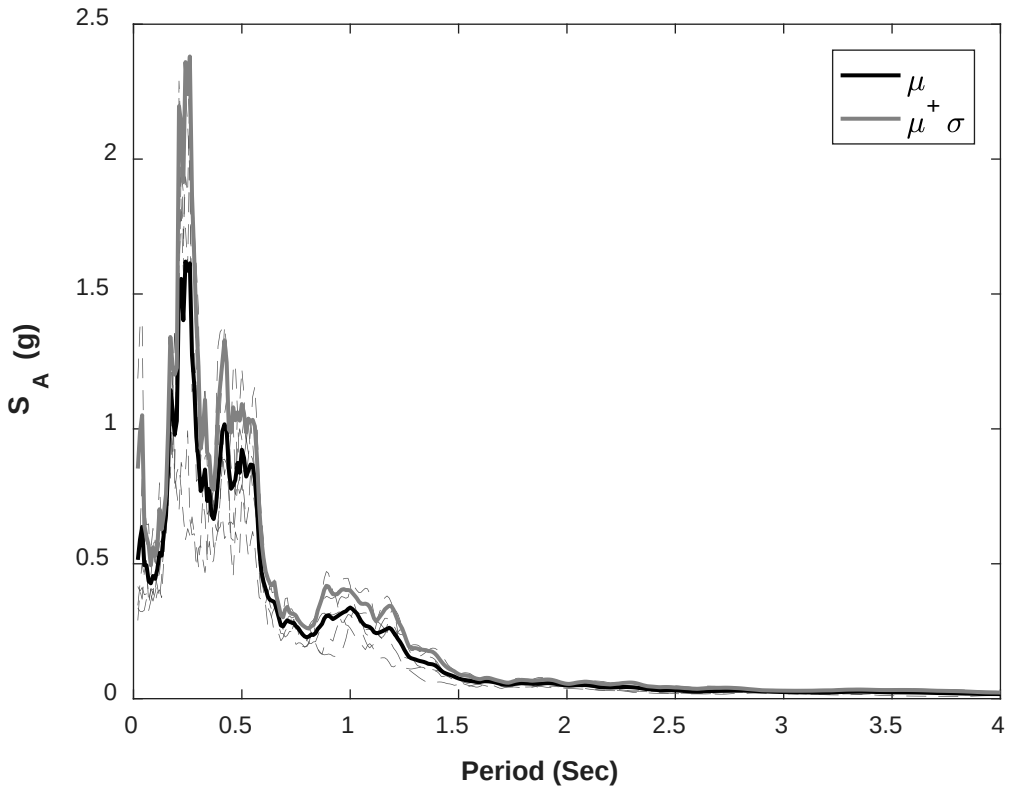

Figure 5.2. Response spectra mean and mean plus standard deviation for vertical accelerations, 15 Tons

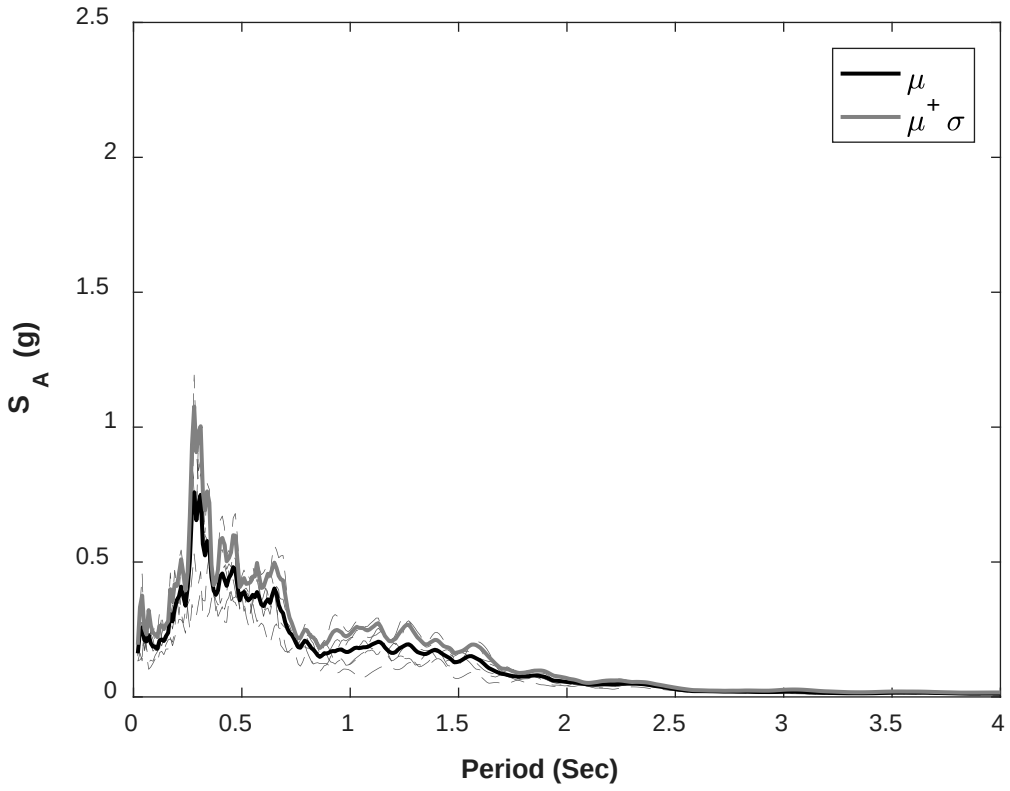

Figure 5.3. Response spectra mean and mean plus standard deviation for vertical accelerations, 50 Tons

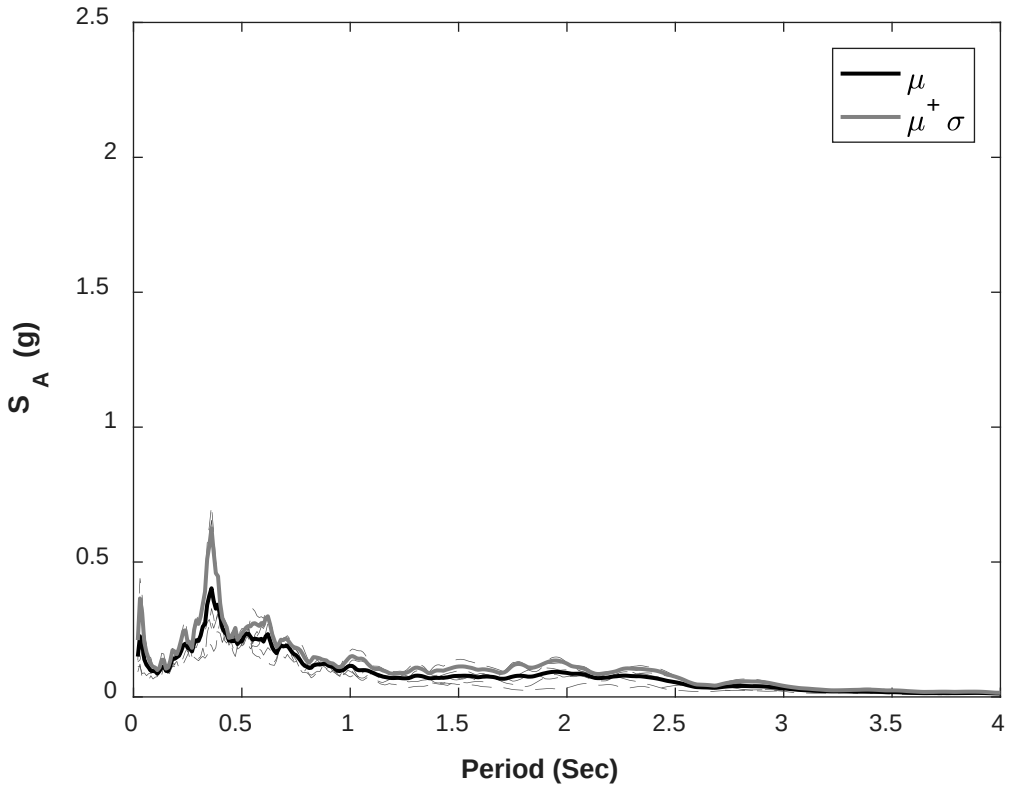

Figure 5.4. Response spectra mean and mean plus standard deviation for vertical accelerations, 100 Tons

Spectrum for Horizontal Direction

The Start and Stop Motion Cases were selected to obtain the spectrum graphs in horizontal direction because they were deemed most critical for horizontal impact and vibrations. The Start and Stop Motion Cases included three instances of starts and stops (see Figure 4.2). To prevent interaction between Starts and Stops in the analysis, which would not mimic real life actions, the time histories were broken up and each Start and Stop instance was treated as a new time history to calculate the corresponding spectrum. The "Start and Stop" motion cases were carried out four times for each load case. There were three accelerometers measuring horizontal accelerations in

each experiment therefore there were 36 total acceleration time histories for each load case, and therefore, 36 unique response spectra can be obtained.

As with the vertical acceleration time histories, the response spectra accelerations are significantly affected by the operator during each incident, who applied various degrees of breaking as evidenced by the time histories in Figure 4.2 and Appendix B. To account for this variability, while remaining aware of realistic emergency stop scenarios, a composite μ spectra and $\mu + \sigma$ spectra have also been calculated.

Figure 5.5 presents the horizontal spectra for the 15 Tons Load Case. The μ spectra and $\mu + \sigma$ spectra are also presented with solid black gray lines, respectively. The estimated PPA for the 15 Tons Load Case in the $\mu + \sigma$ spectrum is approximately 0.34g. The period of the maximum pseudo acceleration is at a period of 0.57 seconds with an acceleration of 0.6g. After this peak, the resulting spectral accelerations decrease almost linearly, but not as dramatically as seen in previous graphs, indicating significant response across all structure periods considered. The maximum acceleration and the period of the maximum acceleration are highly dependent on the duration of the Start and Stop impulse, as well as the peak value. It is reasonable that a short duration pulse will excite stiffer structures more and a slower stop would excite a more flexible structure.

Figure 5.6 presents the horizontal spectra for the 50 Tons Load Case. The μ spectra and $\mu + \sigma$ spectra are also presented with solid black and gray lines, respectively. The estimated PPA for the $\mu + \sigma$ spectrum is 0.24g. The period of the maximum pseudo acceleration is at a period of 0.71 seconds with a maximum horizontal pseudo acceleration of 0.47g. Similar to the 15 Tons spectra, after the maximum point, there is a nearly linear acceleration decrease, differing considerably from the vertical spectra in the previous section.

Figure 5.7 presents the horizontal spectra for the 100 Tons Load Case. The μ spectra and μ + σ spectra are also presented with solid black and gray lines, respectively. The estimated PPA for the μ + σ spectrum is 0.18g, considerably lower than the 15 Tons and 50 Tons Load Cases. The maximum pseudo acceleration occurs at a period of 0.86 seconds with a pseudo acceleration of 0.32g, also considerably lower than the 15 Tons and 50 Tons Load Cases.

As with the vertical spectra, the maximum pseudo accelerations decrease significantly as the SPMT load increases. Furthermore, as the payload increases, the period of the maximum pseudo acceleration response increases. Because of the significant motion case differences, the horizontal accelerations are thought to be more of a function of the deceleration rather than maximum velocity. Consider that, if the operator imposes maximum breaking force, as in a worst case emergency stop, the deceleration rate will be constant (limited by the hydraulics, payload and operator capability) as the vehicle comes to a stop. It is clear from the observed variability in the Start and Stop Motion Case acceleration time histories (see Appendix B) that the operator, even when trying, cannot apply the same maximum deceleration. For this reason the μ + σ composite spectra are considered adequate for development of design spectra.

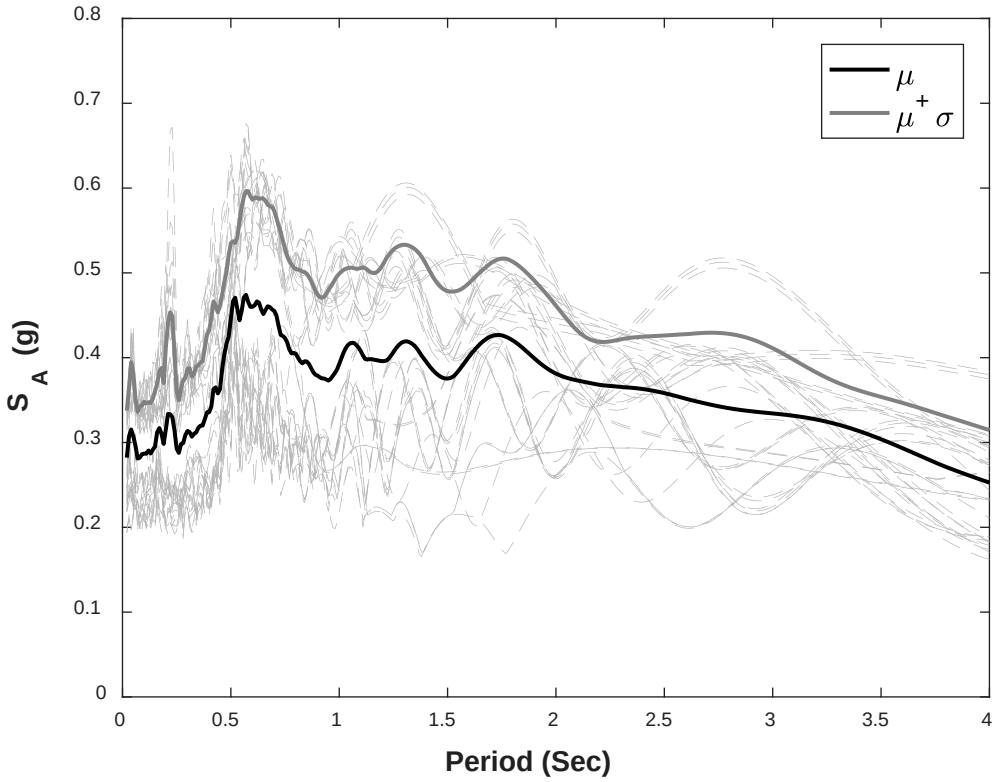

Figure 5.5. Response spectra mean and mean plus standard deviation for horizontal accelerations, 15 Tons

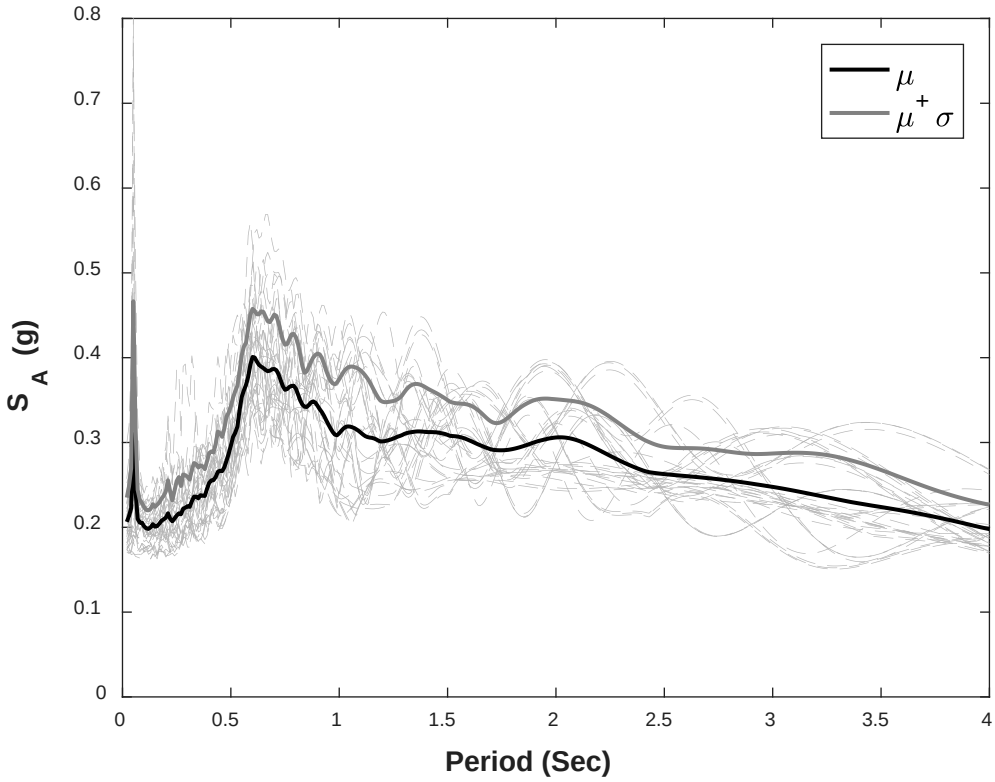

Figure 5.6. Response spectra mean and mean plus standard deviation for horizontal accelerations, 50 Tons

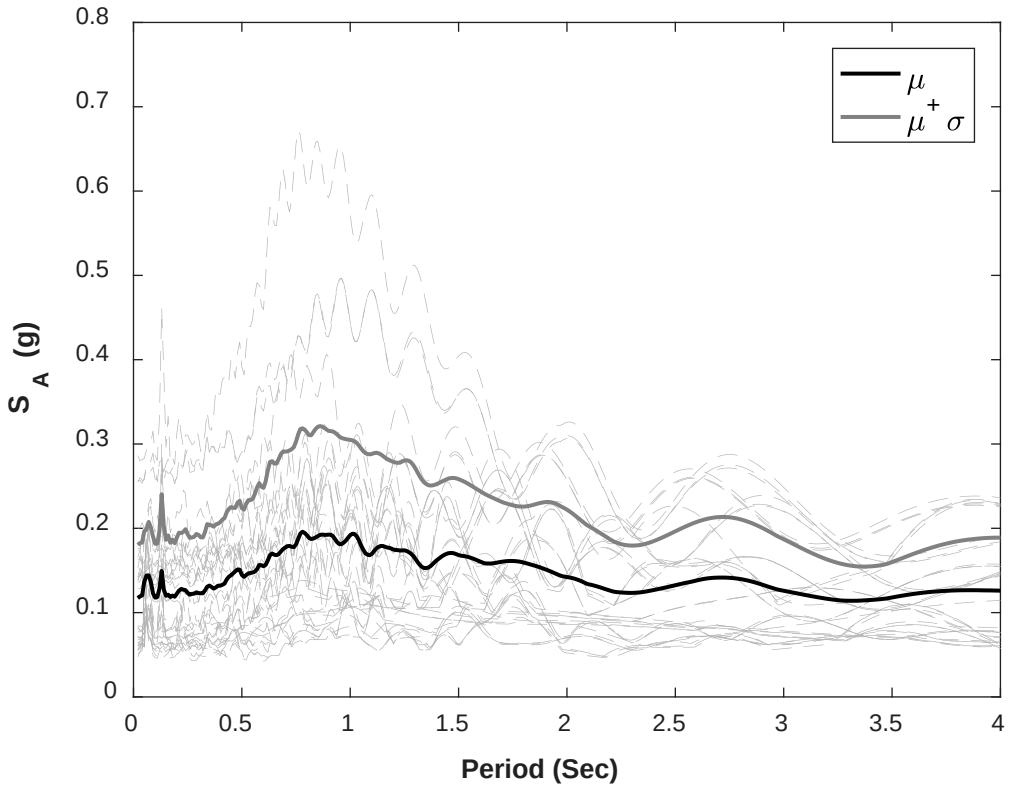

Figure 5.7. Response spectra mean and mean plus standard deviation for horizontal accelerations, 100 Tons

Chapter 6: Design Spectra Development and Recommendations

The spectra plots developed in the previous chapter were based on individual load cases and motion cases. For design purposes, the spectra need to be generalized based on the payload relationship. This section presents the methodology for developing the Vertical and Horizontal Design Spectra.

Vertical Design Spectra

The vertical design assumptions are that of rigid falsework and flexible bridge. When the SPMT and the cargo is subjected to vertical acceleration, the platform transmits the vibration through rigid diaphragms and connections to the bridge. Therefore, assuming a rigid false work during the vertical bouncing is realistic and the PPA for vertical accelerations (PPAV) can be used for falsework design and the spectral acceleration (SAmax) is used to determine the dead load amplification on the bridge structure.

The PPAV for each load case are plotted in Figure 18 including a best fit exponential curve suitable for design. The proposed design equation for the PPAV based on the percent of SPMT capacity (C) is as follows:

$$PPA_V = 0.7533e^{-0.03C} \quad (2)$$

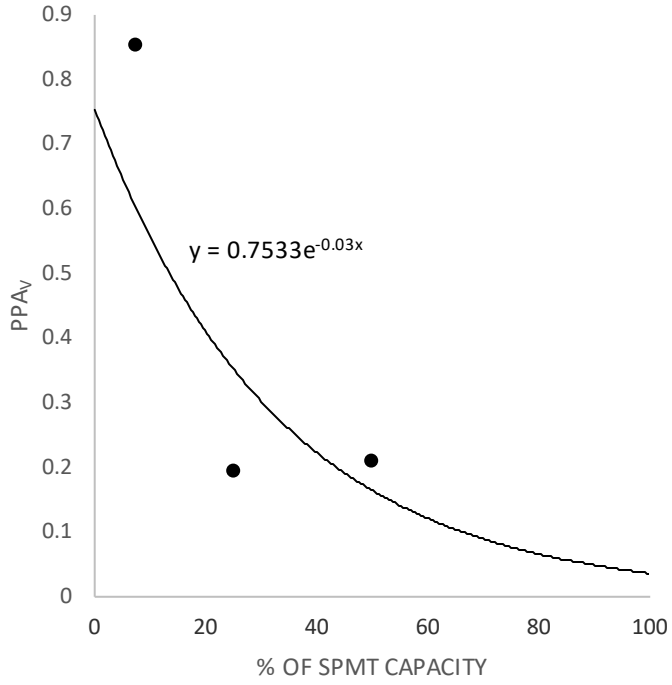

Figure 6.1. PPAV versus % SPMT capacity

To generate the design spectrum for vertical acceleration, the design spectral acceleration (S_{Amax}) is calculated using following equation:

$$S_{Amax} = \begin{cases} 3 \times PPA_V & 0 \le T_n \le T_1 \\ 3\left(\frac{T_1}{T_n}\right) PPA_V & T_n > T_1 \end{cases} \quad (3)$$

Where T_1 is equal to 0.5 second and T_n is the nominal period of the to be analyzed structure. The shape of S_{Amax} is provided in Figure 6.2. The spectral acceleration is only a function of PPAv and the period of the structure.

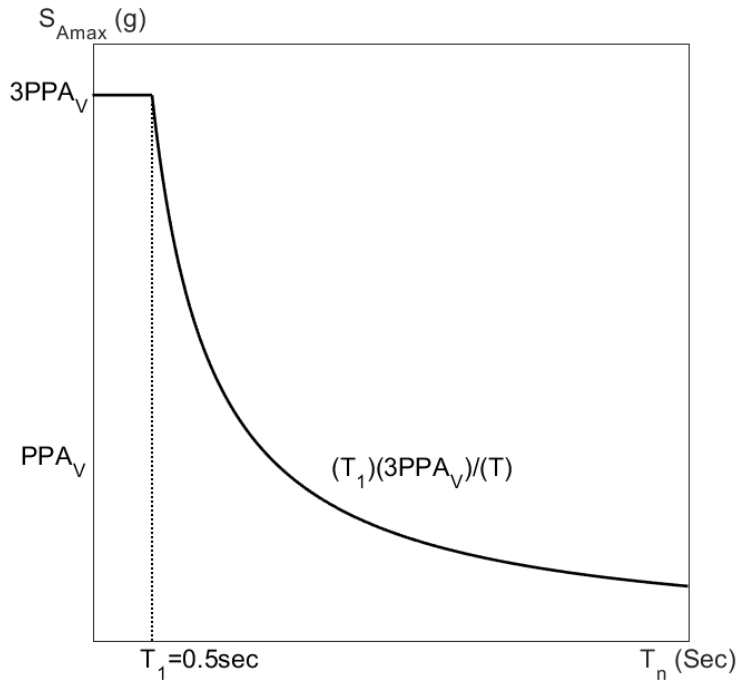

Figure 6.2. Vertical acceleration design spectrum

For comparison purposes Figure 6.3 through Figure 6.5 present the Vertical Design Spectrum overlaid on the computed time history spectra, the $\mu + \sigma$ composite spectrum developed in the previous sections, for each load case. Notice that the ramp up from zero period to $3PPA_V$ is neglected for the design spectrum for simplicity and to discourage designers from underestimating the period of the structure to obtain lower loading.

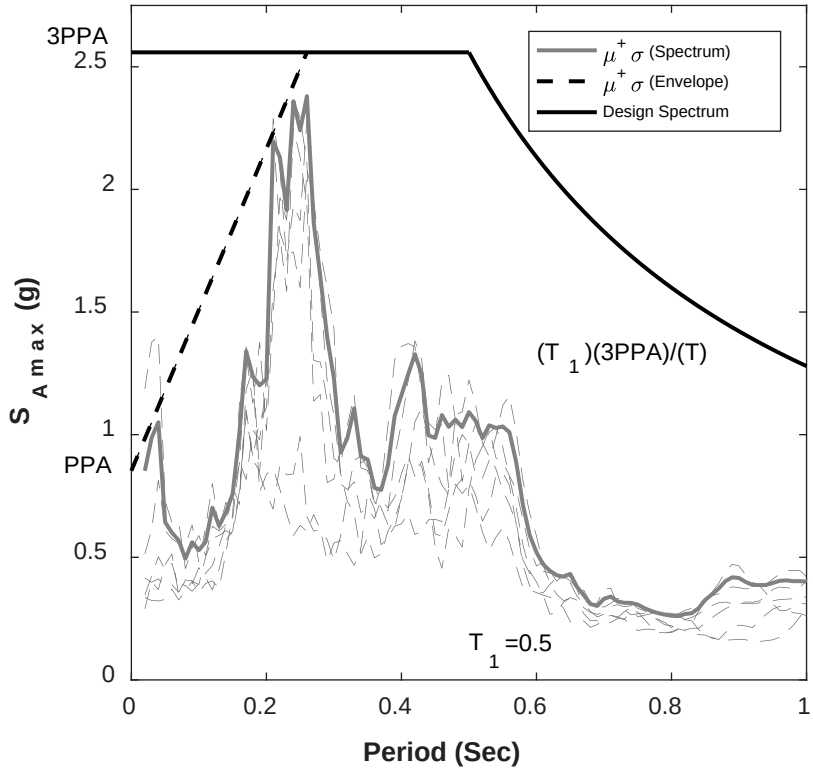

Figure 6.3. Design spectrum for vertical acceleration on light load case spectrums, with dash gray lines as spectrum for each critical vertical time history, solid gray line as $\mu+\sigma$ composite of all spectrum, dash black line as $\mu+\sigma$ envelope, and solid black line as the vertical design spectrum.

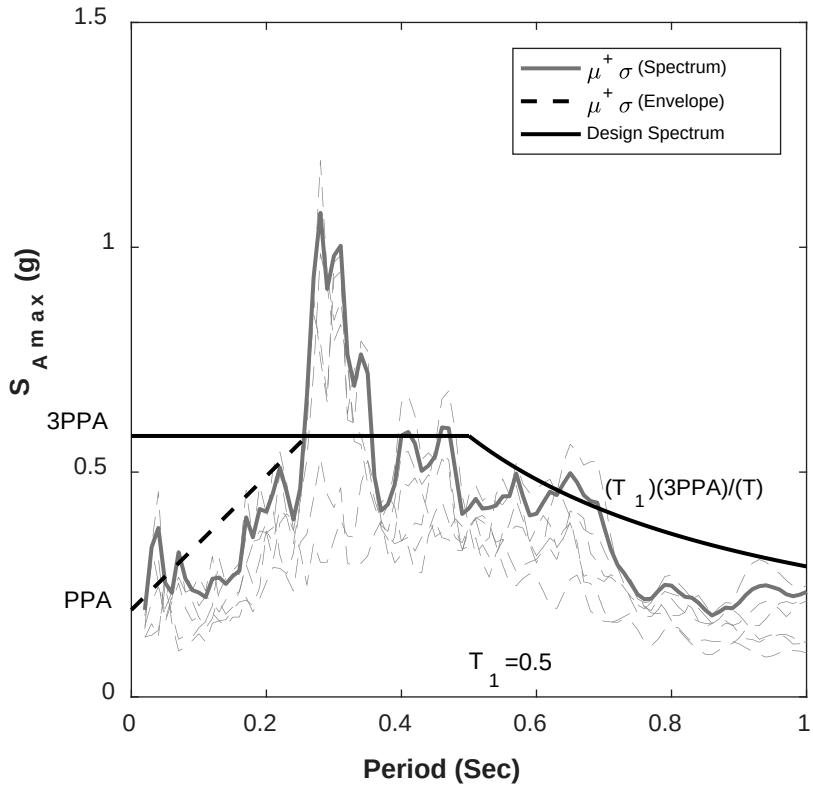

Figure 6.4. Design spectrum for vertical acceleration on medium load case spectrums, with dash gray lines as spectrum for each critical vertical time history, solid gray line as $\mu+\sigma$ composite of all spectrum, dash black line as $\mu+\sigma$ envelope, and solid black line as the vertical design spectrum.

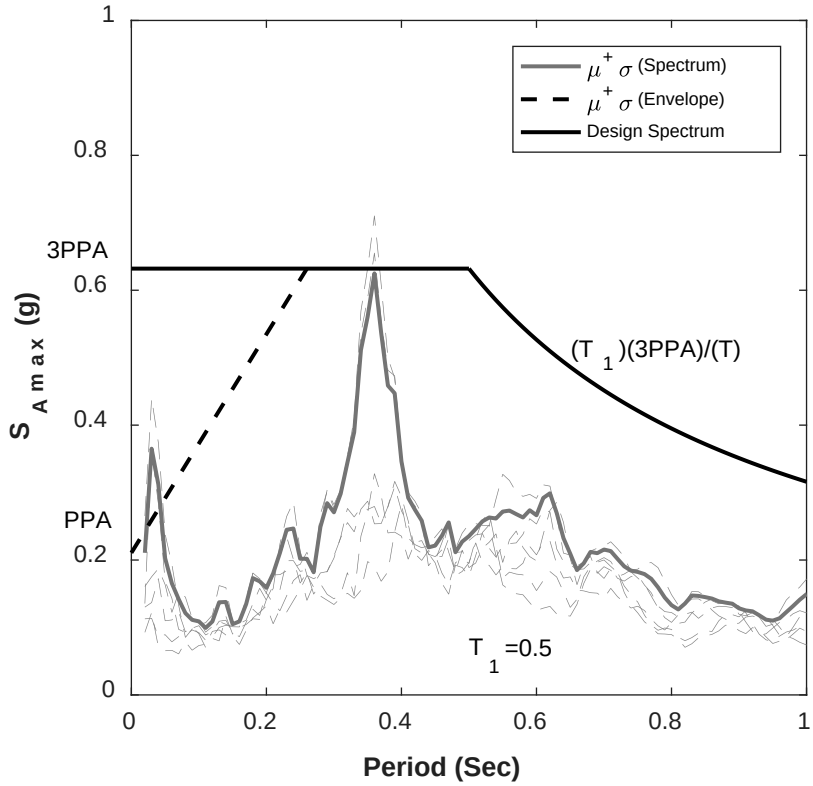

Figure 6.5. Design spectrum for vertical acceleration on heavy load case spectrums, with dash gray lines as spectrum for each critical vertical time history, solid gray line as $\mu+\sigma$ composite of all spectrum, dash black line as $\mu+\sigma$ envelope, and solid black line as the vertical design spectrum.

As discussed previously, the value of PPA_V is dependent on the velocity of the SPMT. Because the vertical accelerations are caused by the roughness of the driven surface, this is a reasonable assumption. If the driving surface was assumed to be a sine wave displacement excitation or any other periodic excitation (see Figure 6.6.), then the displacement due to the sine wave can be expressed in following equation:

$$u(t) = Dsin\left(\frac{2\pi}{T}t\right) \tag{4}$$

Where D is the amplitude of the roadway roughness, T is the period of the sine wave function and $\boldsymbol{t}$ is time. Then the velocity V, and acceleration A, are first and second derivative of equation (4):

$$V(t) = D\left(\frac{2\pi}{T}\right)cos\left(\frac{2\pi}{T}t\right) \tag{5}$$

$$A(t) = -D\left(\frac{2\pi}{T}\right)^2 sin\left(\frac{2\pi}{T}t\right) = \left(\frac{2\pi}{T}\right)^2 u(t) \tag{6}$$

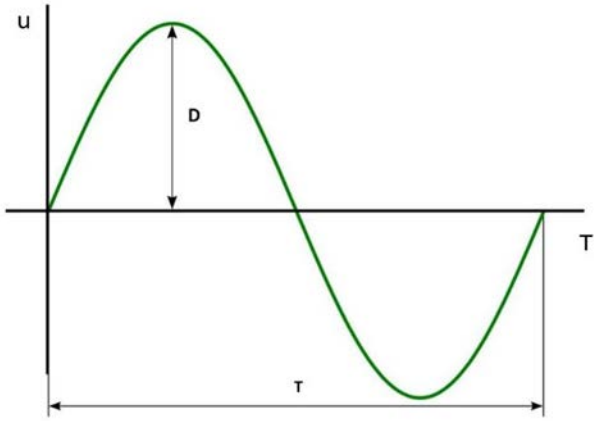

Figure 6.6. The sine wave excitation

Therefore, a change in velocity would affect the acceleration by the power of two. In other words, if the vertical acceleration measured at velocity of V is equal to A, then the vertical acceleration at $V/2$ would be equal to $A/4$.

During the Long Run Load Case, the SPMT speed was estimated at 4 mph, or a fast walk, however, functionally, this is unlikely in practice where it is likely limited to 2.5 mph. Using this information, the design accelerations can be modified in the proposed specification. This is handled using by using a load reduction factor of (2.5 mph/4 mph)^2 = 0.4 to account for service limit state and a worst case 1.0 for the ultimate limit state.

Horizontal Design Spectra

The horizontal design assumption is that of a rigid bridge/cargo (i.e., rigid diaphragm action) and flexible falsework. When the SPMT is subjected to the horizontal deceleration, the platform transmits the impulse through the falsework and into the bridge which will be minimally affected by the horizontal decelerations. Therefore, the critical design case for horizontal accelerations is the falsework and the S_{Amax} for the horizontal direction, outlined below, should be used.

The PPA for horizontal accelerations (PPA_H) for each Load Case are presented in Figure 6.7 and include the best fit exponential approximation proposed for design. The proposed design equation for the PPAH, based on the percent of SPMT capacity is as follows:

$$PPA_H = 0.3615e^{-0.014C} \quad (7)$$

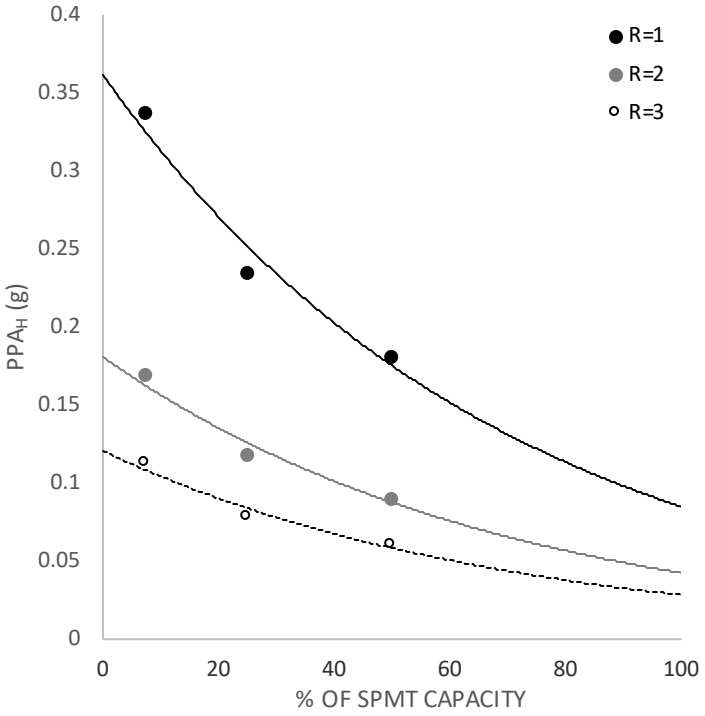

Figure 6.7. The PPA for horizontal accelerations as a function of SPMT capacity

To generate the design spectrum for horizontal acceleration, presented in Figure 6.8, PPA_H is obtained from equation (7) and equation (8) is used:

$$S_{Amax} = \begin{cases} 2 \times PPA_H & 0 \le T_n \le T_1 \\ 2\left(\frac{T_1}{T_n}\right) PPA_H & T_n > T_1 \end{cases} \quad (8)$$

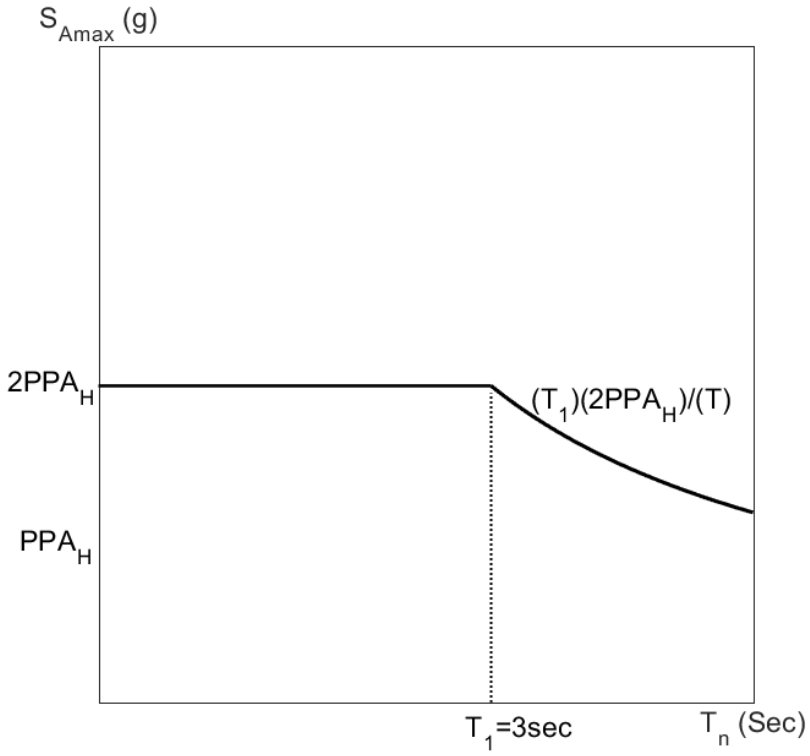

Figure 6.8. Design spectrum for horizontal acceleration, with dash gray lines as spectrum for each critical vertical time history, solid gray line as $\mu+\sigma$ composite of all spectrum, dash black line as $\mu+\sigma$ envelope, and solid black line as the vertical design spectrum.

For comparison purposes, Figure 6.9 through Figure 6.11 present the Horizontal Design Spectrum overlaid on the computed time history spectra and the $\mu + \sigma$ composite spectrum developed in the previous chapters, for each load case. Notice that the ramp up from zero period to $2PPA_V$ is neglected for the design spectrum for simplicity and to discourage designers from underestimating the period of the structure to obtain lower loading.

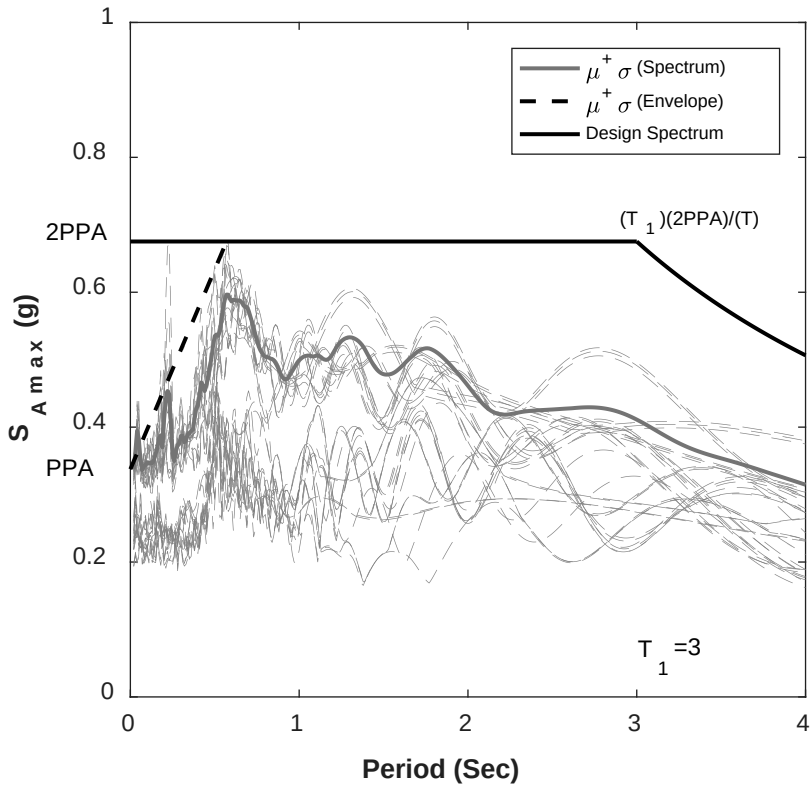

Figure 6.9. Design spectrum for horizontal acceleration on light load case spectrums, with dash gray lines as spectrum for each critical horizontal time history, solid gray line as $\mu+\sigma$ composite of all spectrum, dash black line as $\mu+\sigma$ envelope, and solid black line as the vertical design spectrum.

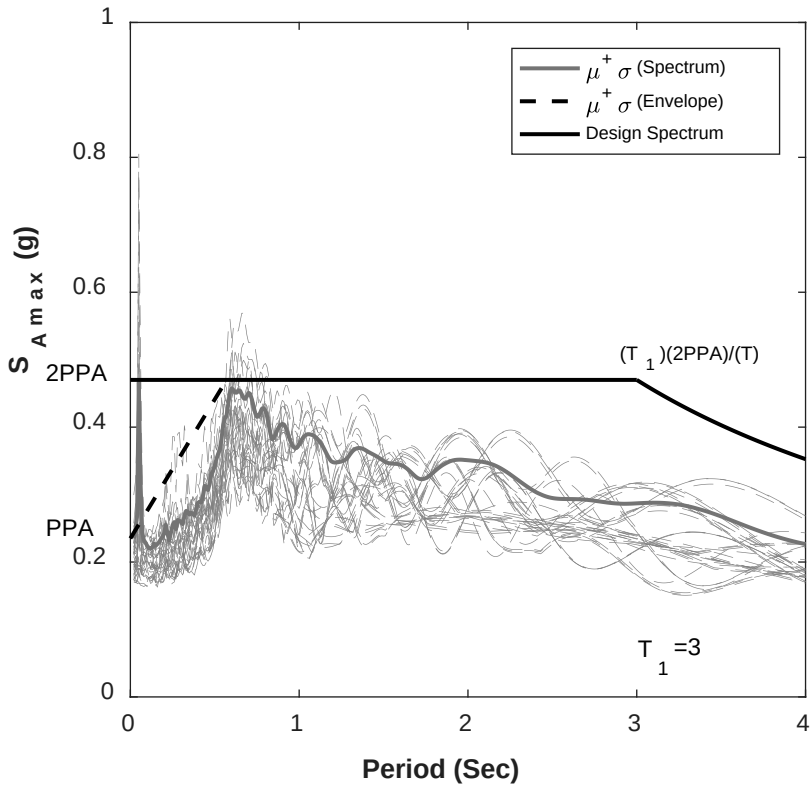

Figure 6.10. Design spectrum for horizontal acceleration on medium load case spectrums, with dash gray lines as spectrum for each critical horizontal time history, solid gray line as $\mu+\sigma$ composite of all spectrum, dash black line as $\mu+\sigma$ envelope, and solid black line as the vertical design spectrum.

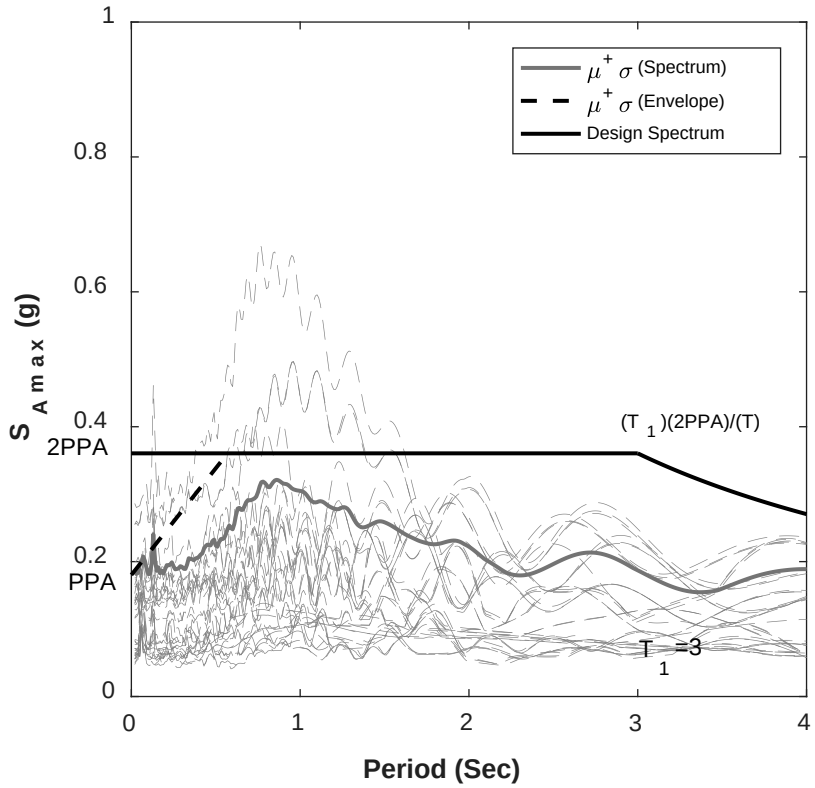

Figure 6.11. Design spectrum for horizontal acceleration on heavy load case spectrums, with dash gray lines as spectrum for each critical horizontal time history, solid gray line as $\mu+\sigma$ composite of all spectrum, dash black line as $\mu+\sigma$ envelope, and solid black line as the vertical design spectrum.

Justification for reducing the vertical acerbations for the service limit states was presented in the previous chapter. However, for the horizontal case, a similar justification cannot be made. Furthermore, since the horizontal accelerations apply mostly to the falsework, which is a temporary structure, some level of damage is considered acceptable. For this reason, the falsework designer shall be allowed to use the response modification ratio (R) to modify the equation (8). It is recommended that if the bridge supports have limited ductility (rigid) use $R = 2$ and if the bridge supports have medium ductility (semi rigid) use $R = 3$. For the case of very rigid connections

directly to the SPMT platform designers are encouraged to use $R = 1$. Demonstration of how to use the R values is presented in Figure 6.7..

Part Two: Friction Values for Slide-In Bridge

Chapter 7: Introduction

Advancements are being made which are altering the typical methods of standard bridge construction. Innovative ideas are improving the planning process, the design process, the materials used, and construction methods, to reduce construction time for new bridges as well as bridges being replaced. These developing methods are categorized under what is known as Accelerated Bridge Construction (ABC). With ever growing traffic demands on today's roads and bridges, the need to reduce construction time, particularly for bridge replacements, is of high importance and can have significant impacts for the general public. One of these ABC methods is called Slide-In Bridge Construction (SIBC).

Slide-In Bridge Construction can be very useful when an existing bridge is in need of replacement. Slide-In Bridge Construction is a method that is used to replace existing bridges. The superstructure for the new bridge is constructed adjacent to the existing bridge so that during construction of the new bridge, the old one can continue to be in service. The replacement bridge is built or assembled on top of tracks used to slide the structure into place once the old one is removed. Typical bridge replacements can shut down traffic for anywhere from a couple of months to over a year. SIBC on the other hand, generally allows the road to be open to traffic during the full construction period other than for a couple days or weeks.

The method used to slide the bridge on the sliding track and into place, typically uses sliding bridge bearings that have two flat sliding surfaces which have low coefficient of friction (COF) values when used together. The surfaces used for the sliding bearings include a polymer called polytetrafluoroethylene (PTFE) and stainless steel. PTFE is most commonly known and

recognized as Teflon which is DuPont's trademark name for PTFE. Since Teflon is a trademark name, PTFE is the proper name that will be used when referring to this material.

The use of PTFE and Stainless Steel interfaces in bridge bearings has been a common practice since around the 1960's. These applications have mainly been for bearings that are designed to reduce stresses that are induced in the bridge structures due to things like thermal expansion and contraction, seismic activity, dynamic loading from traffic, and more. Each of these requires more of a long term bearing, whereas using the bearings for SIBC is a short term use. The need to study how these bearings could be used for SIBC was necessary in order to develop appropriate specifications for SIBC.

The main goal in using these bridge bearings is to reduce the amount of force required to push or pull the bridge across the slide track and into its final resting place. This force is governed by the amount of friction between the sliding surfaces which resists the bridge from moving. The amount of friction varies depending on many different parameters. The research team chose to investigate the effect of four parameters that were believed to have significant influence on the COF values. This was based on results from past studies by other researchers using PTFE-Stainless Steel interfaces (Stanton 2010). The parameters chosen to investigate are the following:

(1) Surface Roughness of the mating material which the PTFE slides on,

(2) Lubrication used between PTFE and the mating surface (e.g. stainless steel),

(3) Sliding Speed of the bridge during as it is being pushed into place, and

(4) Contact Pressure - determined by ratio of bridge weight to PTFE contact area.

Details of how each of these parameters were varied, results were obtained, and conclusions made from the findings, are discussed in detail in the following chapters. The project was not a comprehensive research project on all of the possible parameters that influence the COF

for PTFE-Stainless Steel bridge bearings, but there were some important discoveries found in regards to the four parameters that were researched. These findings are being used in the development of new guidelines and specifications by the Federal Highway Administration for SIBC practices.

Chapter 8 provides a literature review on the subject. Chapter 9 illustrates the materials and test parameters. The tests setup and procedures are demonstrated in Chapter 10. In Chapter 11, the results of the tests are provided in Chapter 12 the results are discussed.

Chapter 8: Literature Review

Along with SPMT bridge moves and conventional crane moves, the scan team that went to Japan and Europe mentioned above also found that the countries they visited also used the following methods to move bridge structures: horizontal skidding or sliding, incremental launching, floating bridges into place, rotating or pivoting into place, and vertically lifting bridges.

Any of these methods that requires skidding or sliding involves overcoming friction forces which can be pretty high. Lateral slides, also known as horizontal slides, consist of building the bridge superstructure on temporary piers next to the current bridge it will replace, and then sliding it into place once the old one has been removed. According to the Wisconsin DOT Bridge Manual "One common method is to push the bridge using hydraulic rams as the bridge slides on a smooth surface and Teflon coated elastomeric bearing pads. Other methods have also been used, such as using rollers instead of sliding pads, and winches in place of a hydraulic ram" (Wisconsin DOT, 2013). The Strategic Highway Research Program 2 (SHRP2) has created an addendum to the Innovative Bridge Designs for Rapid Renewal: ABC Toolkit on Lateral Slides. It talks about applicability of using the method, design considerations, and key components when implementing a bridge slide (SHRP2, 2013). It also discusses the different types of sliding bearings that can be used: rollers, slide shoes, and slide plates. Typically, Teflon (PTFE) and stainless steel are used on the contact surfaces to reduce friction. Sometimes even lubricants like dish soap are used to reduce the friction (SHRP2, 2013).

FHWA had an implementation guide for Slide-In Bridge Construction (SIBC) developed. UDOT and the Michael Baker Corporation are the authors of the guide (FHWA, 2013). SIBC is an ABC technology where the new bridge structure is built adjacent and parallel with the current bridge and then once it is complete, it is slid into place. This method reduces traffic disruption by

greatly reducing the duration that the traffic needs to be altered. The traffic can continue as normal as the new structure is being built, and then rerouted for a short time while the bridge slide occurs. The duration that the traffic is closed during the move is generally anywhere from overnight to a week or more. Often this is done on a weekend or at other times when the traffic demand is low. The SIBC guide was designed to demonstrate the advantages of using SIBC and show how it can be implemented by state and local agencies (FHWA, 2013). To date, this is the most thorough guide that has been developed in the United States for Slide-In Bridge Construction. Figure 8.1 shows a bridge project on I-80 in Utah where SIBC is used. Using this method for the pair of bridges at Echo road and I-80 eliminated the need for phased construction.

Figure 8.1. Bridge slide project in Utah (Source: FHWA Project #F-ST99(232))

The guide addresses many important aspects that are needed for owners, engineers, and contractors to make a decision on whether or not SIBC is the best approach for their project. It addresses the benefits and the limitations to SIBC, as well as possible savings and potential cost increases for SIBC projects. With some projects the savings will outweigh the extra costs. Sometimes a project will cost more to use SIBC than conventional construction but has such great benefits that are worth the extra cost. The guide also gives design considerations for the following: abutments, bridge superstructure, substructure reuse, temporary works and bridge slide system,

connections, and tolerances. There are different types of slide systems that can be used and the manual explains them and their advantages and disadvantages. There are industrial rollers that can be used, which can be a single big bearing, or multiple smaller bearings; or Teflon pads can be used. Both of these methods require some sort of guide or track that they can follow to direct the bridge the proper way. Both types of slide systems also need either jacks or winches to push or pull the bridge into place. These too are explained in the SIBC Implementation Guide and what the advantages/disadvantages are (FHWA, 2013).

Iowa DOT put together an Accelerated Bridge Construction workshop which was held August 11-12, 2008 in Des Moines, Iowa. The workshop brought together officials from Iowa DOT, many other state DOT's, Federal Highway Administration, National Steel Bridge Alliance, Iowa State University, local engineering consultants and contractors, and many other professionals who have been a part of ABC projects or research. The workshop was invitation only and had over 90 participants who went. Multiple presentations were given in order to bring all the participants up to date on ABC projects across the U.S. and current ABC methods. After several hours of presentations in the morning, groups were created to facilitate collaboration throughout the afternoon. During these workshops groups brainstormed on ideas of how ABC methods could be used, how to improve prefab design details, and then discussed opportunities and obstacles for their ideas. The groups also discussed research that needed to be done, needed policy changes, and areas where specifications could be developed. Ideas and methods were discussed for several of Iowa's upcoming bridge projects and what action could be taken to implement accelerated bridge construction on those projects (Iowa DOT, 2009).

In Dec of 2013 Michigan DOT (MDOT) also held an Accelerated Bridge Construction workshop. The workshop was organized and put together for reasons similar to the workshop that

Iowa DOT held. In 2008 prefabricated bridge elements were used for the first time in Michigan. Following the success of the project MDOT built several other bridges using the same method. MDOT wanted to expand the use of ABC techniques to incorporate bridge slides and the use of SPMTs in their projects. The purpose for the workshop was to leverage knowledge and experience about how they could use these innovative techniques for the design and construction of future Michigan bridges. Not only was the workshop set up to expand the knowledge of MDOT, but also for local agency engineers and Michigan's consulting, construction, and prefabrication industry. During the workshop there were presentations that were given on the following topics:

- Scoping, decision-making, planning, and cost
- Contracting
- Rapid demolition methods for ABC projects
- Structural analysis and design
- Structural move plans
- Contingency plans
- Construction
- Monitoring during moves
- Maintenance of traffic (MOT)
- Workforce management
- Observations and lessons learned.

Some of the things that were discussed for Bridge Slides were static and dynamic coefficients of friction and how MDOT would use the coefficients to select required jacking hydraulics to move the bridge. Often with slide-in systems, Teflon laminated neoprene steel reinforced pads are used on a track system. It is set up so that the Teflon surface is in contact with

stainless steel coated steel carriages to produce low friction coefficients. The group discussed lateral restraints that are needed to keep the bridge structure aligned as well as the complications of sliding a multi span structure. Figure 8.2 is a picture of Teflon (PTFE) pads being used for a bearing system.

Figure 8.2. Bridge slide using PTFE sliding bearings (Source: SHRP2 Renewal Project Ro4)

When discussing the implementation of SPMTs for moving bridge structures into place, the main thing that was considered was possible issues with the geotechnical aspect of the project. The geotechnical design should evaluate the loads that will be applied to it while the bridge is being transported on SPMTs and design accordingly. An approach for the SPMTs also needs to be carefully assessed. Another issue that was talked about was the bracing needed for the bridge structure while it was being transported. The workshop helped MDOT develop plans on how ABC would be used for future Michigan bridges (Aktan et al., 2014).

The Wisconsin Department of Transportation sponsored the University of Washington (UW) to conduct tests for determining coefficients of friction between several different stainless-steel finishes and a Teflon (PTFE) coated surface. Graduate student Josef C. Taylor and Professor John F. Stanton are the ones who carried out the research and authored the report Friction

Coefficients for Stainless Steel (PTFE) Teflon Bearings (Taylor and Stanton 2010). The purpose of the report is to provide the Wisconsin DOT with the results in a clear and straightforward way and to be implemented by the Bureau of Structures for bridge design.

Bearings used for bridge slides are often made with sheet Teflon (PTFE) and stainless steel polished to a #8 mirror finish. There are many different types of surface finishes for stainless steel. A #8 mirror finish is much smoother and glossier than a #2B rolled finish. AASHTO LRFD Design Specifications use a #8 finish which is the only type of finish that they provide values for. Since stainless steel polished to a #8 finish is more expensive and can be more difficult to obtain than other finishes, Wisconsin DOT had UW test #2B rolled finish and rough as-rolled finish stainless steel, and then compare the results to #8 polished Stainless steel. The report explains the most important parameters which cause friction to vary when using PTFE and stainless steel. They are surface finish, contact pressure, sliding speed slide path and temperature. The tests conducted in the study addressed all of those except for temperature because special equipment is required for low temperature testing (Taylor and Stanton 2010).

Most of the results they obtained produced expected results, but the slide path test produced consistently counter-intuitive results. The coefficient of friction for the #8 mirror finish increased as the slide path increased, whereas for the #2B rolled finish it stayed constant, and for the rough as-rolled finish it decreased. Based off of the tests that were conducted an equation was developed to help predict the friction coefficient as a function of the surface finish, the contact pressure, the sliding speed and the slide path. After all of the tests were done and the results analyzed they determined that stainless steel with a #2B surface finish is an appropriate alternative to a #8 mirror finish. However, it is important to note the tests did not analyze how temperature change effects

the coefficient of friction and that this was one of the important parameters that should be considered (Taylor and Stanton, 2010).

Another ABC method of constructing bridges is the Incremental Launching Method (ILM). This method is one that has been around for many years. There have been many Europe bridges that have been constructed using this method. In the past the use of ILM has not been used that much in the United States. However, it has been increasing in the U.S. as it can be a very effective way to build a bridge in areas with site restrictions such as deep valleys, water crossings or environmentally protected areas.

In 2007 a report was created titled Bridge Construction Practices Using Incremental Launching. The report was compiled at the request of AASHTO. It was prepared by Mike LaViolette of HNTB Corp., as well as the following individuals from The Bridge Engineering Center at Iowa State University: Terry Wipf, Yoon-Si Lee, Jake Bigelow and Brent Phares. The purpose for this work was to report available information about incremental launching method (ILM), applications of it, limitations and benefits. The group conducted a comprehensive literature review for ILM which is contained in the report. They also provided recommendations for bridge owners, designers and contractors regarding the best practices for planning, designing and construction techniques using ILM, and explain possible applications and limitations (LaViolette et al., 2007).

While replacing a bridge over the Iowa River, Iowa DOT implemented an incremental bridge launch for a girder bridge and monitored multiple parts of the substructure and superstructure during the launch, as seen in Figure 8.3, (Wipf et al., 2004). Some of the things they monitored were strain, deflection, tilt and load data. The bridge was erected in six full-span launches and data was collected for all of the launches. The data was used to monitor the flexural

behavior of the girders, contact stress between the girders and bridge roller bearings used to launch the bridge, global and local pier column behavior, and cross-frame force distribution and magnitudes.

Figure 8.3. Incremental bridge launch over Iowa River (courtesy of Iowa DOT)

When looking at the pier columns there were observed residual or "locked in" stresses built up at the end of the day. There were extremely large contact stresses measured on the bottom flange and web of some of the girders as they rolled over the temporary supports. Based off of the results obtained and the experience of launching the bridge, there were a few recommendations made. They advised that the design of the girders should include the girder to roller contact stresses which can be very high when launching a bridge. To reduce these high localized stresses in the girders that are developed while moving across the rollers, they suggest using either bigger diameter rollers or multiple small rollers. Doing this will spread out the load so that it is not as concentrated but is instead spread out over a larger area of the bottom flange of the girder as it moves across the roller.

Another piece of advice was given when in the design stage. They said to consider that there may be unequal vertical bearing forces applied from the girders to the supports as the

structure is being launched. This is due to it shifting and not being perfectly centered between the supports. It is important to recognize that these uneven forces may cause warping of the bridge structure as a whole during the launch and that measures should be taken to prevent this (Wipf et al., 2004).

Sponsored by FHWA, Michael Culmo authored a manual titled Accelerated Bridge Construction – Experience in Design, Fabrication and Erection of Prefabricated Bridge Elements and Systems (Culmo, 2011). As of 2011 the manual represents the "State of the Practice" for all aspects of ABC. It covers what Accelerated Bridge Construction is and what the benefits are when using ABC technologies. It fills in many of the gaps where information is lacking in previous manuals. Many aspects of ABC are covered in adequate detail in other manuals published, and so this manual does cover those topics but does so in less detail. The following are some of the ABC techniques that are discussed in the manual: Foundation Wall Elements, Rapid Embankment Construction, Prefabricated Bridge Elements and Systems (PBES), Structural Placement Methods, and Fast Track Contracting (Culmo, 2011).

In the Structural Placement section, it describes five ways in which the structure can be moved into place. These five methods include: Self-Propelled Modular Transporters (SPMTs), Longitudinal Launching, Horizontal Skidding or Sliding, Other Heavy Lifting Equipment and Methods, and Conventional Cranes. For each method an overview is given of the process, examples are used to illustrate the usefulness of the method and in what types of situations each method excels. Each of these methods have parameters and limitations that need to be considered when deciding on the bridge placing method to be used, and this manual helps decision makers in making that decision.

FHWA also had a manual created for using SPMTs to remove and replace bridges. It was created in 2007 and is titled Manual on the Use of Self-Propelled Modular Transporters to Remove and Replace Bridges (FHWA, 2007). This manual gives details throughout the process of using SPMTs to remove or install a bridge from conception to completion. It describes the equipment and their capabilities, lists the benefits and costs, and identifies criteria needed in deciding which projects are appropriate to use SPMTs. Since this method of using SPMTs can reduce construction time considerably implementing SPMTs should be considered for all bridge replacement projects where construction time is a priority.

This manual also includes example calculations for design, diagrams, plan sheets and specifications that can be used in getting started on a bridge move project that will use SPMTs. There are several case studies that are also included in the document which can be referenced. Design requirements and guidelines are included for ground bearing capacity, prefabricated superstructures, and substructures. The manual is a great resource for designers, contractors, and project managers to use when using SPMTs to move a bridge structure. As information and experience increases in the industry revisions will be made and additional material will be added to the manual to provide a more thorough resource on the use of SPMTs in removing and replacing bridges.

Utah State University graduate student Erik Rosvall, worked with Dr. Marvin Halling in collecting and analyzing data for five Utah bridge moves that occurred in 2008. All of these bridges were built in a temporary location and then moved into place using SPMTs. Each of the bridges had multiple strain gauges connected to them which allowed them to monitor the stresses in the superstructures while lifting them from temporary supports, during transportation on SPMTs, and during placement in their final position on top of the substructure. Once the data was collected, the

measured stresses were compared to the calculated stresses determined by analysis. Sensors were located on the webs of the girders near the lift points and on the bottom of the deck at the mid-span of the bridge structure.

When the structure was on the temporary supports it acted as a simply supported beam with the max moment in the center of the span, but when the structure was lifted the moment diagram changed because the lifting points were located in away from the ends. The bottom flanges of the girders did not remain in tension and the top flanges/deck in compression across the length of the bridge. Instead the bottom of the bridge experienced a reversal in stresses from tensile to compressive and vice versa for the top. There were three different types of stresses that were identified; stress due to lifting, temperature stress, and dynamic stress. The data, evaluation, interpretation, and conclusions for these bridge moves can be found in Rosvall's thesis Data Analysis of Utah's I-80 Bridges – For the Use in the Development of Accelerated Bridge Construction Standards (Rosvall and Halling, 2010).

With Accelerated Bridge Construction becoming more common in the U.S. and the need for standardized ABC systems for bridges, the Transportation Research Board (TRB) under the 2nd Strategic Highway Research Program (SHRP2) has put together a Toolkit entitled Innovative Bridge Designs for Rapid Renewal: ABC Toolkit (SHRP#2B, 2010). This design toolkit was created for prefabricated bridge elements and systems (PBES) and includes standard design concepts for the substructure and superstructure of bridges as well as systems for the foundation. It contains ABC standard concepts, sample design calculations, recommended design specifications for load and resistant factor design (LRFD), as well as recommended LRFD construction specifications. This can help decrease the time needed for design and construction making ABC more appealing and cost effective for agencies to use. It can also help professionals

new to ABC with the learning curve by giving them step-by-step guidance to follow. One of the things that has prevented bridge owners from using ABC techniques is the slow engineering process as a result of each solution needing to be custom engineered. With pre-engineered systems that can be implemented using conventional construction equipment; more owners, engineers, and contractors will want to use ABC for their projects. The toolkit was created with the understanding that additional content will be added as more knowledge and experience is acquired such as for lateral sliding and other areas of ABC that need developed.

Chapter 9: Test Parameters

Deciding which parameters to test

Bridge bearings that use PTFE and stainless steel sliding surfaces have been used for years to reduce unwanted forces in bridge structures. Many researchers, as discussed in the literature review, have studied these types of bridge bearings and how the coefficient of friction (COF) is influence by changing different parameters. There are many parameters that can affect the COF for PTFE bearings. These parameters were discussed and which ones would be the best ones to focus on for this project. It was impractical to attempt to test all of the parameters and the team decided to focus on the ones that had a significant influence on the COF, and that could be controlled easily during the planning and implementation of a bridge slide.

The four parameters chosen for this project were:

(1) Surface Roughness of the mating material (e.g. stainless steel),

(2) Lubrication used between PTFE and the mating surface,

(3) Sliding Speed of the bridge as it is being slid into place, and

(4) Contact Pressure - determined by ratio of bridge weight to PTFE contact area.

The reasons each of these parameters were chosen, and how they were varied is discussed below.

Surface Roughness

When using PTFE bearings for permanent bridge bearing applications, AASHTO specifies the mating surface to be stainless steel with a #8 mirror finish. This is because the #8 mirror finish is the most polished and consequently the smoothest stainless steel available which corresponds to low friction values when used with PTFE. For Slide-In Bridge Construction the requirements to

use a #8 mirror finish may be unnecessary since the bearings are typically not used for permanent bridge bearing applications, but are usually just used as a temporary means to slide a bridge into place.

When planning and designing how the bridge will be slid into place, it is critical that the horizontal force, which is directly correlated to the COF of the sliding surface, not exceed the capacity of the bridge's super structure, the bridge falsework, or the sliding equipment (e.g. hydraulic rams, cables). So, if materials that are cheaper and more common can be used for the mating surface, and the horizontal forces do not exceed what they should, then there should be no reason to limit contractors to only using #8 mirror finish stainless steel. Stanton and Taylor's research (Stanton, 2010) found that stainless steel with a 2B finish performed almost as good as the #8 mirror finish for the tests that they did (they did not use lubrication for any of their tests).

Lubrication

It is common practice to use lubrication in conjunction with dimpled PTFE pads to reduce the friction for PTFE sliding bearings. Small concave dimples are drilled out of the PTFE pads so that there is a place for the lubricant to be retained. The team decided to compare tests using different kinds of lubricants, as well as tests with no lubricants (referred to as "dry" tests). The dry tests were to be used as a base point to compare the lubricated tests to. The following four lubricants are the ones that the team felt would be good to investigate: soap, grease, oil, and graphite.

Soap

There have been multiple bridge slides where the contractors used dish soap on the PTFE pads to lubricate them. It may sound a little odd at first to use soap as a lubricant, but it is easy to

acquire and can be much more environmentally appealing than other types of lubricants. This had never been researched in the past and so it was an important lubricant to test out and see how it compared with others.

Grease

There are several reasons why grease was chosen as one of the lubricants to be tested. Grease is the lubricant that AASHTO specifies to be used for permanent bridge bearings. It is a common lubricant for many different applications, and stays in place after applied to a surface without being washed away very easily. It also repels water and does not dry out in the sun like soap does.

Oil

Oil is one of the most common lubricants that is used and seemed to be a logical lubricant to test. Automotive motor oil is very accessible and there are different viscosities that are easily available to buy in large quantities.

Graphite

As other lubricants were discussed that could be tested, graphite was one that seemed like it may work even though it is a little more difficult to obtain large containers of graphite since it is typically not used for big projects like this.

Although there are many different lubricants out there that could have been tested, these are the four that were decided to be good ones to test. More about the specifics of the lubricants will be discussed later in the materials chapter.

Sliding Speed

The speed at which the PTFE and the mating surface slide against each other is known to have an effect on the COF as well. Once again using AASHTO specifications for permanent bridge bearings as a starting point, it made sense to run tests at the speed that they specify for testing PTFE bearings which is 2.5 in/min. This is a pretty slow speed, and so the other speed that was chosen to run tests at was 10 in/min. The 10 in/min seemed to be a more reasonable speed at which contractors would want to push/pull a bridge at.

Contact Pressure

It seems a little counter intuitive at first, but as the contact pressure (between the PTFE and the mating surface) increases, the COF decreases. Extensive testing was done for the NCHRP Report 432, High-Load Multi Rotational Bridge Bearings (NCHRP, 1999) where the researchers proposed that the COF decreases linearly as the contact pressure increases for pressures less than 3000 psi, and as the pressure increases into higher pressures the COF remains fairly constant. Based on this the team decided to run tests at the following four pressures: 1500 psi, 3000 psi, 4500 psi, and 8000 psi.

PTFE can start to deform at high pressures such as 8000 psi, especially if the PTFE is not reinforced with fiber fillers. However, since these pads were not to be tested as long term bearings, but just as temporary sliding bearings, it may not matter to much if they deform slightly. The plan was to just run a couple of tests at 8000 psi just to see how the COF changed as the pressure increased to such a high pressure and to see if the pads deformed much.

Test Matrix

With the four parameters that were chosen and the proposed ways in which they would be varied, this creates 120 different combinations of tests. This was not practical to do with the funds

available and time allowed. A test matrix was created and presented to the NCHRP board on what tests the team planned on doing, which was based off of what would be practical for a bridge slide in the field, as well as to be able to compare results easily. The following test matrix below in Table 9.1 shows which tests were completed during this project.

Table 9.1. Test matrix shows proposed/completed tests each labeled with identifying code

Test Matrix		Lubricants Used between PTFE and Stainless Steel Surfaces				
Slide Speed (in/min)	Pressure (psi)	Dry Smooth(sm) or Dimpled (dim)	Dish Soap	Silicone Grease (SAE-AS 8660)	Automotive Motor Oil	Graphite
No. 2B Stainless Steel						
10 in/min	1500	X	X	X		
	3000	X	X	X		
	4500	X	X	X	X	X
	8000	*	*	*		
2.5 in/min	1500	X	X	X		
	3000	X	X	X		
	4500	X	X	X	X	X
	8000	*	*	*		
No. 1 Stainless Steel						
10 in/min	1500	X	X	X		
	3000					
	4500	X	X	X	*	*
	8000					
2.5 in/min	1500	X	*	*		
	3000					
	4500	X	*	*	*	*
	8000					
Carbon Steel						
10 in/min	1500	*	X	X		
	3000					
	4500	*	X	X	*	*
	8000					
2.5 in/min	1500	*	*	*		
	3000					
	4500	*	*	*	*	*
	8000					

X Primary tests to be performed

* Secondary tests may be performed based on the results of the primary tests performed

Chapter 10: Materials and Test Setup

The research team used Utah State University's structure lab to simulate forces required for bridge slides. Since the testing was done during the winter months of January, February, and March, the lab was heated and kept between about 55 - 65 degrees Fahrenheit. This lab is not designed for temperature controlled testing which is why the temperatures varied between that range. The materials that were chosen to be used in the testing will be discussed below as well as the reasoning why these decisions were made.

Materials

PTFE Pads

PTFE which is the acronym for Polytetrafluoroethylene is a fluorocarbon-based polymer that naturally has very low friction properties as well as other properties that make it a favorable material to use for bridge bearings. During manufacturing some of these properties can be altered to increase the performance of the pads for the desired application. Some of these other properties include high resistance to weathering, high and low temperature capability, and high chemical resistance.

Fillers such as glass and carbon fibers can be added to the PTFE during the manufacturing process to improve strength and resistance to wear, which is great for some applications, but it also increases the friction of the pads. So the PTFE that was used for this project was "Unfilled." The samples were also "Virgin" PTFE. This means that it did not contain any recycled PTFE. Virgin PTFE also has slightly lower friction than non-virgin PTFE which is why virgin PTFE was used for this project.

The team decided to use both dimpled and smooth PTFE pads. The dimpled ones were used for the tests using lubricants, whereas the smooth pads were used for the dry tests. The dimples are designed to retain some of the lubricant so that while sliding the PTFE stays lubricated longer. Figure 10.1 below shows both a dimpled and smooth PTFE pad.

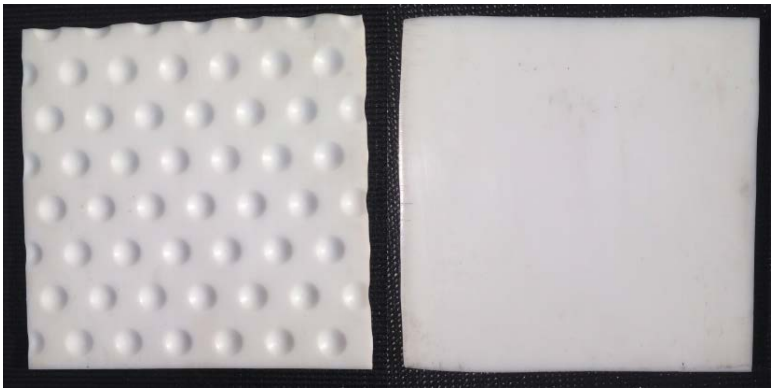

Figure 10.1. PTFE pads; dimpled and smooth

Contact pressure is calculated by finding the portion of the bridge weight concentrated on each PTFE pad and then dividing that load by the surface area of the pad. So in determining the size of pads to be used, it was decided that 4" x 4" PTFE pads would be a good size that would allow the vertical load, simulating the weight of the bridge, to be in a manageable range. The calculations for this were based off of the maximum contact pressure to be tested on the pads, which was 8000 psi. Multiplying this pressure by the area of 16 square inches would mean that a vertical load of 128,000 lbs would be needed to achieve that pressure (Force = Pressure X Area). This load was a reasonable amount that could be simulated in the lab which is why this size of PTFE pads was chosen.

Two companies that manufacture and sell bridge bearings were contacted in order to get the PTFE samples donated for the project. Both companies, D.S. Brown and R.J. Watson, were happy to help out in donating the PTFE. It was unnecessary to have them send completely assembled bearings that they typically sell, since the only thing being investigated was the

interaction between the two sliding surfaces. This made it easier to get the material donated since all that was needed were samples of PTFE and stainless steel. Twelve PTFE pads were donated by R.J. Watson and twelve by D.S. Brown. Each company sent 4 smooth pads and 8 dimpled pads.

Stainless Steel and Carbon Steel

The stainless steel used for the testing was Type 304 stainless. This type of stainless was chosen because it is the type specified for a similar application for permanent bridge bearings in the AASHTO LRFD Bridge Design Specifications. The goal was to compare stainless steels that had different surface roughness. Figure 10.2 shows the two kinds of stainless steel that were used and also the carbon steel used. The specimen on the left of the photo is stainless steel with a #2B finish, and the middle specimen is stainless steel with a #1 finish. The specimen on the right of the photo is carbon steel.

There are many different types of finishes for stainless steel. Each one goes through a different process when being made which gives it a different finish and consequently a different surface roughness. Table 10.1 shows the available finishes, the grit number, and the processes that they go through to create the finish they have. The #2B finish is the most common and cheapest to buy.

Depending on how thick the stainless is, it will either be referred to as plate or sheet stainless steel. If the stainless is equal to or thicker than 3/16 inch (0.1875in), then it is considered plate stainless steel. If it is less than that thickness (0.1874 in or less) then it is sheet stainless steel. The standard way of measuring sheet stainless steel is in gauges. The #2B stainless steel sheets that were used were 12 gauge (0.105 in thick), and the # 1 stainless as well as the carbon steel plates used were 3/16” thick. The # 1 finish for stainless steel is only made as plate stainless which is why the stainless was 3/16 in thick for those specimens.

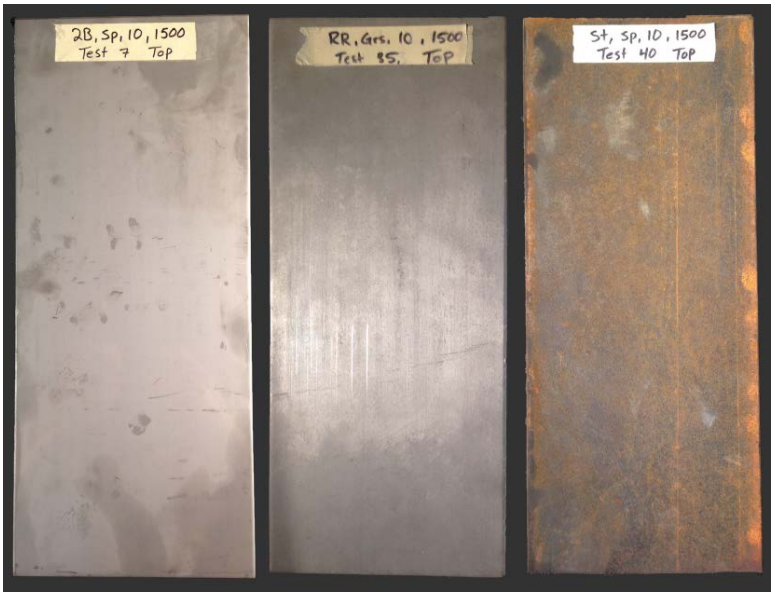

Figure 10.2. Left: #2B stainless steel; Center: rough rolled (#1) stainless steel; Right: Carb

Table 10.1. Stainless steel finishes

STAINLESS STEEL FINISHES		
Finish #	**Grit #**	**Metallurgy Process**
#1 Finish	60	Hot-rolled, annealed and descaled
#2D Finish	80	Hot-rolled, annealed and descaled, dull finish
#2B Finish	100-320	Cold-rolled, annealed, bright finish
#3 Finish	100-120	Intermediate polished finish, usually 120 grit, one or both sides
#4 Finish	120-220	General purpose polished finish, usually 180 grit, one or both sides
#6 Finish	240	Dull satin finish, Tampico brushed, one or both sides
#7 Finish	320	High luster finish or near mirror (has some lines)
#8 Finish	400-500	Mirror finish

For the #2B stainless steel there were a couple important differences between the sheets that were purchased. The first order of #2B stainless was for sheets that were 8” x 18”. Some of these sheets were scratched during transport. The ones that had really bad gouges were not used for testing due to the concern of the scratches causing higher COF values. The sheets that just had light scratches on them but were still pretty smooth were still used. These sheets were used for the

first three #2B tests. More #2B stainless was purchased and since they no longer needed to be as big as the ones from the first order, these were ordered at 6” x 14” in order to reduce the cost. All of the following tests using #2B stainless used these smaller ones.

The larger #2B sheets seemed to be slightly rougher than the smaller #2B sheets and also had the small scratches on them. These tests were used for the first three tests which were the three at 1500, 3000 and 4500 psi using #2B stainless, at 10 in/min, and no lubrication (dry). The results for these test produced slightly higher COF values than expected which will be discussed further in the results section.

Lubricants

The soap that was used as a lubricant was liquid Dawn dish soap. The oil that was used was SAE 10W-40 Motor Oil. The grease used was SAE-AS8660 dielectric grease made by Jet-Lube. SAE-AS8660 is what AASHTO specifies when using lubricants on PTFE sliding bearings for regular bridge bearings. The graphite used was just a standard powdered graphite purchased at a local hardware store. Each of these lubricants are shown in Figure 10.3 below.

Figure 10.3. Lubricants used for tests

Steel Substrate

Steel substrates were used to confine the PTFE pads to help prevent them from deforming as a contact pressure was applied. An area of 4" X 4" was machined into the steel plates where the PTFE pads could sit. The recess was machined to a depth of 3/32 of an inch. Once the PTFE pads were inserted into the recess, half of the pad would stick out since the PTFE was 3/16 inch thick. Most of the PTFE pads fit very snug in the substrate, but a few of them had a little slop and so a thin shim was put in to make them fit tight.

Test Setup

The testing was done in a structures lab at Utah State University in Logan Utah. The lab has a reaction frame in which the test setup was mounted. Figure 35 below is a sketch of how the team planned on using this reaction frame to attach everything to it. Two vertical rams were used to simulate the vertical load caused by the weight of a bridge, by applying a load to a spreader beam which pushed down on the PTFE pads and sandwiched them. Once this vertical load was applied, the horizontal actuator would then slide the specimens back and forth with the only resistance being the friction between the PTFE pads and the stainless steel.

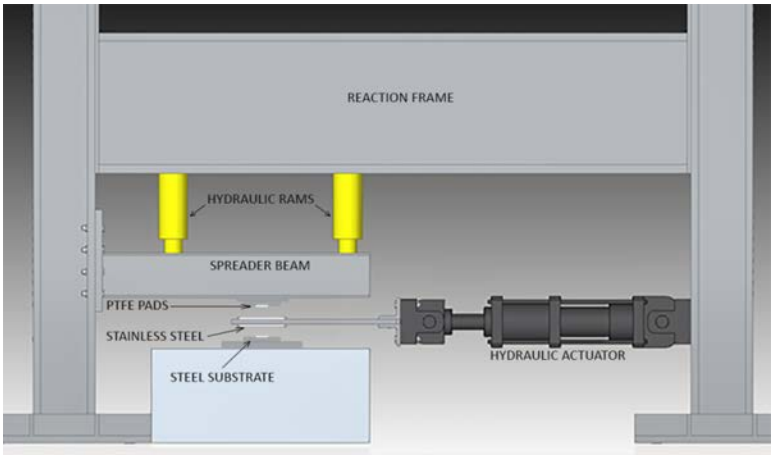

Figure 10.4. General test setup

In order to keep the spreader beam from moving when the actuator moves back and forth, it was necessary to secure the beam to the reaction frame. Slotted holes were cut into the end plate of the spreader beam so that while the vertical load was being applied the bolts could be loose enough for the beam to slide up and down freely without binding up. Once the desired vertical load was set, the bolts would be tightened by hand just enough to take out any slop but still loose enough to prevent them from carrying any load. Figure 36 shows a zoomed in area of the slots in the end plate of the spreader beam.

Figure 10.5. Slotted connection for spreader beam

When using sliding bearings in a bridge slide, the PTFE bearing pads are usually placed on a track with the PTFE surface facing up and then there usually a stainless steel slide shoe on the underside of the superstructure of the bridge that slides across the PTFE bearings. However, with the setup in the lab there needed to be two PTFE pads and two stainless steel plates used in order for the system to work properly and not have any extra resistance from the use of a roller or some

other type of setup. This meant that the friction would be doubled since there were two sliding surfaces. This was accounted for in calculating the COF and will be discussed later.

Initially the plan was to attach the PTFE pads to the steel tongue and push them back and forth sliding along the stainless steel plates. If it had been done this way however, it would have created a slightly eccentric loading on the pads as they slid from one end of the stroke to the other. To avoid this issue, it was decided to keep the pads stationary by attaching them to the spreader beam above and the concrete block below. Then the stainless steel plates would be attached to both sides of the steel tongue and slid back and forth.

Figure 37 shows how the stainless steel and PTFE were attached and how they were sandwiched together. The steel substrates used to confine and hold the PTFE were tack welded to the spreader beam and large plates below on the concrete block. The friction between the large steel plates and the concrete block was always higher than the friction between the PTFE pads and stainless steel, and that is what kept the base plate from sliding on top of the concrete block.

Figure 10.6. Test setup showing PTFE pads attached to steel substrates, and stainless steel sheets attached to steel tongue

Load cells were placed between the vertical rams and the spreader beam to measure the vertical load for each ram. In order to prevent eccentric loading on the vertical rams or the load cells, spherical bearings were used. These were placed just under the load cells and on top of the spreader beam. Figure 38 below shows the full test setup. The horizontal actuator (shown on the right in this figure) is a servo hydraulic ram that is made by MTS. This actuator has a load cell built into it to measure the horizontal load needed to slide the specimens. It also has built in sensors that measured the horizontal displacement, the speed, and the number of cycles continuously during the testing.

Figure 10.7. Test setup in structures lab

Chapter 11: Test Procedures and Test Results

Tests Performed

At the beginning of this project a test matrix was created with the proposed tests that the team planned on doing. This matrix has been discussed and shown previously in Table 9.1. Each of the primary tests that were originally proposed to be done were completed, as well as most of the secondary tests and other tests that were determined would be good to do. Decisions on whether or not to do certain tests were made during the testing process based on similar tests and how they performed.

The following test matrix shown below in Table 11.1 shows which tests were completed. Each test that was completed during the project is represented by its equivalent label shown in the matrix of the table. These labels are also helpful when looking at photos of test specimens to identifying what the parameters were for that test. Table 11.2 shows what each of the abbreviations in Table 11.1 stands for.

Table 11.1. Test matrix of completed tests represented by code used label test parameters

Test Matrix		Lubricants Used between PTFE and Stainless Steel Surfaces				
Slide Speed (in/min)	Pressure (psi)	Dry Smooth(sm) or Dimpled (dim)	Dish Soap	Silicone Grease (SAE-AS 8660)	Automotive Motor Oil	Graphite
No. 2B Stainless Steel						
10 in/min	1500	2B,D-sm,10,1500	2B,Sp,10,1500 †	2B,Grs,10,1500	2B,Oil,10,1500	
	3000	2B,D-sm,10,3000	2B,Sp,10,3000	2B,Grs,10,3000	2B,Oil,10,3000	
	4500	2B,D-sm,10,4500	2B,Sp,10,4500 †	2B,Grs,10,4500	2B,Oil,10,4500	2B,Gph,10,4500
	8000	2B,D-dim,10,8000	2B,Sp,10,8000	2B,Grs,10,8000	2B,Oil,10,8000	
2.5 in/min	1500	2B,D-dim,2.5,1500	2B,Sp,2.5,1500	2B,Grs,2.5,3000‡		
	3000	2B,D-dim,2.5,3000	2B,Sp,2.5,3000	2B,Grs,2.5,3000		
	4500	2B,D-dim,2.5,4500	2B,Sp,2.5,4500	2B,Grs,2.5,4500	2B,Oil,2.5,4500	2B,Gph,2.5,4500
	8000					
No. 1 Stainless Steel						
10 in/min	1500	RR,D-sm,10,1500	RR,Sp,10,1500	RR,Grs,10,1500	RR,Oil,10,1500	
	3000					
	4500	RR,D-dim,10,4500	RR,Sp,10,4500	RR,Grs,10,4500	RR,Oil,10,4500	*
	8000					
2.5 in/min	1500	RR,D-sm,2.5,1500	*	*		
	3000					
	4500	RR,D-sm,2.5,4500	*	*	*	*
	8000					
Carbon Steel						
10 in/min	1500	*	St,Sp,10,1500	St,Grs,10,1500	St,Oil,10,1500	
	3000					
	4500	*	St,Sp,10,4500	St,Grs,10,4500	St,Oil,10,4500	*
	8000					
2.5 in/min	1500	*	*	*		
	3000					
	4500	*	*	*	*	*
	8000					

* Tests considered before testing began, but were not done based on results of prior tests.
† Additional tests were done using Soap and adding water during testing to simulate effects of rain.
‡ This test was done at the wrong pressure. 3000 Psi was used instead of the 1500 psi.

Table 11.2. Acronyms used in test codes to identify parameters used for each test

Terms Used for Labeling and Identifying Tests	
Term	**Description**
2B	Stainless steel mating surface with a #2B surface finish
RR	Stainless steel mating surface with a #1 surface finish which is also known as rough rolled (RR) stainless steel
St	Carbon steel mating surface
D-sm	Dry test (no lubrication used), with smooth (sm) PTFE pads
D-dim	Dry test (no lubrication used), with dimpled (dim) PTFE pads
Sp	Soap was used for lubrication
Grs	Grease was used for lubrication
Oil	Oil was used for lubrication
Gph	Graphite was used for lubrication
10	A sliding speed of 10 in/min was used
2.5	A sliding speed of 2.5 in/min was used
1500	Contact pressure of 1500 psi was used
3000	Contact pressure of 3000 psi was used
4500	Contact pressure of 4500 psi was used
8000	Contact pressure of 8000 psi was used

Data Acquisition and Data Processing

Two data acquisition units were used to collect the data. The MTS ram had its own system set up to it, and the two vertical rams were hooked up to a separate system. The vertical data acquisition only measured the vertical force for both vertical rams and time. The MTS data acquisition was set up to measure the horizontal forces, horizontal displacement, cycle count, and time. The sampling rate was set at 100pts/second to make sure that the spikes in force as seen in Figure 39 below were captured.

The sliding speed was set to be constant at either 10 in/min or 2.5 in/min depending on the test. The ram was set to push the samples back and forth ± 1 inch, corresponding to a stroke of 2

inches. In order to produce a sliding speed that was constant, the MTS actuator was programed to run a ramp waveform, instead of a sinewave or square wave.

As the ram would reach the end of the stroke it would switch directions and start moving the other way. When this change in direction happened the force required to push it would spike higher due to the static friction. Figure 39 shows a graph of the horizontal force on the y-axis and displacement on the x-axis. This graph shows all 101 cycles for the test. The highest spike in force on the left hand side is the static friction for the first cycle. The force decreased quite a bit after the first cycle, and then slowly continued to decrease as the cycles (or slide path) increased.

It is easier to see the trend of the force decreasing over time when the cycles are spread out on a force versus time plot. Figure 40 shows the first 12 cycles of a test. The Static Friction is highest on the first cycle, and then decreases slowly for each progressing cycle.

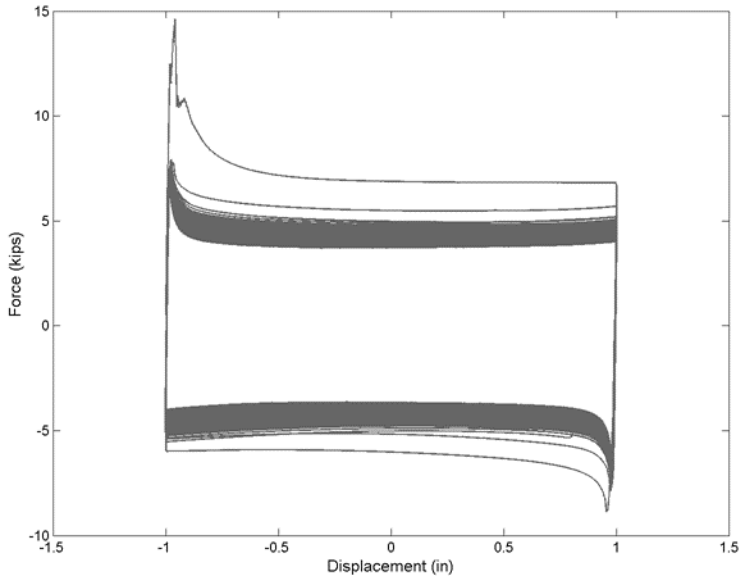

Figure 11.1. Typical graph of force versus displacement for all 101 cycles

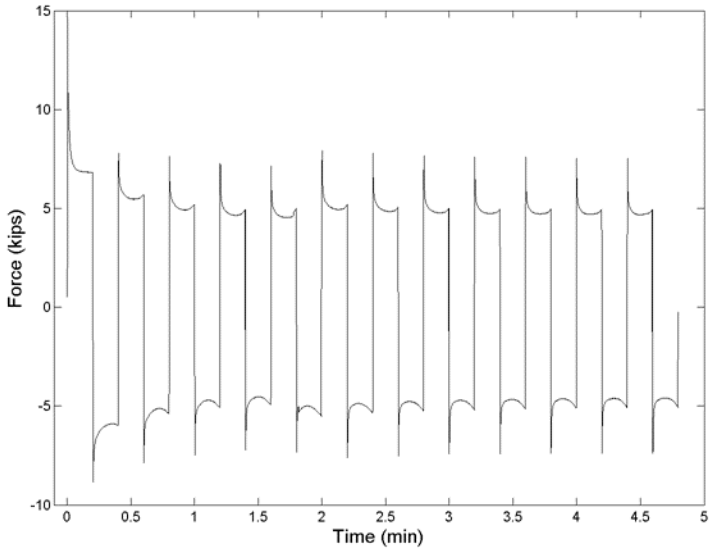

Figure 11.2. Typical graph of force versus time (cycles 1-12)

The coefficient of friction (COF) is calculated using a simple equation relating the vertical force (or Normal Force (*N*)) to the horizontal force (or Friction Force (*F*)):

$$F = \mu \times N \tag{9}$$

where μ is COF.

Since the setup used had two sliding surfaces there are two friction forces so the proper equation for this project then becomes:

$$F = 2 \times \mu \times N \tag{10}$$

Rearranging the equation to solve for the COF gives the equation in this form:

$$\mu = \frac{F}{2 \times N}, \qquad COF = \frac{Horizontal\ Force}{2 \times Vertical\ Force} \tag{11}$$

Once the COF was found for each test, graphs were created to easily compare and analyze the data. When the COF is plotted, as shown below in Figure 11.3, it looks much like the last plot of force vs time but with different values.

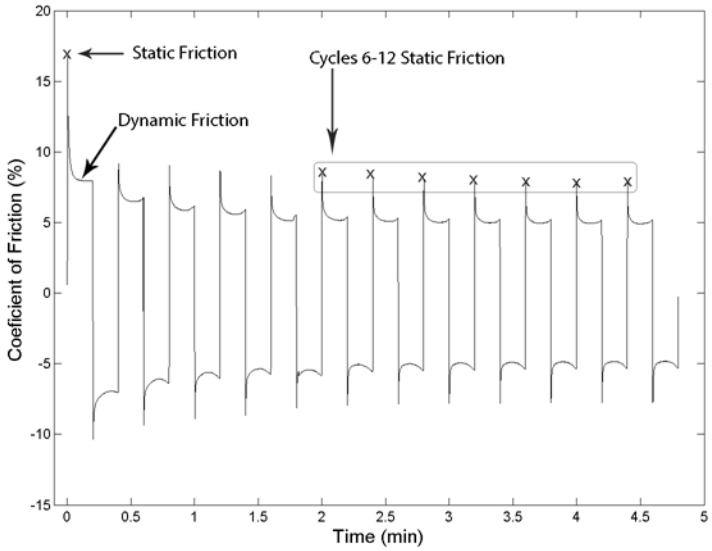

Figure 11.3. Typical plot of the coefficient of friction versus time (cycles 1-12)

There are two main types of friction: static and dynamic. The static friction is the amount of friction that keeps an object from moving. In order for an object to start sliding it has to overcome the static friction force. Dynamic friction is the friction present once the object is in motion. The Dynamic friction is always lower than the static friction and so the values for the static friction are what will be focused on.

In order to understand and summarize the behavior of each test, three important values have been recorded in

Table 11.3 below. The three values are the static friction for cycle 1, the average of cycles 6-12, and cycle 101. Figure 11.3 above shows static friction for cycle 1 and also cycles 6-12. The figure does not show the point at the 101st cycle since it is zoomed in on only the first 12 cycles.

Table 11.3. Static coefficient of friction values for all tests (cycles: 1, mean of 6-12, and 101)

STATIC COEFFICIENT OF FRICTION (%)																		
Slide Speed	10 in/min									2.5 in/min								
Roughness	**2B Stainless**			**RR Stainless**			**Carbon Steel**			**2B Stainless**			**RR Stainless**			**Carbon Steel**		
Cycle	*1*	*6-12*	*101*	*1*	*6-12*	*101*	*1*	*6-12*	*101*	*1*	*6-12*	*101*	*1*	*6-12*	*101*	*1*	*6-12*	*101*
1500 Psi																		
Dry	7.75 *	3.24 *	3.03 *	14.12	6.53	5.85	-	-	-	4.23	4.24	3.16	-	-	-	-	-	-
Soap	5.66	2.28	2.84	24.25	6.99	4.05	18.35	7.63	4.63	4.50	1.90	2.90	-	-	-	-	-	-
Grease	5.15	0.99	1.55	4.20	2.81	3.26	6.86	4.30	3.81	-	-	-	-	-	-	-	-	-
Oil	4.04	1.05	1.49	16.07	5.92	3.10	20.15	6.22	4.32	-	-	-	-	-	-	-	-	-
Graphite	-	-	-	-	-	-	-	-	-	-	-	-	-	-	-	-	-	-
3000 Psi																		
Dry	16.76 †	7.93 †	6.81 †	-	-	-	-	-	-	2.57	2.11	2.27	-	-	-	-	-	-
Soap	2.18	1.27	1.87	-	-	-	-	-	-	5.07 ‡	1.85 ‡	1.97 ‡	-	-	-	-	-	-
Grease	2.02	0.55	1.11	-	-	-	-	-	-	1.86	0.50	1.12	-	-	-	-	-	-
Oil	1.51	0.87	1.09	-	-	-	-	-	-	-	-	-	-	-	-	-	-	-
Graphite	-	-	-	-	-	-	-	-	-	-	-	-	-	-	-	-	-	-
4500 Psi																		
Dry	12.1 †	4.90 †	4.75 †	4.10	2.47	2.33	-	-	-	2.99	1.42	1.89	-	-	-	-	-	-
Soap	2.45	1.20	1.57	5.02	3.97	3.49	7.05	3.27	2.01	0.70	0.50	0.84	-	-	-	-	-	-
Grease	1.06	0.46	0.81	4.11	2.28	2.92	2.75	1.73	1.72	0.48	0.40	1.01	-	-	-	-	-	-
Oil	2.75	0.77	0.79	5.99	2.60	1.47	6.85	3.19	1.86	1.08	0.68	0.74	-	-	-	-	-	-
Graphite	9.49	9.67	6.12	-	-	-	-	-	-	6.16	5.85	6.11	-	-	-	-	-	-
8000 Psi																		
Dry	2.94	0.88	0.69	-	-	-	-	-	-	-	-	-	-	-	-	-	-	-
Soap	1.44	0.88	1.26	-	-	-	-	-	-	-	-	-	-	-	-	-	-	-
Grease	0.67	0.32	0.47	-	-	-	-	-	-	-	-	-	-	-	-	-	-	-
Oil	0.90	0.46	0.47	-	-	-	-	-	-	-	-	-	-	-	-	-	-	-
Graphite	-	-	-	-	-	-	-	-	-	-	-	-	-	-	-	-	-	-

* Stainless steel previously used for a grease test was used for this test. Small remnants of grease remained which reduced the friction
† Tests used 2B stainless steel sheets that were a little rougher than the others, which is likely to have increased the friction slightly
‡ 3000 psi was applied to the PTFE pads for 32 hours before testing to see if static COF for cycle 1 would increase after being loaded for a long time

Typical Tests

Dry

Dry tests were done using #2B stainless steel as well as # 1 stainless steel. There were no dry tests done on the carbon steel based off of the assumption that the coefficient of friction would be higher than desirable. Three of the dry tests were done with #2B stainless that had a little

rougher surface than the other #2B sheets. This was previously mentioned in the materials section when the stainless steel was discussed. See that section for why these stainless sheets had rougher surfaces. Figure 11.4 below is a picture of one of the dry tests that used the smaller #2B stainless steel sheets that were the more typical ones used. Both dimpled and smooth PTFE pads were used for the dry tests in order to see which ones worked better when no lubrication was used. See the test matrix to see which ones used smooth PTFE pads and which ones used dimpled pads.

Figure 11.4. Dry test which used dimpled PTFE instead of smooth

Soap

Dawn dish soap was applied to both the PTFE pads as well as the stainless steel or steel plates. Dimpled PTFE pads were used for all of the soap tests. Figure 11.5 is a typical picture of how much soap was applied to the PTFE and Stainless steel or steel. Figure 11.6 shows a better view of the PTFE pad and how thick the layer of soap typically was.

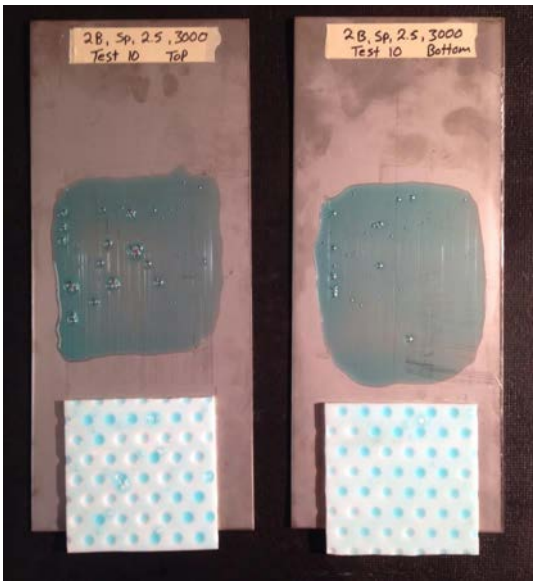

Figure 11.5. Typical soap test; shows how much soap was applied to the sliding surfaces

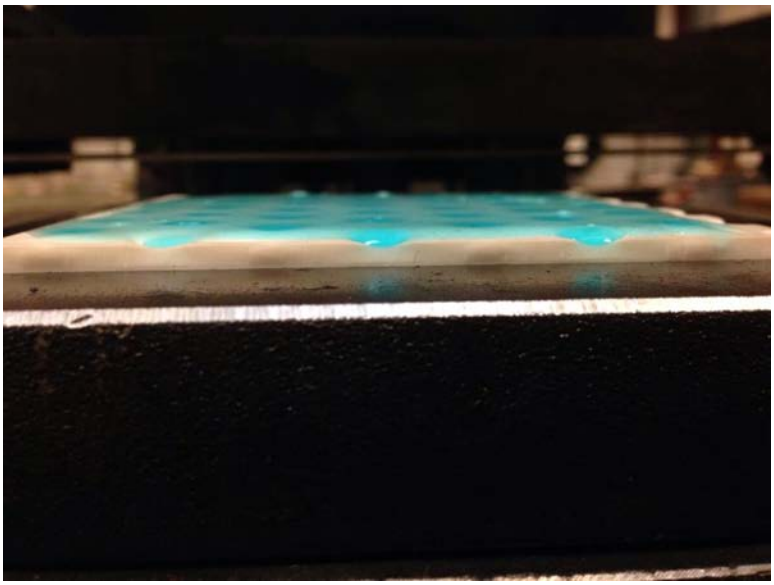

Figure 11.6. Typical soap test; shows the layers of Dawn dish soap on a dimpled PTFE pad

Grease

The type of grease that was used was chosen based on what AASHTO specifies for permanent bridge bearings in the LRFD Bridge Design Manual. AASHTO specifies SAE-AS8660 which is a silicone based dielectric grease. Dimpled PTFE pads were used for all of the grease tests. A thick layer of grease was applied to the PTFE pads so that all of the dimples were filled and there was an even layer of grease on the whole pad.

A layer of grease was also applied to the stainless steel and carbon steel plates. Figure 11.7 shows the before picture for one of the grease tests, and Figure 11.8 shows the same specimens after the test was complete. Even though the majority of the grease would get pushed off to the side, the sliding surfaces stayed pretty lubricated throughout the tests.

Figure 11.7. Typical grease test; grease was applied to PTFE pads and stainless steel or steel plates

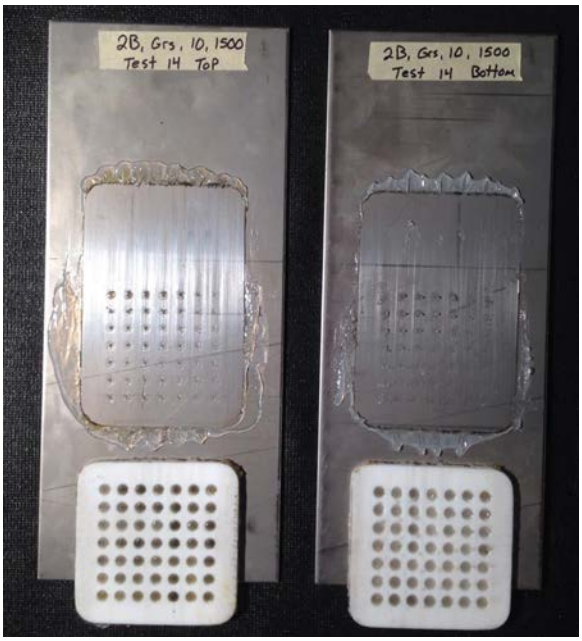

Figure 11.8. Typical grease test after testing

Oil

The type of oil that was used for the testing was 10W-40 automotive engine oil. An adequate layer of oil was applied to the specimens and the tests seemed to stay pretty well lubricated throughout the testing. Figure 11.9 below shows the amount of oil used on the tests, and what kind of oil was used.

Figure 11.9. Typical oil test; shows oil on PTFE and stainless steel before testing

Graphite

For the graphite tests standard tubes of powdered graphite was purchased from a local hardware store. Figure 11.10 shows a picture of one of the tubes that was used for the graphite tests. Both the PTFE and the stainless steel were coated with the graphite. The graphite tests did not perform very well at all, and so only two tests were done using graphite. For the first graphite test a lot of graphite was dumped on the pad, with the idea that after the majority of it was pushed off, there would still be an adequate layer of graphite left on the sliding surface. Very poor performance was seen during this tests. The friction force was very high and the PTFE pads deformed quite a bit due to too much heat caused by the friction. It was suspected that there was too much graphite put on the test specimens and that using smooth PTFE instead of dimpled would possibly give better results. Figure 11.11 shows how much graphite was used for the first test. This test was done using dimpled PTFE pads.

Figure 11.10. Tube of graphite powder used for the graphite tests

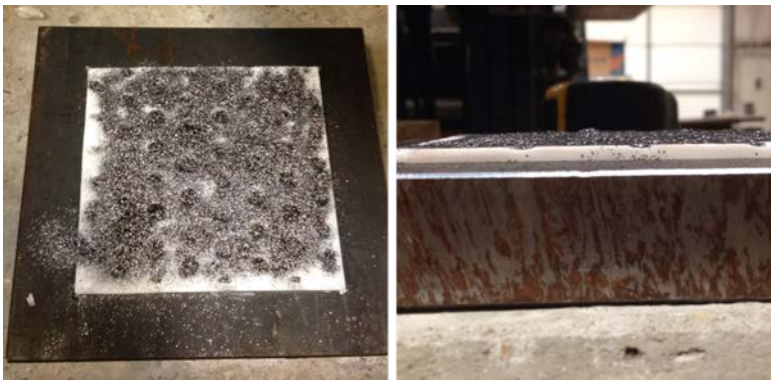

Figure 11.11. Test used too much graphite and produced poor performance

Figure 11.12 below shows how the PTFE pad deformed and started curling out from under the steel substrate due to the high amount of friction that was present. At the end of the tests the steel substrate holding the PTFE and the steel tongue holding the stainless steel, were hot to the touch. It's assumed that they heated up around 20 to 30 degrees above the temperature they were at before the test started. Figure 11.13 is a good picture that illustrates how much the PTFE pad deformed. Half of the thickness of the pad was confined by the steel substrate which is why part of the pad retained its square shape as shown on the right side of Figure 11.13. This was the original size and shape of the pad.

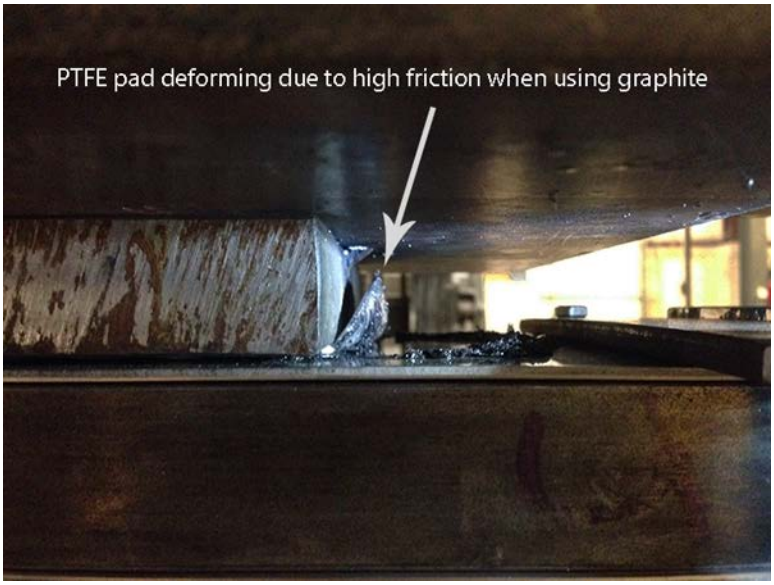

Figure 11.12. Graphite on dimpled PTFE pad sitting in steel substrate

Figure 11.13. Deformed PTFE pad after testing using graphite

For the next graphite test that was performed, smooth PTFE pads were used instead of dimpled, and only a light even coating of graphite was applied in hopes to get lower COF values than with the first test. Figure 11.14 is a picture of the stainless steel and PTFE pad used on top. This shows the before and after pictures of the same specimens. Notice how this test did not deform nearly as much as the test that used dimpled PTFE and had a lot of graphite. This test also had a lower COF than the other one.

Figure 11.14. Stainless steel and PTFE pad before and after graphite test was done

Chapter 12: Analysis and Discussion of the Results

When comparing results of the different tests, it is important to only vary one parameter at a time in order to accurately assess how that parameter influences the COF. Each of the four parameters will be evaluated this way by referring to the COF values in Table 9.1 above. The parameters will be discussed in the following order: (1) Contact Pressure, (2) Lubricants, (3) Surface Roughness, and (4) Sliding Speed.

Contact Pressure

Upon examination of how the COF was influenced by the contact pressure as it was adjusted, revealed the pattern that as the contact pressure increases, the COF actually decreases. Even though this may seem counterintuitive for most, this pattern has been found by many other researchers in the past that have looked at how contact pressure affects the COF for PTFE sliding surfaces. Both Stanton and Taylor (1999) as well as Campbell and Kong (1987) reported finding this to be true during their research.

The general pattern for this can be seen by comparing tests that vary with pressure but use the same lubricant, sliding speed, and surface roughness. This pattern can be seen by looking at the three graphs below which are groupings tests for soap, grease, and oil respectively. Each of these groups of tests used #2B stainless, and ran at a sliding speed of 10 in/min. These graphs show the static coefficient of friction on the y-axis, and cycles 1-12 and cycle 101 on the x-axis. The values used in these plots are the same values shown in Table 11.3 which was presented above. This type of graph allows comparison of the static friction for the first cycle, how it behaves right after the first cycle, and finally whether it increases or decreases as the cycle progresses to cycle 101.

Figure 12.1 compares the contact pressure for the soap tests, Figure 12.2 compares the tests that used grease, and Figure 12.3 compares the oil tests. Each of these graphs are pretty consistent in showing that during the full slide path of the tests the friction decreases as the pressure is increases. Note that in Figure 12.1 either the 3000 psi test is lower than expected, or the 4500 psi test is higher than expected for the first couple of cycles but then the lines quickly cross so that the COF for the 3000 psi tests is higher than the one for the 4500 psi. It appears that there is something that caused the first cycle to be a little off for one of these tests but it is unsure what that cause was.

A similar thing happens with the oil tests but for these tests the cause is known. It is simple. Each of these oil tests used the same PTFE and stainless steel sheets; however, the first test to use them was the one at 4500 psi. Then the specimens were used for another oil test that was at 4500 psi but at a sliding speed of 2.5in/min. (this test is not part of this group in the plot). Nest the PTFE and SS specimens were respectively used for the 1500, 3000, and 8000 psi tests shown in the plot. So in other words, the test at 4500 psi had to break in the samples for the first couple of cycles since it was the first test to use them, which caused the friction for that test to increase slightly.

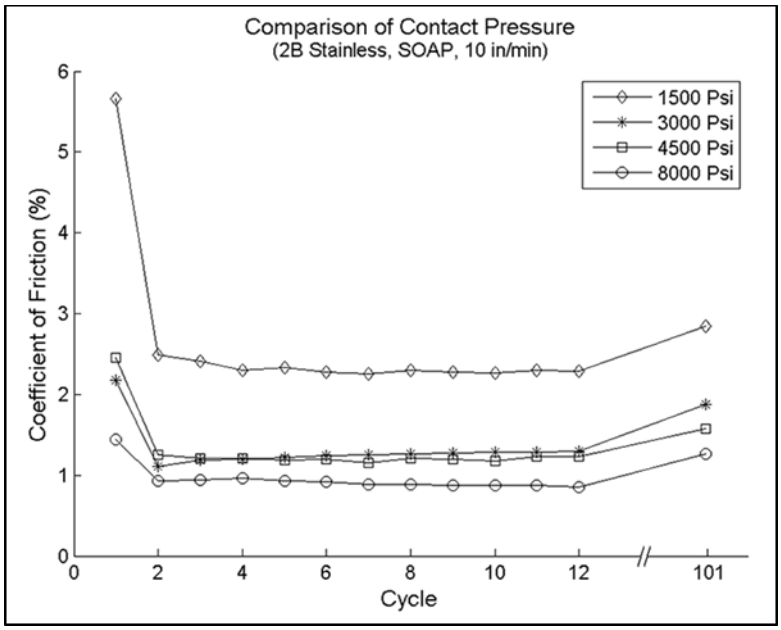

Figure 12.1. Pressure comparison for soap tests, using #2B stainless and 10 in/min

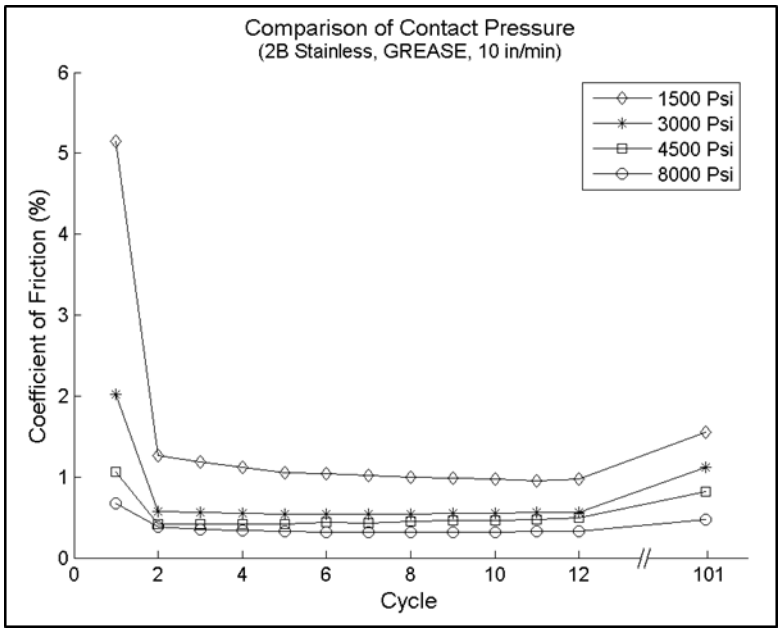

Figure 12.2. Pressure comparison for grease tests, using #2B stainless and 10 in/min

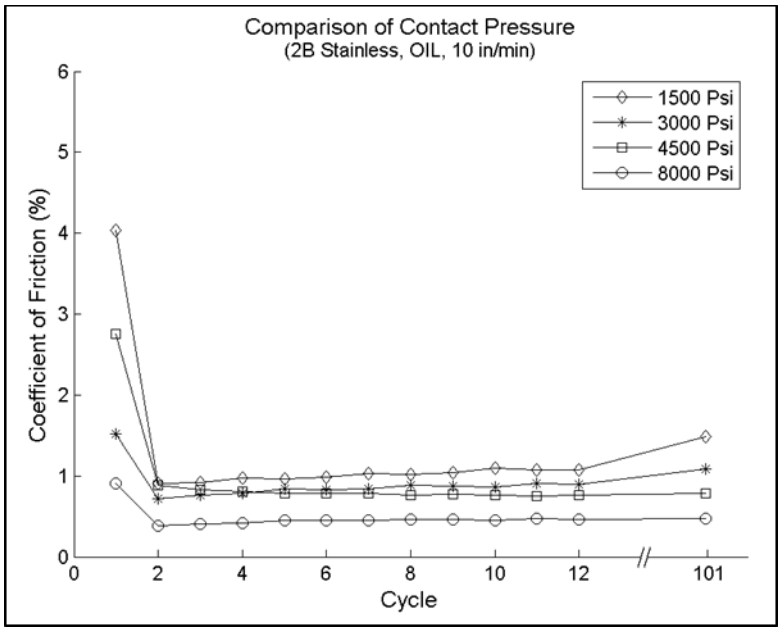

Figure 12.3. Pressure comparison for oil tests, using #2B stainless and 10 in/min

The group of dry tests that goes with the three plots above (using #2B stainless and 10in/min) follows the same pattern and shows a bigger difference in the COF between the pressures. These tests are shown in Figure 12.4 below. Note that this plot also has a test that seems to be off. The 1500 psi test in this group has a lower COF than the 3000 psi and 4500 psi test. Being the first test out of the 47 tests completed, there was an issue with the way the data acquisition was set up for this test, and this test needed to be redone. This issued was unknown until most of the other tests had been completed and so it wasn't redone until most of the other tests were completed.

Because of this the stainless steel that was used for the tests was a pair of sheets that had been used for three other tests that used grease. When deciding to use this pair it was assumed that the grease could be cleaned off really well and it would perform similar to the other dry tests that used #2B stainless. However, after the test had been completed and the specimens taken out of the setup, it was obvious that remnants of grease had remained. This little bit of grease caused the

friction to be lower than if they were completely dry with no remnants of grease on them. This is why all of the friction values for the 1500 psi test are lower than the ones for the 3000 psi and 4500 psi tests.

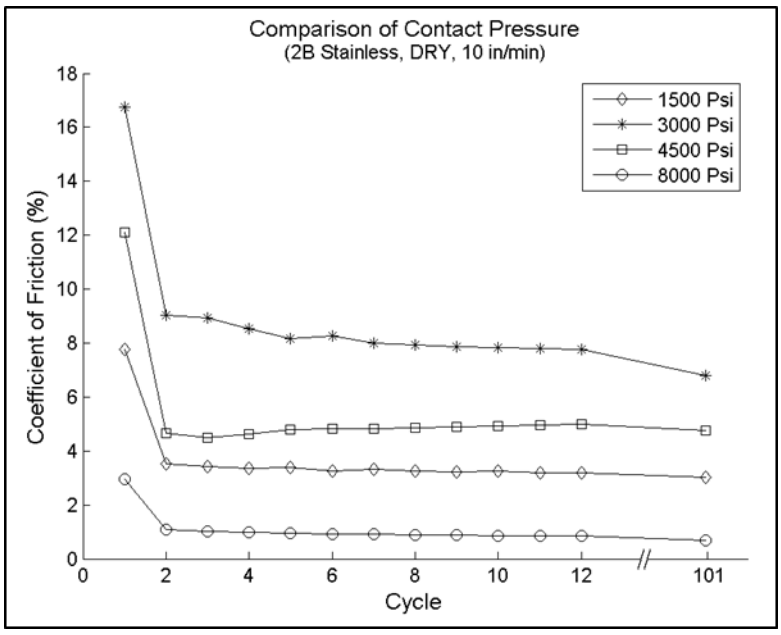

Figure 12.4. Pressure comparison for dry tests, using #2B stainless and 10 in/min

In summary, the test results obtained for this project agrees with other researchers in that the coefficient of friction decreases as pressure increases. There were a couple of tests that did not follow this pattern but there is good reason why they did not. The overall pattern of all the tests does follow the pattern. To see how the COF varied as with contact pressure for other groups of tests not discussed here (such as for tests at 2.5 in/min).

Lubrication

When using lubricants in combination with dimpled PTFE pads, friction values are significantly reduced, with exception to using graphite. The performance of the various lubricants relative to each other can be compared by looking at Table 11.3. Using this table, it is easy to see that the dry tests and graphite tests produce the highest COF values. Soap performed a little better

than the dry tests over all, and grease and oil performed the best. Note that there are a couple of tests that have numbers that don't match the pattern of the others. There are brief explanations in the foot notes of the table.

To help be able to see the patterns of how the different lubricants performed, a couple of plots will be shown below with different groupings of tests just as was done above when looking at contact pressure. The first group of tests includes all of the tests that used a #2B surface roughness, a sliding speed of 10 in/min, and a contact pressure of 1500 psi. Figure 12.5 shows a comparison of the COF values for these tests. Again, this plot shows cycles 1-12, and cycle 101.

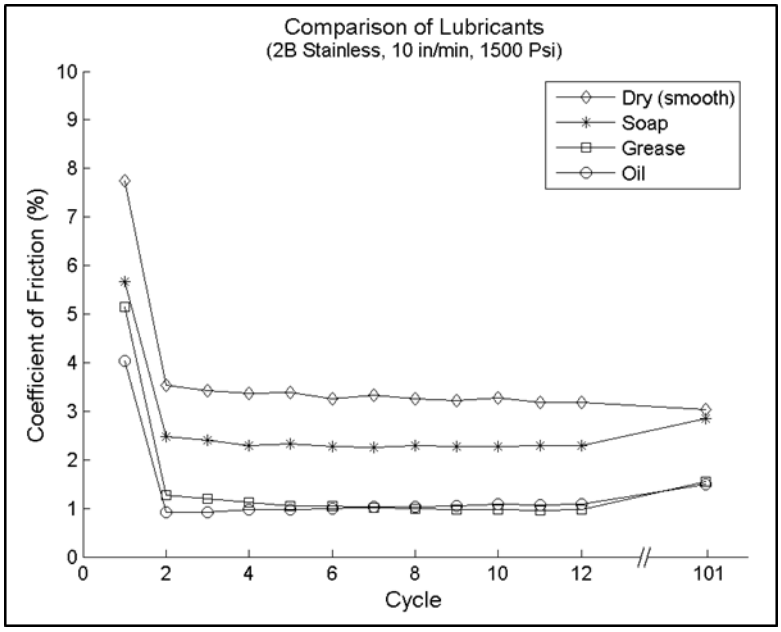

Figure 12.5. Lubricant comparison at 1500 psi, using #2B stainless and 10 in/min

The grease and oil tests performed very similarly to each other and produced much lower COF values than the dry test as well as the soap test. The points at cycle 1 are the most important values in this group of tests since they are the highest points for the plots. Looking at the first cycle, oil performed 50 percent better than the dry test. It dropped to about 1% for the subsequent cycles, and then only increasing slightly to 1.5% at the end of the test. The specimens seemed to

stay pretty well lubricated with the oil throughout the test. The oil that was used was SAE 10W-40 automotive engine oil.

The grease test had the next best results after oil with a COF value of 5.15% for cycle 1, then it dropped just like the oil test to around 1%, and then increased slightly as the slide path increased. The Soap started with a 5.7% COF for cycle 1, and dropped to an average of 2.3%, and then increased to just below 3% at cycle 101.

The dry test had a COF that started at 7.75% for cycle 1, then dropped to around 3.5% for cycles 2-12. However, unlike the lubricated tests, the friction for the dry test actually decreased as the slide path increased. This is due to the PTFE pads wearing and becoming smoother.

After comparing the tests at a pressure of 1500 psi, the tests of the next group that were compared were at a pressure of 3000 psi. Figure 12.6 plots the COF for this group. Each of the tests used #2B stainless steel, a sliding speed of 10 in/min, and 3000 psi. As noted previously, the dry test for in this group used a stainless steel sheet that had a gouge across the surface that likely raised the COF a little for it.

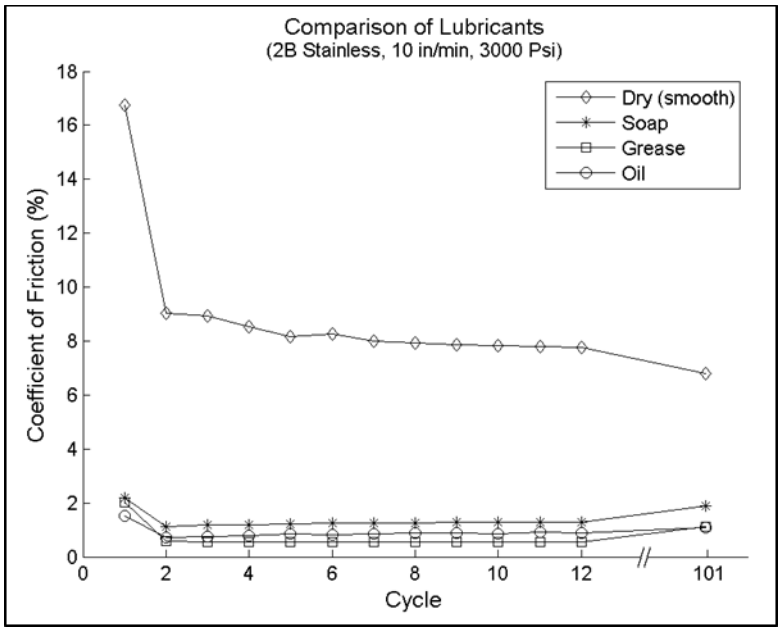

Figure 12.6. Lubricant comparison at 3000 psi, using #2B stainless and 10 in/min

Notice that in comparison to Figure 12.7 the lines showing the COF for the soap, oil, and grease all dropped quite a bit. Again this shows that as the pressure increases, the COF decreases. Oil, grease, and soap all performed very similar with this group of tests. The grease and soap tests started out at just over 2%, and the oil performed the best for the first cycle producing a COF of 1.5%.

This next group of tests will now be at 4500 psi. So the common parameters between these tests are #2B stainless steel, 10 in/min sliding speed, and 4500 psi. Once again the grease, oil and soap are very low compared to the dry test.

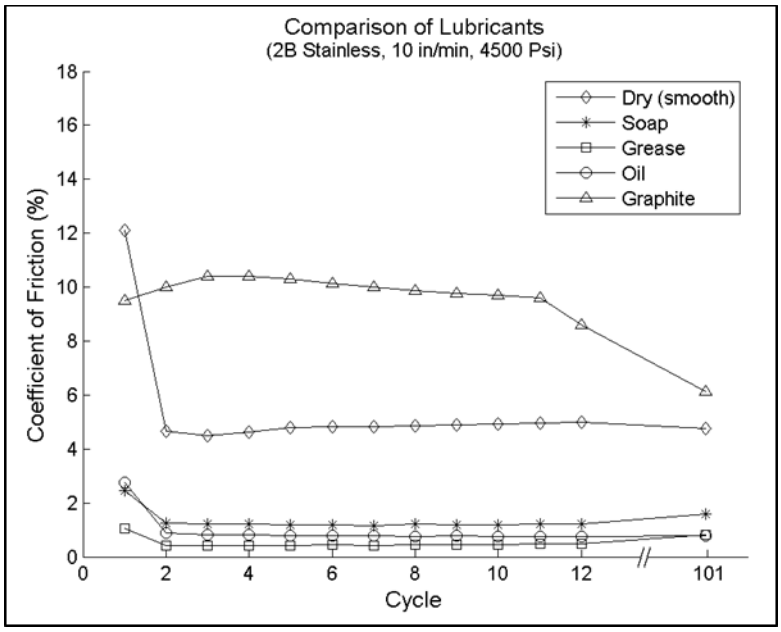

Figure 12.7. Lubricant comparison at 4500 psi, using #2B stainless and at 10 in/min

This group also includes a graphite test, which as shown in the plot, performed very poorly. A significant amount of deformation of the PTFE pads was observed during the graphite test, as was discussed earlier under the materials section. Refer back to Figure 11.12 and Figure 11.13 to see how the PTFE pad deformed and started curling out from the confining substrate due to the high amount of friction.

The second graphite test that was done used less graphite and a smooth PTFE pad in hopes to reduce the friction values in comparison to the first test that was done. The performance was much better for this. The PTFE pads hardly deformed at all in comparison to the test that used more graphite and dimpled PTFE. Also, as is illustrated in Figure 12.8 below, the COF values were quite a bit lower for the test that used the smooth PTFE pads and light coating of graphite (Test #2B,Gph,2.5,4500). The friction was lower for the beginning cycles, and then they both eventually ended up converging to the same point towards the end of the cycles. Note that the two

tests were also done at different speeds, which also had an effect in the 2.5 in/min test having lower values.

Based on the performance of these two tests it was decided that graphite is not a good lubricant to use and no more tests were done using it. It produces COF values that are just as high as or higher than when using no lubrication at all.

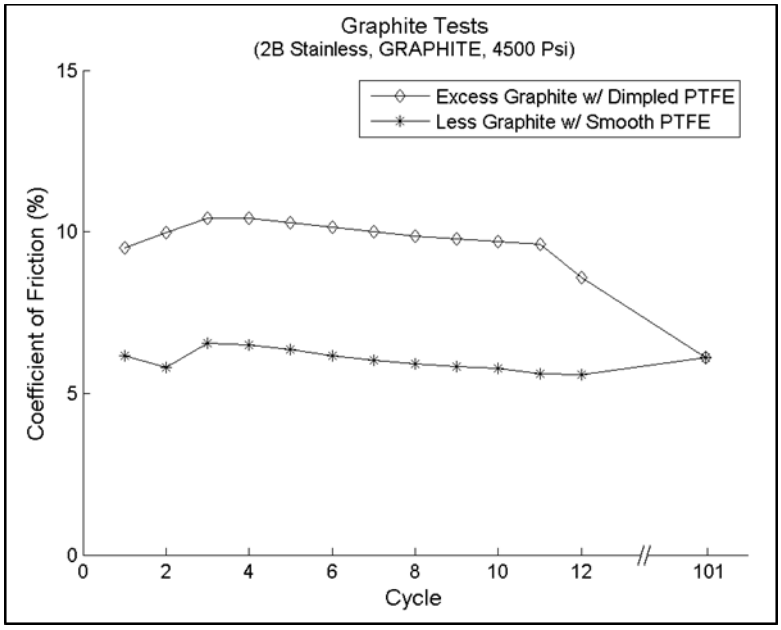

Figure 12.8. Graphite tests compared

In summary the oil tests performed really well, and did a really good job at keeping the pads lubricated throughout the testing. The COF values dropped significantly using oil versus dry. The grease tests performed just as well as the oil tests in most cases and since it repels water is assumed that it won't wash away as easily as the oil may during a rain storm. The soap tests also performed well. The friction values for the soap were often not much higher than what was seen for the oil and grease tests. The grease performed very poorly and is not recommended to be used in bridge slides. It is also recommended that dry PTFE is not used since these tests also gave much higher COF values than what can be obtained using lubricants.

Surface Roughness

The three types of surface roughness that were tested were #2B stainless steel, rough rolled stainless steel, and carbon steel. These materials are discussed in more detail in the materials section of this document. Overall, the #2B stainless steel produced much lower COF values than the #1 rough rolled (RR) stainless and also the carbon steel (St).

The following figures show how the COF compares when looking at the different surfaces that each has a different surface roughness. The graphs are grouped first by soap, then grease, and then oil. All of these groups of tests are at a sliding speed of 10 in/min, and 4500 psi. To see the other graphs that are similar to these for other parameters, such as for 1500 psi. These three graphs are a good representation of how the contact surfaces performed in comparison with each other. As can be seen in Figure 12.9, Figure 12.10, and Figure 12.11 below, the COF for the #2B tests was always lower than the rough rolled and steel tests.

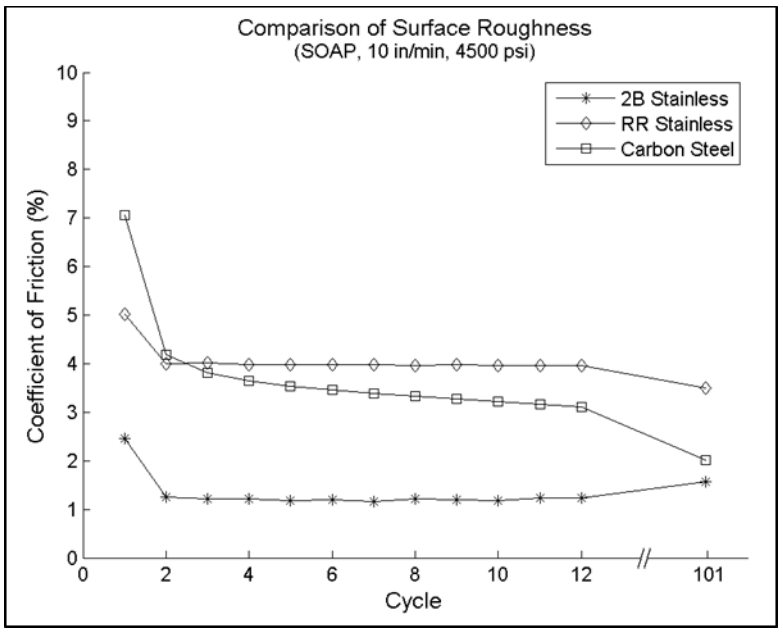

Figure 12.9. Comparison of surface roughness for soap tests

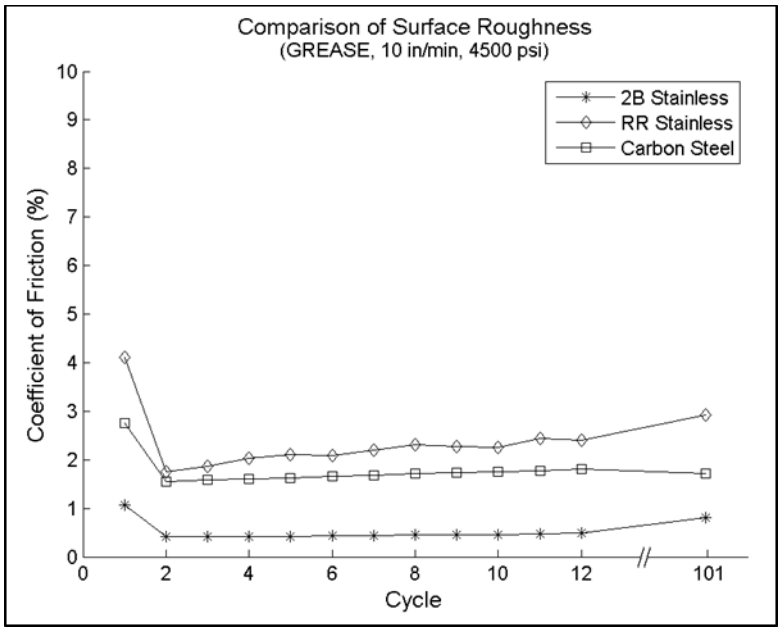

Figure 12.10. Comparison of surface roughness for grease tests

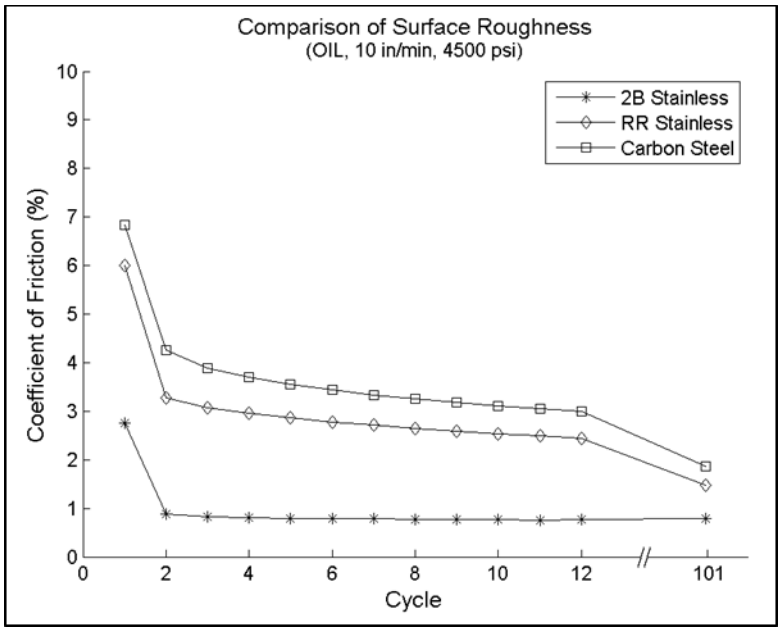

Figure 12.11. Comparison of surface roughness for oil tests

On average the COF values for the #2B surfaces were 3 times lower than the COF for the rough rolled and carbon steel surfaces. That is a big difference, which is why it is recommended that all bridge slides use either #2B stainless steel sliding surfaces or mirror finish which is the finish specified by AASHTO for bridge bearings. Almost half of the steel and rough rolled surfaces

produced COF values around 15% or higher. Due to these higher values it was decided that other tests beyond what was said would be tested were not tested.

Sliding Speed

The two sliding speeds that were investigated were 10 inches per minute and 2.5 inches per minute. The sliding speed of 2.5 in/min in general produced lower COF values than the 10 in/min. It appears that for the soap tests, varying the sliding speed had a bigger effect on the difference between the COF for the two speeds, than it does for the grease and oil tests. Figure 12.12 shows the friction paths for two of the soap tests at 4500 psi, and compares how the two sliding speeds performed relative to each other. The COF for the 2.5 in/min sliding speed was consistently lower than the COF for the 10 in/min. For the most part this is how all of the soap tests were when comparing the sliding speed.

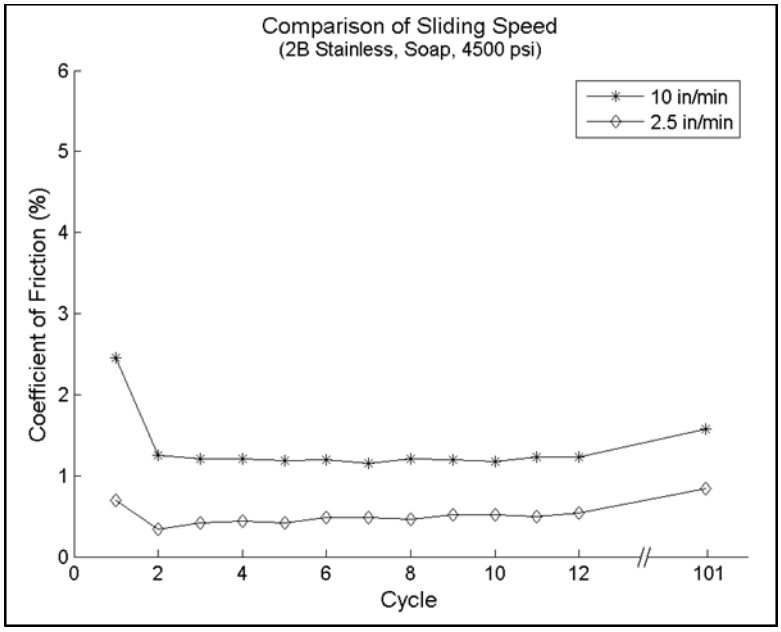

Figure 12.12. Comparison of sliding speed using #2B stainless, soap, and 4500 psi

When the grease tests were compared with each other to see how the sliding speed influenced the COF, most of the graphs illustrated that there was little influence that the sliding

speed had. Figure 12.13 is a good example of how the sliding speed doesn't have much influence when using grease. Some of the other comparisons using grease or oil but at different pressures had a little more variance in the COF for the two sliding speeds, but they were still very similar. Comparisons for the dry tests on #2B stainless do not provide good comparisons when looking at the effects of sliding speed because of inconsistencies with the surface roughness of the stainless steel.

Over all, there is a pattern seen that as the sliding speed is increased, the COF will also increase slightly. When using soap for a lubricant, this increase will be more than if grease or oil were used.

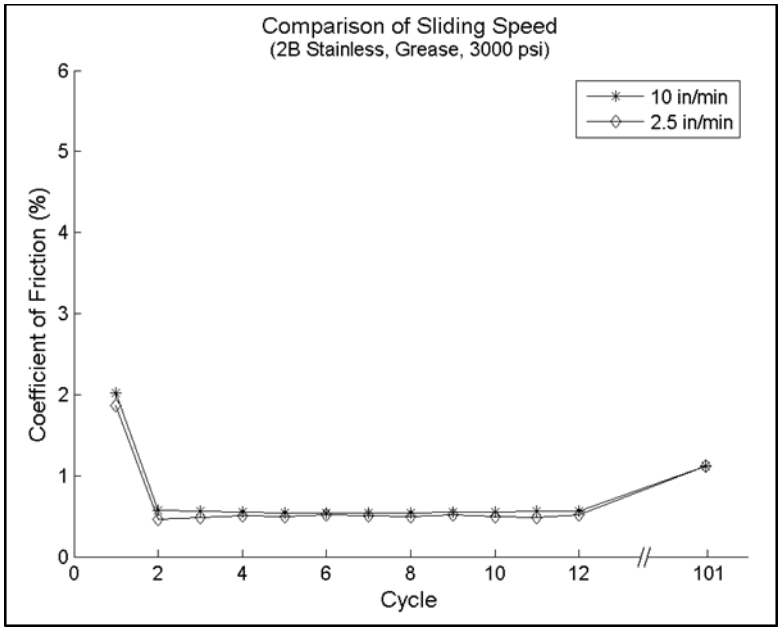

Figure 12.13. Comparison of sliding speed using #2B stainless, grease, and 3000 psi

Part Three: Conclusions

Chapter 13: Bridge Dynamics Conclusion

In the preceding chapters, the dynamic response of lightly and heavily loaded SPMTs were investigated during several common maneuvers. It was found that traversing a long stretch of uneven ground was critical for the vertical direction (The Long Run Motion Case) and rapid decelerations were critical for the horizontal direction (The Start and Stop Motion Case). Transverse accelerations were found to not be critical for the horizontal direction. Increasing the payload of the SPMT was found to decrease measured accelerations significantly. Acceleration data was recorded from the platform in various locations during these maneuvers. The data collected was used to develop design response spectra, treating the problem similarly to an earthquake design scenario.

The following conclusions can be made based on the testing and analysis of SPMT dynamic loads:

- Vertical accelerations were controlled by the Long Run Motion Case
- Vertical accelerations are related to SPMT transport speed
- Vertical accelerations affect the falsework and the cargo differently: The cargo is considered flexible for design and the falsework can be considered rigid. The vertical design spectrum is recommended for vertical design of the flexible cargo and applying the PPAV to the falsework is considered acceptable.
- Horizontal accelerations were controlled by the longitudinal direction of the Start and Stop Motion Case.
- Horizontal accelerations are not affected by the speed of the SPMT, but are affected by the ability of the operator to perform a braking operation.

- Horizontal accelerations affect the falsework and the cargo differently: The cargo is considered rigid for design and the falsework is considered flexible. The horizontal design spectrum is recommended for horizontal design of the flexible falsework and horizontal forces acting on the rigid bridge are considered negligible.
- Transverse accelerations were considerably lower than the longitudinal accelerations, therefore longitudinal accelerations are recommended for both horizontal directions when designing.
- Significant reductions in PPA were measured as payload increased. Contractors are recommended to use large loads, with respect to SMPT capacity, to reduce design forces.
- Design spectra were developed for the horizontal and vertical directions, which are based only on an estimation of PPA for the SPMT loading.
- Justifications for reducing PPA and the design spectra were presented for both directions.
- Vertical accelerations can be reduced by limiting the speed of the SPMT during transport
- Horizontal accelerations can be reduced because some level of damage is likely acceptable to the falsework and response modification factors may be applied to the developed spectra, similar manner currently used for AASHTO LRFD earthquake design.

Chapter 14: Friction Value Conclusion

The research team tested four parameters which influence the coefficient of friction (COF) for sliding bearings which use PTFE-Stainless Steel sliding interfaces. The project focused on testing the effects each of these parameters have when using PTFE sliding bearings for Slide-In-Bridge Construction. The four parameters that were tested are: (1) Surface Roughness, (2) Lubrication, (3) Sliding Speed, and (4) Contact Pressure.

Surface Roughness

There were three surfaces roughness tested: stainless steel with a #2B surface roughness (2B), rough rolled stainless steel which has a #1 surface roughness (RR), and standard carbon steel (St) which is readily available at construction sites. As expected the rough rolled stainless steel, as well as the carbon steel, produced COF values much higher than what the stainless with a #2B surface produced.

For permanent bridge bearings, which are a more long-term application of sliding bearings, AASHTO specifies to use stainless steel with a #8 finish (commonly known as a mirror finish). This type of finish has a very polished surface which yields low friction values. However, it is much more expensive than #2B stainless steel and not as readily available. It is roughly 50% less expensive to use #2B stainless than the #8 mirror stainless. Since the #2B stainless steel performed similar to the #8 mirror stainless steel, it is recommended that either one of these stainless finishes be used for Slide-In Bridge Construction. Although rough rolled #1 stainless and carbon steel did not yield as low of fiction values as did the #2B, it is recommended that these materials be allowed for use as a mating surface as long as the extra capacity needed for a higher friction force be accounted for in the design. If either carbon steel or rough rolled stainless steel is used as a mating

surface it's recommended to use a lubricant as well as a contact pressure above 3000 psi in order to reduce the COF.

Lubricants

The lubrications that were tested were standard liquid dish soap, dielectric silicone grease (SAE-AS8660), automotive motor oil (10W-40 viscosity), powdered graphite, as well as dry tests which used no lubricants. Each of these lubricants were tested in combination with dimpled PTFE pads. Some of the dry tests used dimpled, and some used smooth PTFE pads for better comparison. The dry tests and graphite tests had very high friction values, whereas the soap, grease, and oil all performed really well. The oil and grease tests gave the lowest friction values and for many of the tests the soap was not a whole lot higher. Either of these lubricants would work great and are recommended for use in bridge slides.

Sliding Speed

There were two sliding speeds that were investigated, 10 inches per minute, and 2.5 inches per minute. The faster speed of 10 in/min gave COF results that were a little higher than for the 2.5 in/min tests. When oil or grease are used the influence that the sliding speed has on the COF decreases to where there is not much of a difference between the two sliding speeds. It is recommended that the specifications for bridge slides be based off of the results for the 10 in/min tests since this speed is much more reasonable for contractors to use, and this would be the more conservative speed to use.

Contact Pressure

It has been well documented by other researchers that as the contact pressure increases, the COF decreases when using PTFE bearing pads. The testing for this project obtained results that agree with this pattern for dry tests as well as soap, grease, and oil. This pattern was also seen for the different sliding speeds as well as surface roughnesses. The pressures that were tested were 1500, 3000, 4500, and 8000 psi. The biggest drop in the COF was seen when going from 1500 to 3000 psi, whereas many of the 3000 and 4500 psi tests had values within a closer range. The tests done at 8000 psi reduced the COF values lower than the ones at 4500 psi, but the drop in COF tends to decrease faster with changes in pressure at lower pressures, than it does at higher pressures.

References

Aktan, H., Attanayake, U., Mohammed, A. (2014). Accelerated Bridge Construction and Structural Move – Workshop, Western Michigan University, Kalamazoo, MI, pp 50.

Ardani, Ahmad A., Lindsey, Rukhsana, Mallela, Jagannath (2010) One-Weekend Job, Rapid Removal and Replacement of 4500 South Bridge in Salt Lake City, Utah. Transportation Research Board, Utah.

Culmo, M. (2011). Accelerated Bridge Construction – Experience in Design, Fabrication, and Erection of Prefabricated Bridge Elements and Systems, CME Associates, Inc., East Hartford, Connecticut, pp 347.

FHWA (2013). Slide-In Bridge Construction Implementation Guide, Project: F-ST99 (232), U.S. Department of Transportation, Federal Highway Administration, Washington, D.C., pp 168.

FHWA (2007). Manual on the Use of Self-Propelled Modular Transporters to Remove and Replace Bridges, Project FHWA-HIF-07-022, U.S. Department of Transportation, Federal Highway Administration, Washington, D.C., pp 118.

Iowa DOT (2009). Iowa Department of Transportation Accelerated Bridge Construction Workshop: Workshop Report, Iowa Department of Transportation, Ames, IA, pp 87.

Kim, S., Holub, C., Elnashai, A. (2011) Analytical Assessment of the Effect of Vertical Earthquake Motion on RC Bridge Piers. American Society of Civil Engineers (ASCE), Vol. 137, pp 252-260.

LaViolette, M., Wipf, T., Lee, Y., Bigelow, J., Phares, B. (2007). Bridge Construction Practices Using Incremental Launching, Iowa State University (ISU), Ames, Iowa, pp 106.

NCHRP (1999). High-Load Multi-Rotational Bridge Bearings, NCHRP Report 432

Ralls, M., Tang, B., Bhidé, S., Brecto, B., Calvert, E., Capers, H., Dorgan, D., Matsumoto, E., Napier, C., Nickas, W., Russell, H. (2005). Prefabricated Bridge Elements and Systems in Japan and Europe. Alexandria, Virginia, pp xii, 13.

Rosvall, Erik, Halling, Marvin, Lindsey, Rukhsana (2010) Induced Stresses from Lifting and Moving Highway Bridges with Self-Propelled Modular Transporters. Utah State University, Logan, Utah, pp 17-25.

Rosvall, Erik, Halling, Marvin (2010). Data Analysis of Utah's I-80 Bridges – For the Use in the Development of Accelerated Bridge Construction Standards. Utah State University, Logan, Utah, pp 90.

Strategic Highway Research Program 2 (2013a). ABC Standard Concepts: The Lateral Slide – Addendum to Innovative Bridge Designs for Rapid Renewal: ABC Toolkit, SHRP2 Renewal Project R04, Publication Draft, Transportation Research Board, Washington D.C., pp 70.

Strategic Highway Research Program 2 (2013b). Innovative Bridge Designs for Rapid Renewal: ABC Toolkit, SHRP2 Report S2-R04-RR-2, Transportation Research Board, Washington D.C., pp 323.

Taylor, J.C., Stanton, J.F. (2010). Friction Coefficients for Stainless Steel (PTFE) Teflon Bearings, University of Washington, Seattle WA, Wisconsin Department of Transportation, Madison WI, Federal Highway Administration, Washington DC.

UDOT (2009). Accelerated Bridge Construction SPMT Process Manual and Design Guide, Utah Department of Transportation, Salt Lake City, Utah, pp 84.

Wipf, T.J., Phares, B.M., Abendroth, R.A., Wood, D.L., Chang, B., and Abraham, S. (2004). Monitoring of the Launched Girder Bridge over the Iowa River on US 20, Iowa State University, Ames, IA, pp 100.

Wisconsin DOT (2013). WisDOT Bridge Manual, CH 7-Accelerated Bridge Construction, Wisconsin Department of Transportation, Madison, Wisconsin, pp 1-35.

Appendix A

Appendix Table A. 1 The sensor specifications

Name	Company	Range	Calibration Factor
A1035	BDI	±2g	1.00281 g/V_{OUTPUT}
A1036	BDI	±2g	1.00648 g/V_{OUTPUT}
A2087	BDI	±5g	325.733 $g/V_{OUTPUT}/V_{EXCITATION}$
A2088	BDI	±5g	326.797 $g/V_{OUTPUT}/V_{EXCITATION}$
A2089	BDI	±5g	332.266 $g/V_{OUTPUT}/V_{EXCITATION}$
A2090	BDI	±5g	319.489 $g/V_{OUTPUT}/V_{EXCITATION}$
A2130	BDI	±5g	2.516 g/V_{OUTPUT}
A2131	BDI	±5g	2.516 g/V_{OUTPUT}
A2132	BDI	±5g	2.516 g/V_{OUTPUT}
A2133	BDI	±5g	2.513 g/V_{OUTPUT}

Appendix B

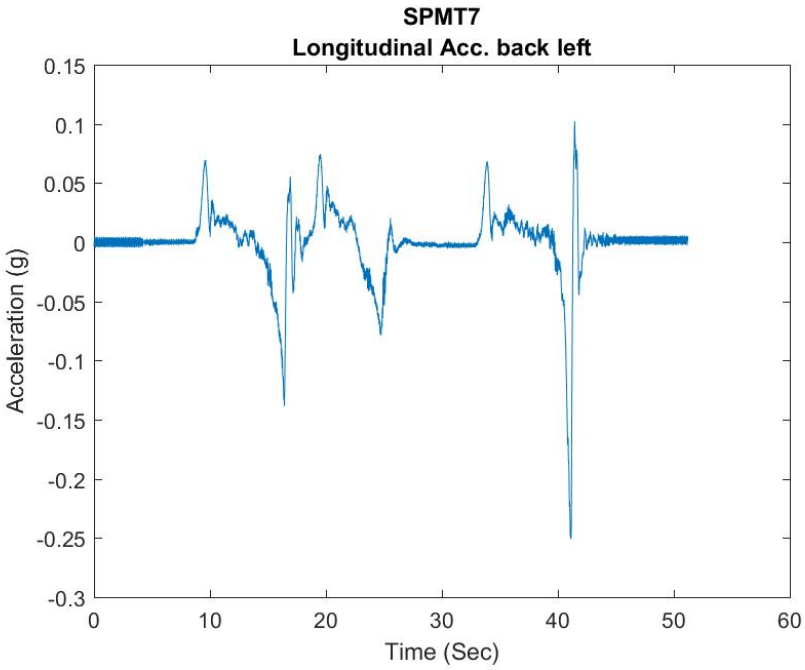

Appendix Figure B. 1 Time history for maximum longitudinal acceleration for Cluster 1 in heavy load case

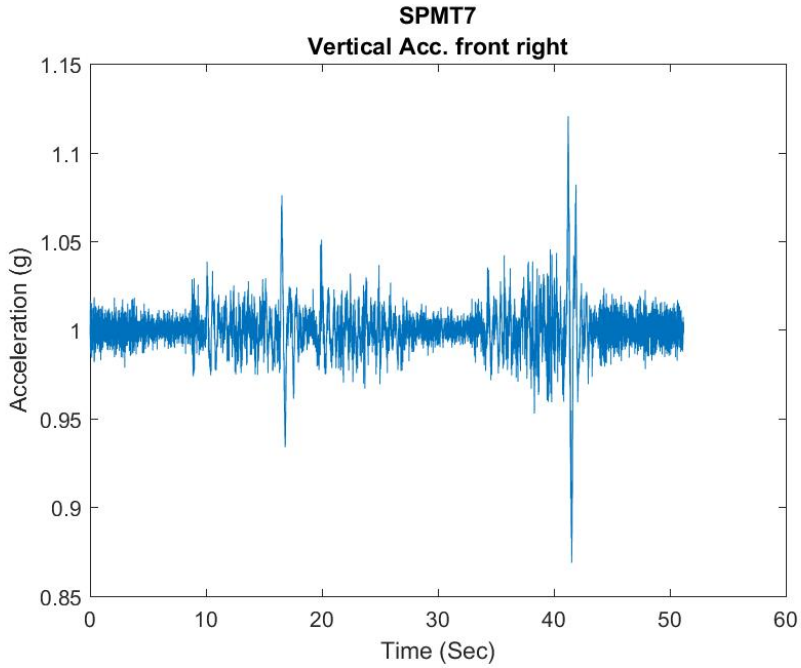

Appendix Figure B. 2 Time history for maximum vertical acceleration for cluster 1 in heavy load case

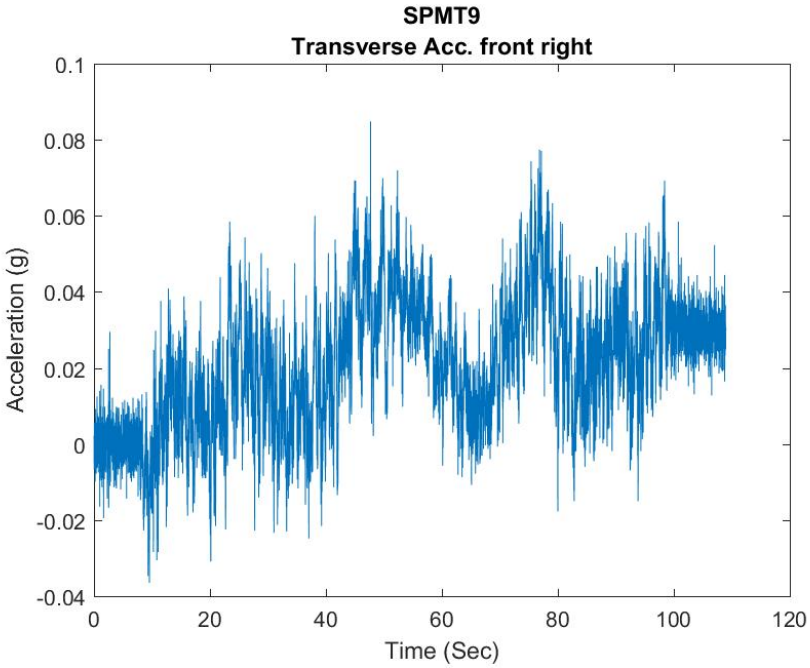

Appendix Figure B. 3 Time history for maximum transverse acceleration for Cluster 1 in heavy load case

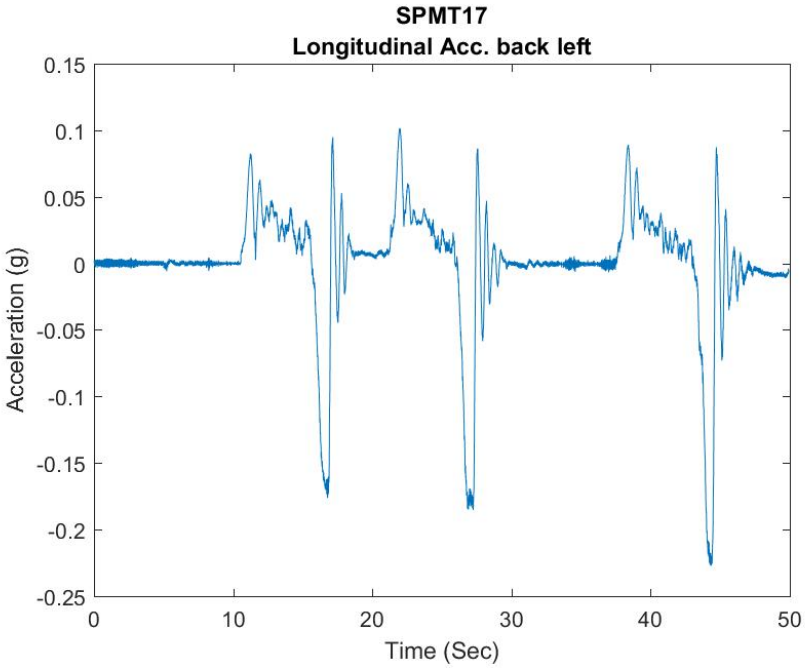

Appendix Figure B. 4 Time history for maximum longitudinal acceleration for Cluster 1 in medium load case

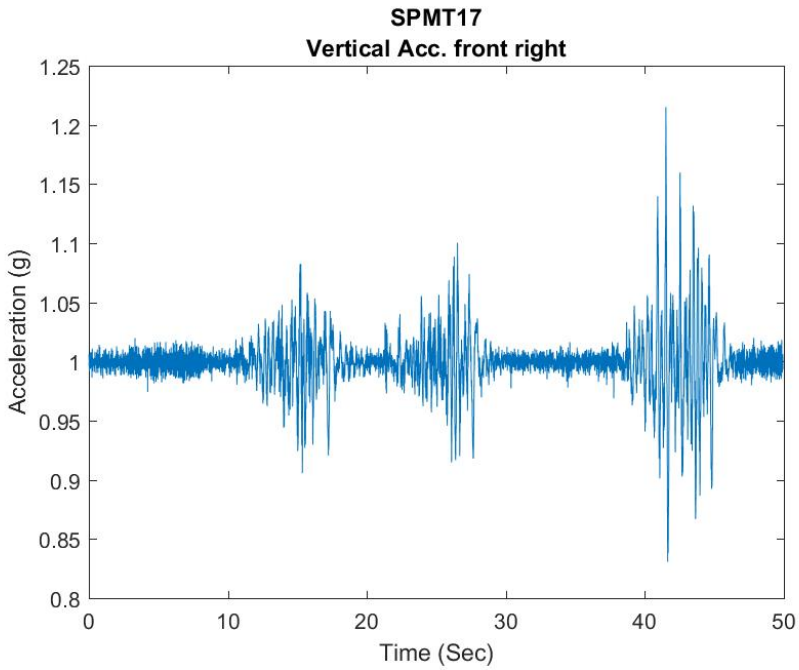

Appendix Figure B. 5 Time history for maximum vertical acceleration for Cluster 1 in medium load case

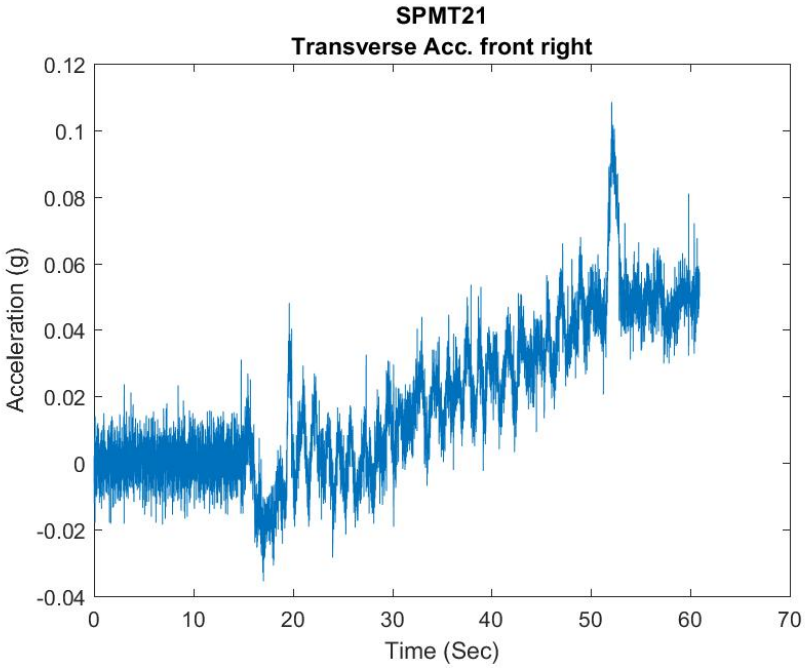

Appendix Figure B. 6 Time history for maximum transverse acceleration for Cluster 1 in medium load case

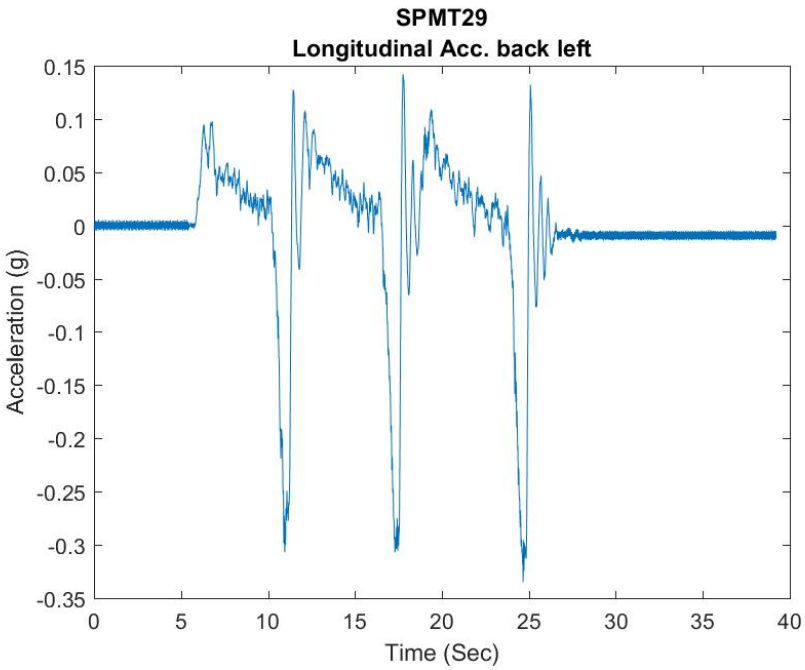

Appendix Figure B. 7 Time history for maximum longitudinal acceleration for Cluster 1 in light load case

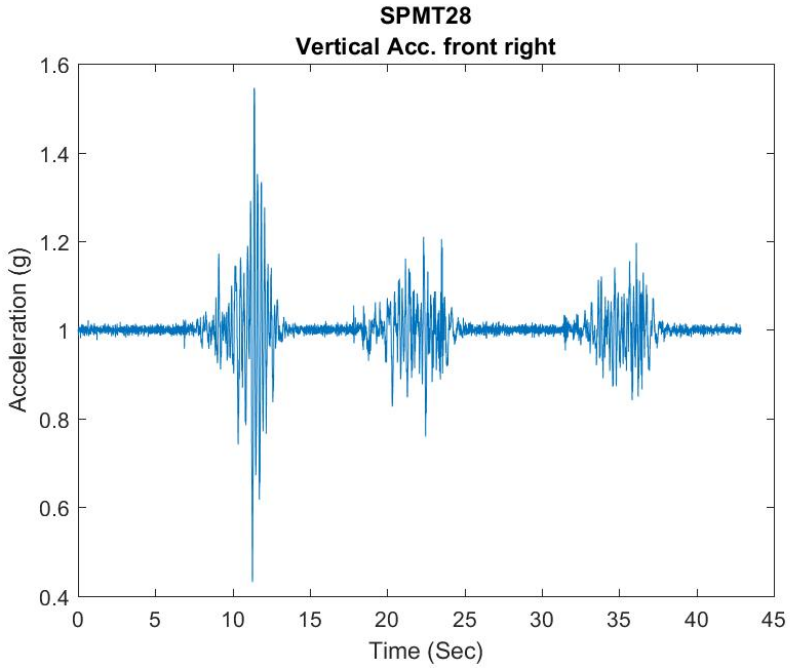

Appendix Figure B. 8 Time history for maximum vertical acceleration for Cluster 1 in light load case

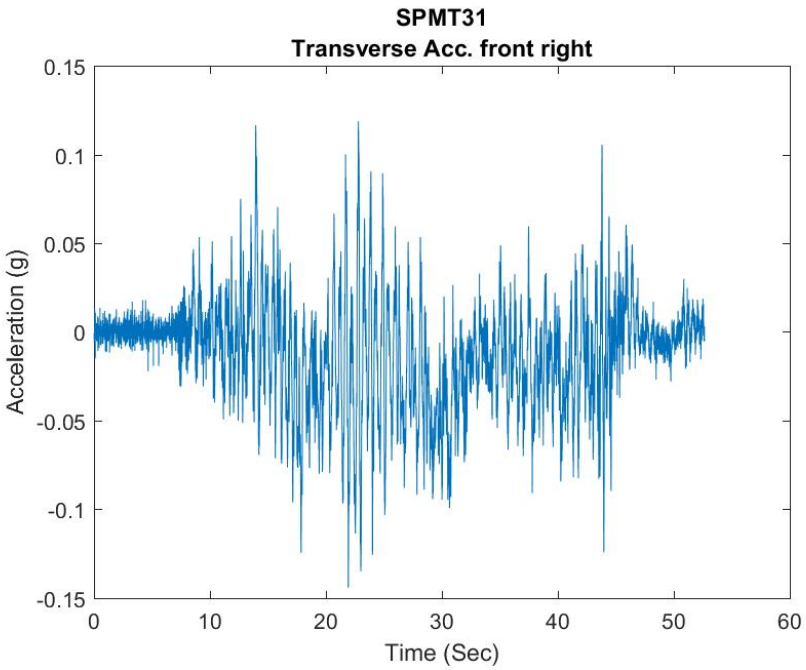

Appendix Figure B. 9 Time history for maximum transverse acceleration for Cluster 1 in light load case

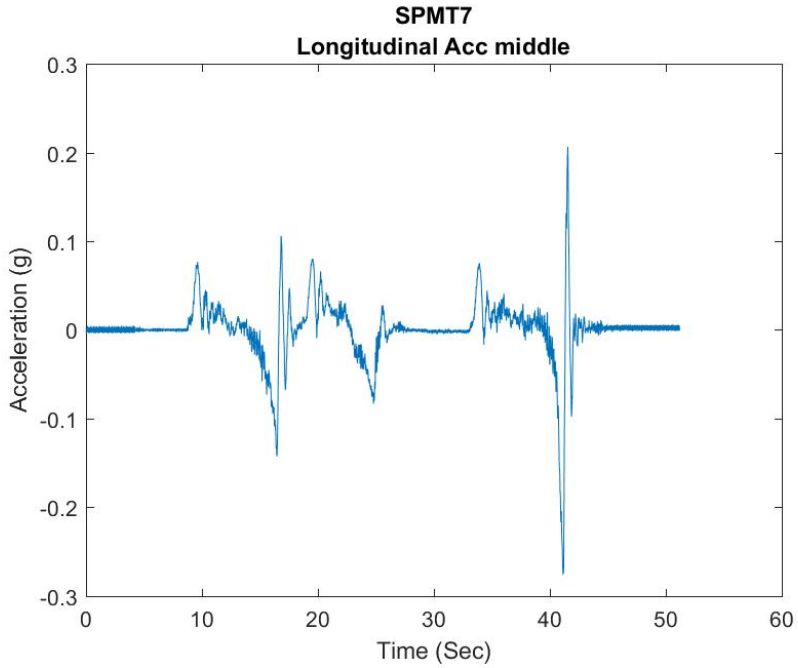

Appendix Figure B. 10 Time history for maximum longitudinal acceleration for Cluster 2 in heavy load case

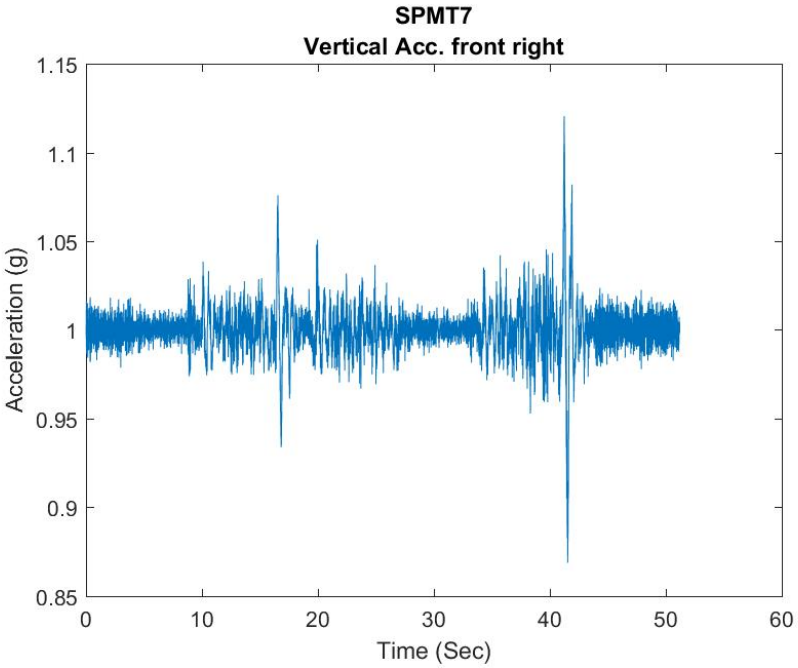

Appendix Figure B. 11 Time history for maximum vertical acceleration for Cluster 2 in heavy load case

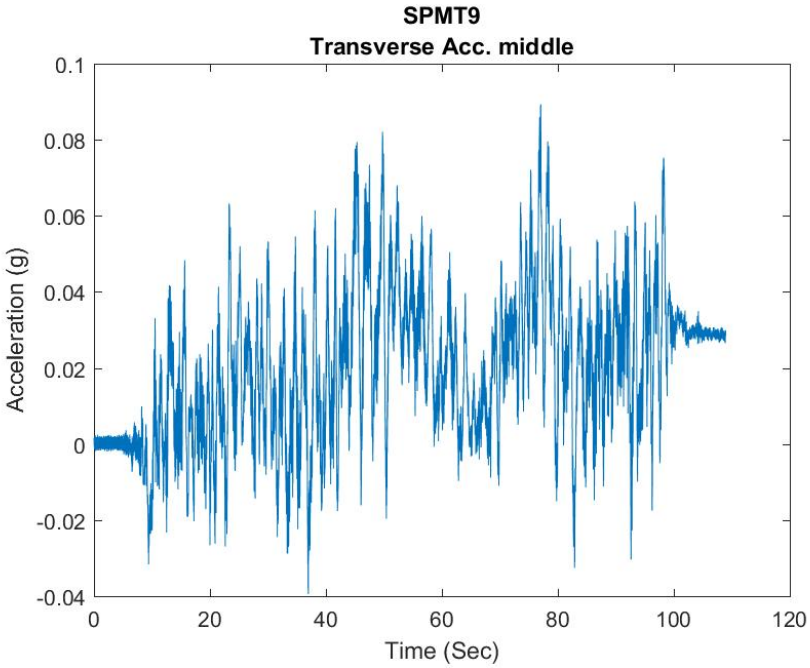

Appendix Figure B. 12 Time history for maximum transverse acceleration for Cluster 2 in heavy load case

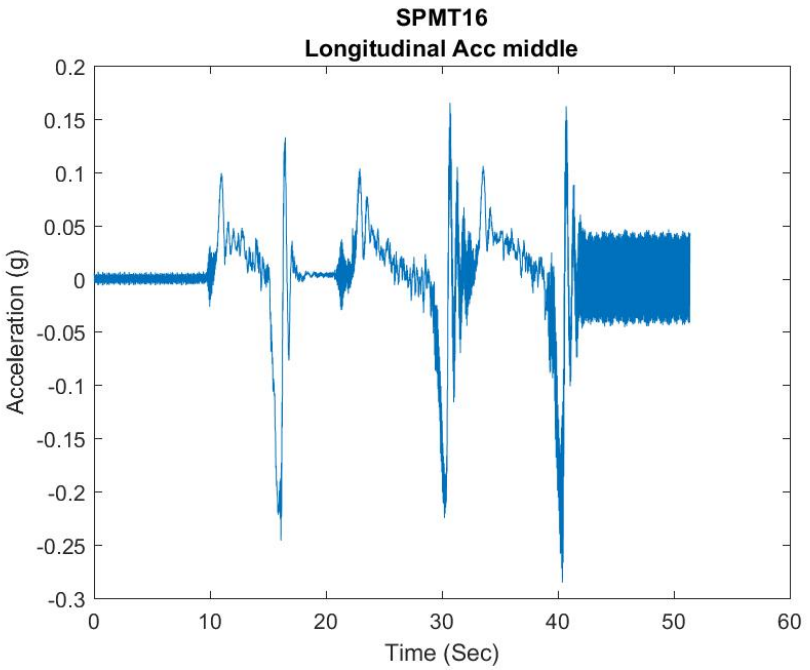

Appendix Figure B. 13 Time history for maximum longitudinal acceleration for Cluster 2 in medium load case

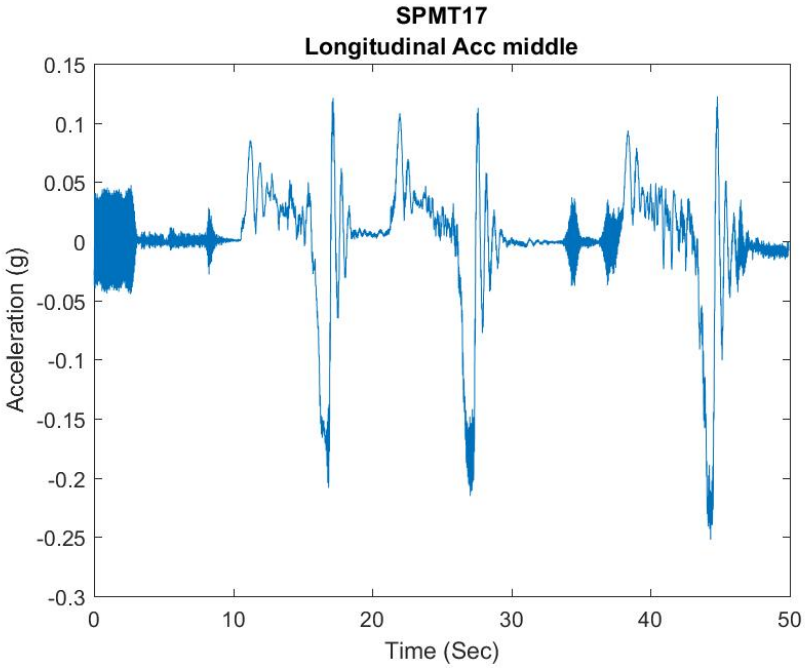

Appendix Figure B. 14 Time history for maximum vertical acceleration for Cluster 2 in medium load case

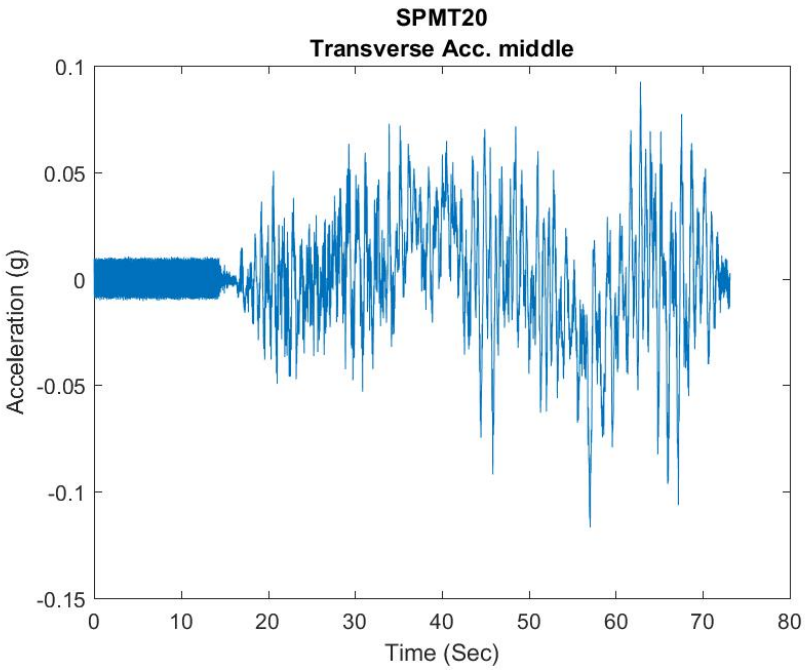

Appendix Figure B. 15 Time history for maximum transverse acceleration for Cluster 2 in medium load case

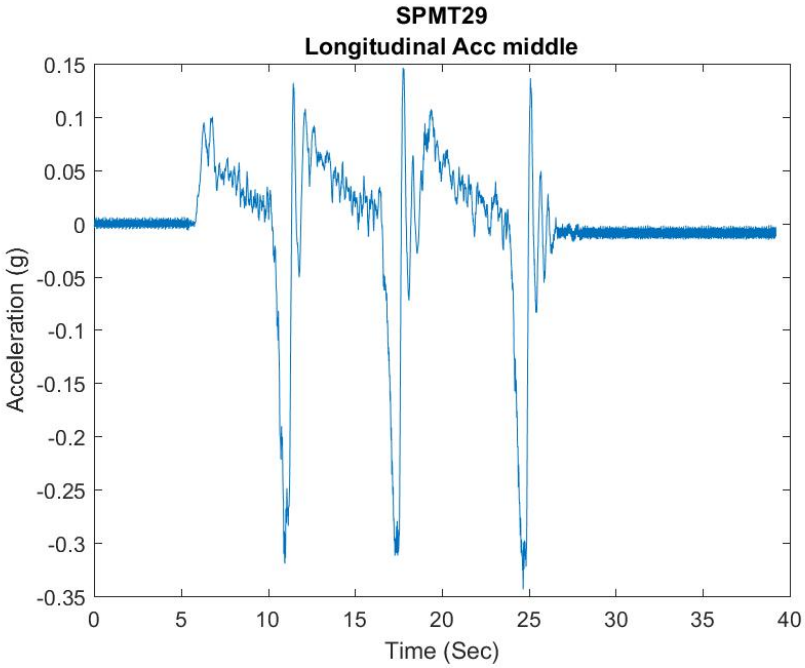

Appendix Figure B. 16 Time history for maximum longitudinal acceleration for Cluster 2 in light load case

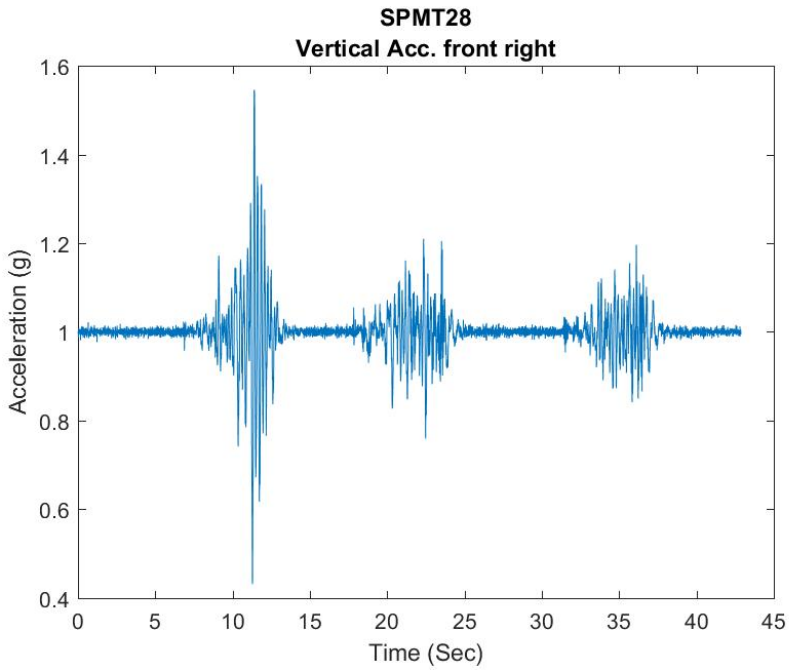

Appendix Figure B. 17 Time history for maximum vertical acceleration for Cluster 2 in light load case

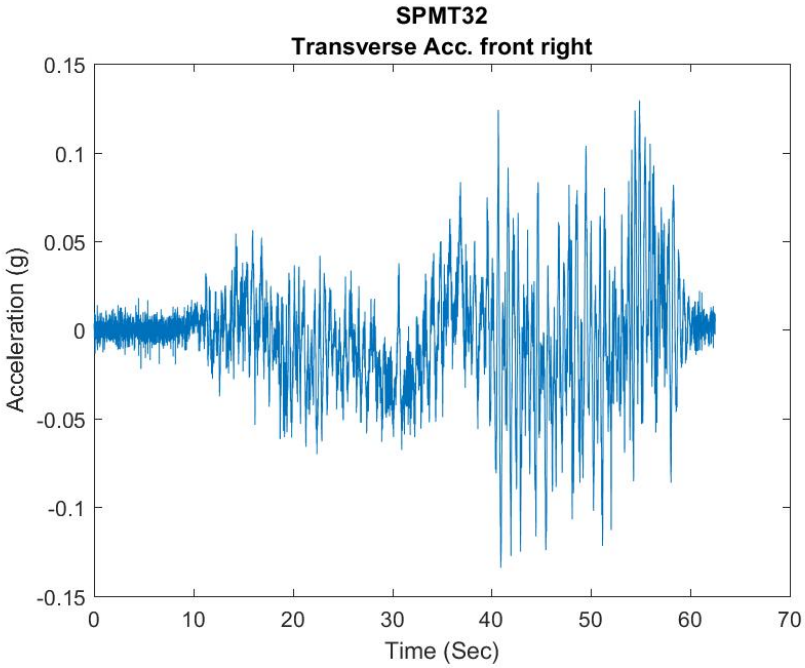

Appendix Figure B. 18 Time history for maximum transverse acceleration for Cluster 2 in light load case

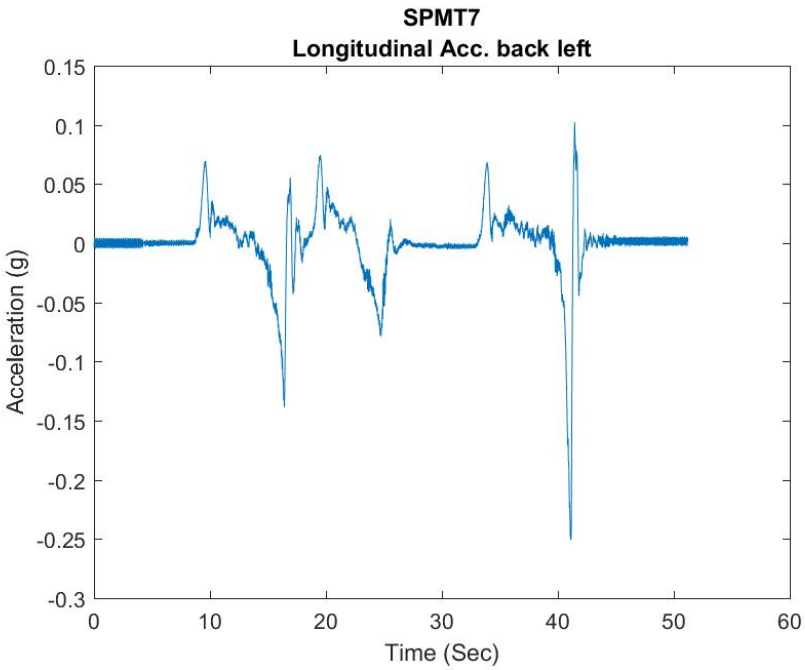

Appendix Figure B. 19 Time history for maximum longitudinal acceleration for Cluster 3 in heavy load case

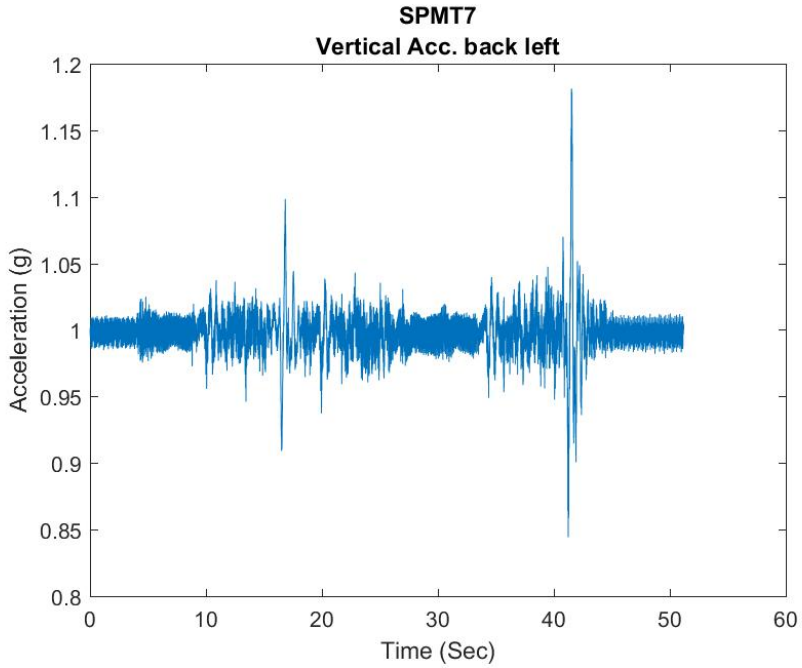

Appendix Figure B. 20 Time history for maximum vertical acceleration for Cluster 3 in heavy load case

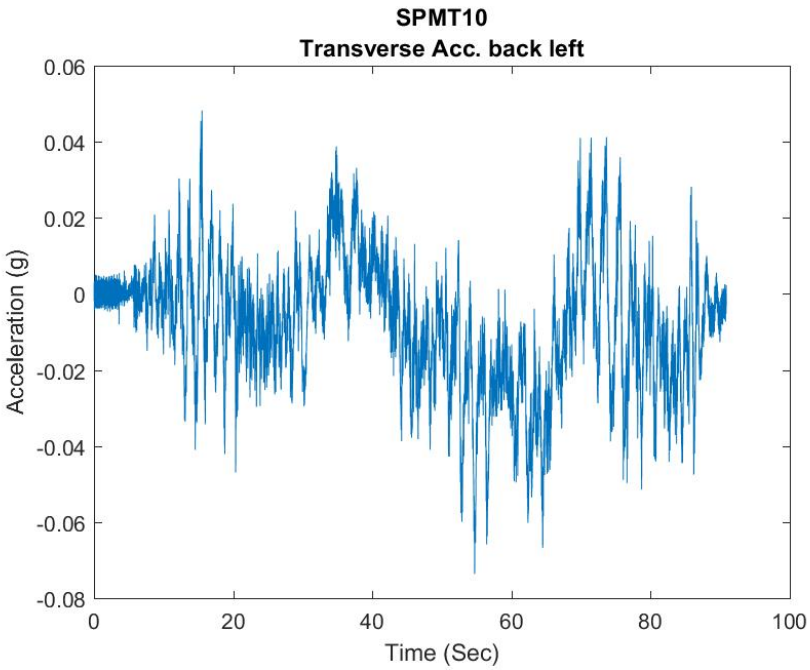

Appendix Figure B. 21 Time history for maximum transverse acceleration for Cluster 3 in heavy load case

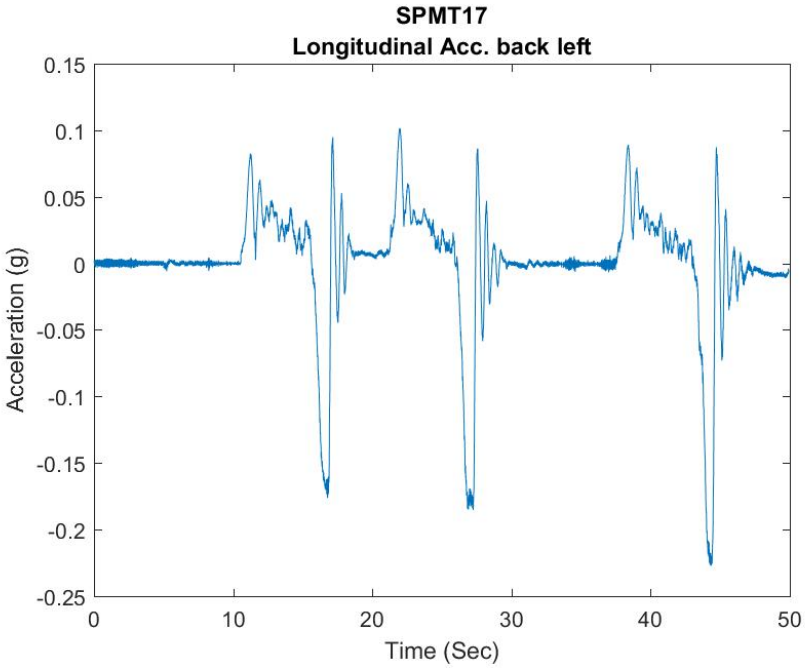

Appendix Figure B. 22 Time history for maximum longitudinal acceleration for Cluster 3 in medium load case

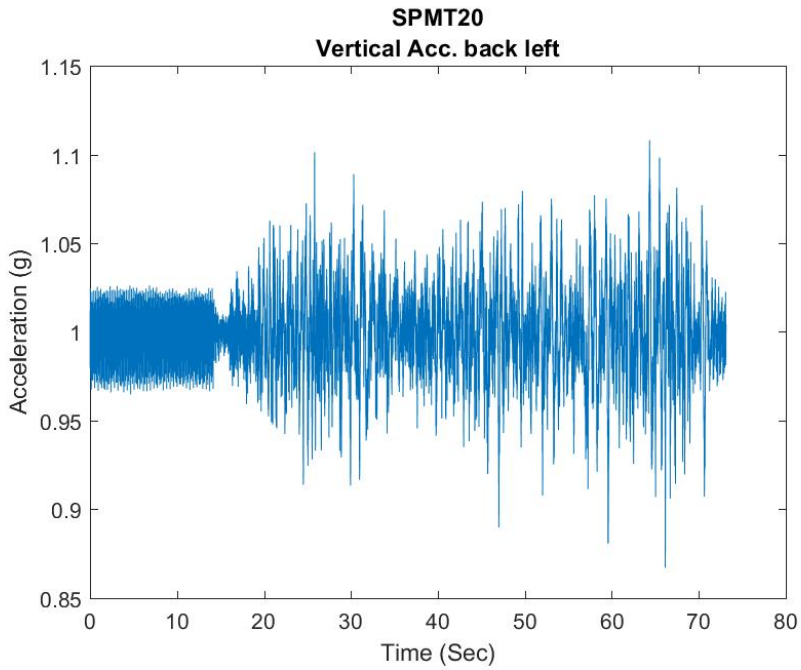

Appendix Figure B. 23 Time history for maximum vertical acceleration for Cluster 3 in medium load case

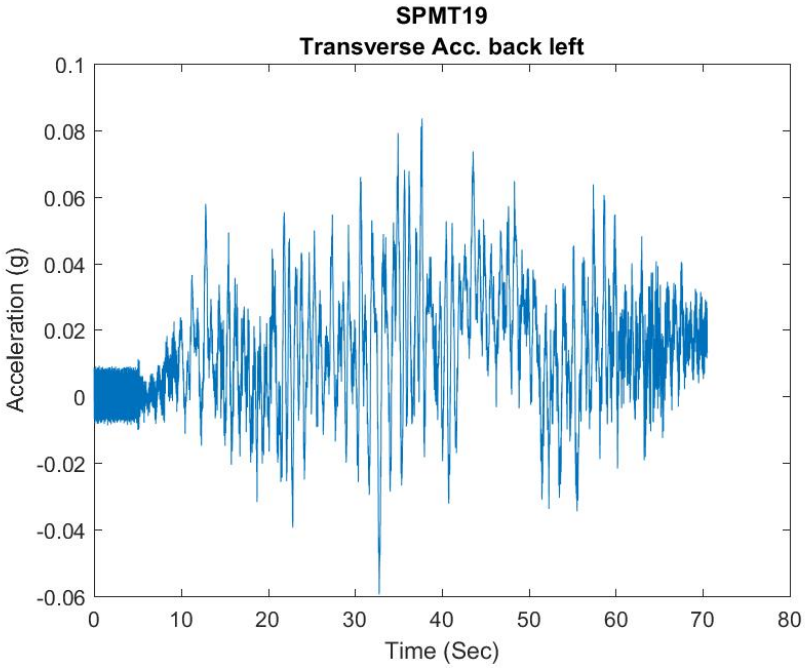

Appendix Figure B. 24 Time history for maximum transverse acceleration for Cluster 3 in medium load case

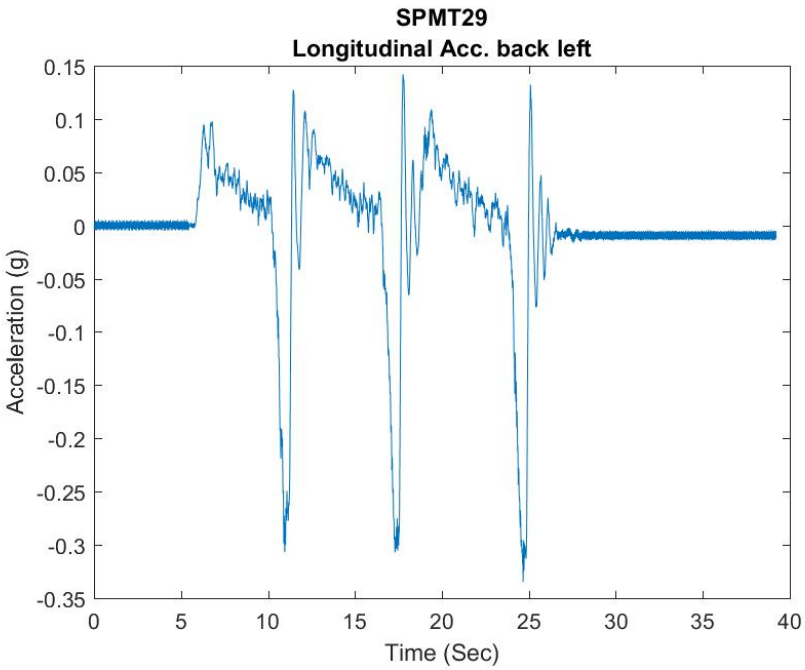

Appendix Figure B. 25 Time history for maximum longitudinal acceleration for Cluster 3 in light load case

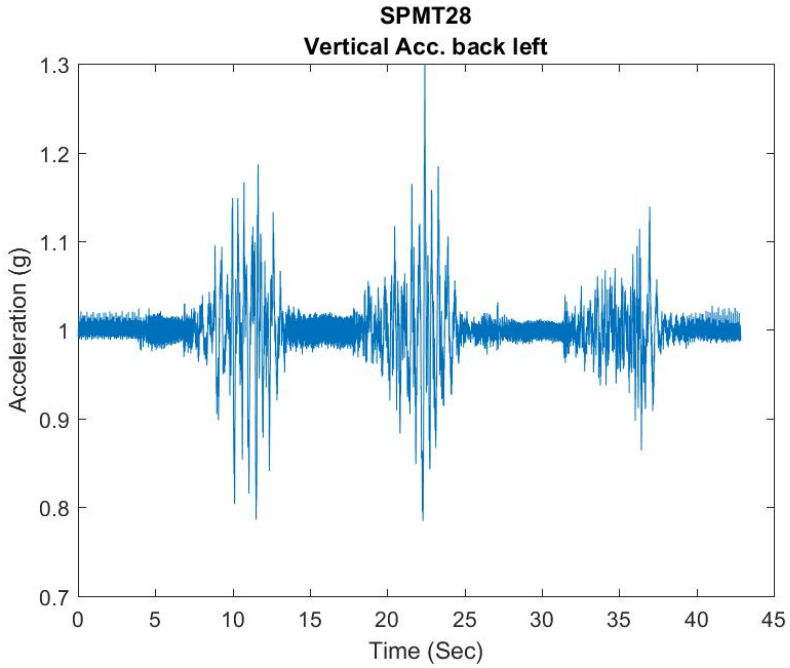

Appendix Figure B. 26 Time history for maximum vertical acceleration for Cluster 3 in light load case

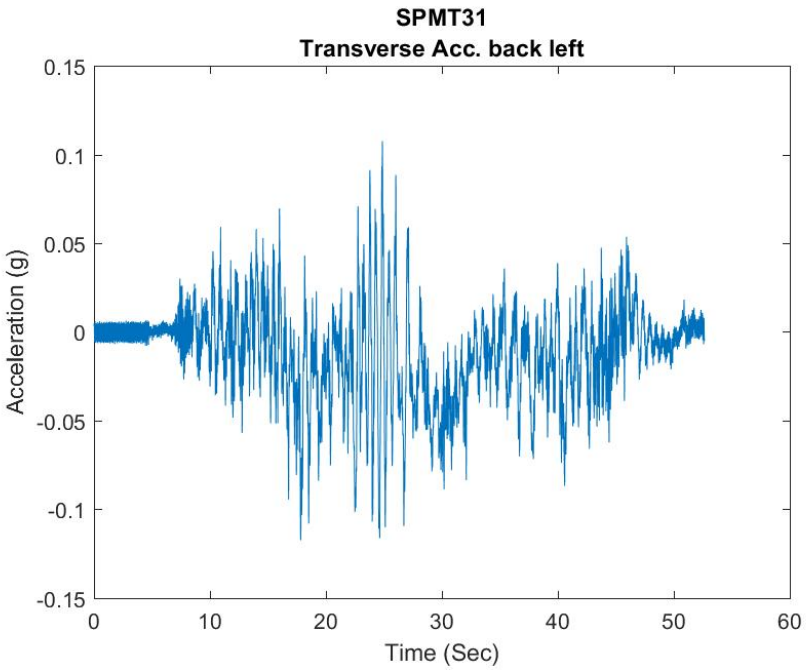

Appendix Figure B. 27 Time history for maximum transverse acceleration for Cluster 3 in light load case